Wegener Center for Climate and Global Change
University of Graz

Scientific Report No. 46-2011

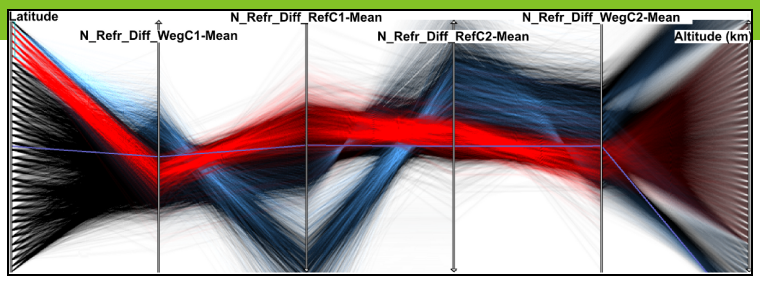

On Upper-Air Climate Data: Interactive Visual Exploration and GPS Radio Occultation as Reference Climate Record

Florian Ladstädter

December 2011

Financially supported by

FWF
Der Wissenschaftsfonds.

Wegener Center
www.wegcenter.at

UNI GRAZ

The **Wegener Center for Climate and Global Change** combines as an interdisciplinary, internationally oriented research center the competences of the University of Graz in the research area „Climate, Environmental and Global Change“. It brings together, in a dedicated building close to the University central campus, research teams and scientists from fields such as geo- and climate physics, meteorology, economics, geography, and regional sciences. At the same time close links exist and are further developed with many cooperation partners, both nationally and internationally. The research interests extend from monitoring, analysis, modeling and prediction of climate and environmental change via climate impact research to the analysis of the human dimensions of these changes, i.e, the role of humans in causing and being effected by climate and environmental change as well as in adaptation and mitigation. (more informationen at www.wegcenter.at)

The present report is the result of a PhD thesis work completed in May 2011. The work was funded by the Austrian Science Fund (FWF) under research grants P18733-N10 (INDICATE) and P21642-N21 (TRENDEVAL).

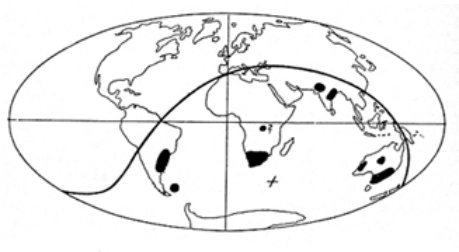

Alfred Wegener (1880-1930), after whom the Wegener Center is named, was founding holder of the University of Graz Geophysics Chair (1924-1930) and was in his work in the fields of geophysics, meteorology, and climatology a brilliant, interdisciplinary thinking and acting scientist and scholar, far ahead of his time with this style. The way of his ground-breaking research on continental drift is a shining role model — his sketch on the relationship of the continents based on traces of an ice age about 300 million years ago (left) as basis for the Wegener Center Logo is thus a continuous encouragement to explore equally innovative scientific ways:
paths emerge in that we walk them (Motto of the Wegener Center).

Wegener Center Verlag • Graz, Austria
© 2011 All Rights Reserved.
Selected use of individual figures, tables or parts of text is permitted for non-commercial purposes, provided this report is correctly and clearly cited as the source. Publisher contact for any interests beyond such use: wegcenter@uni-graz.at.

ISBN 978-3-9503112-3-5

December 2011

Contact: Dr. Florian Ladstädter-
florian.ladstaedter@uni-graz.at

Wegener Center for Climate and Global Change
University of Graz
Leechgasse 25
A-8010 Graz, Austria
www.wegcenter.at

Wegener Center for Climate and Global Change
Institute for Geophysics, Astrophysics, and Meteorology/Institute of Physics
University of Graz

Dissertation
zur Erlangung des akademischen Grades eines Doktors der Naturwissenschaften

On Upper-Air Climate Data: Interactive Visual Exploration and GPS Radio Occultation as Reference Climate Record

Florian Ladstädter

Mai 2011
Editiert: Dezember 2011

Betreuer:
Univ.-Prof. Mag. Dr. Gottfried Kirchengast
Dr. Andrea K. Steiner

Wegener Center for Climate and Global Change, University of Graz, Leechgasse 25, A-8010 Graz, Austria
Institute for Geophysics, Astrophysics, and Meteorology/Institute of Physics,
University of Graz, Universitätsplatz 5/II, A-8010 Graz, Austria

This thesis was submitted in May 2011 and edited in December 2011. Paper D was updated to its final, published version. Minor changes in Section 3.3 were necessary to reflect the updates.

Abstract

While the efforts of the scientific community have lead to a remarkable knowledge of the climate system, there are still many open topics left to be resolved. One of these topics is concerned with upper-air climate change. There has been a debate about upper-air trends in the last decades, and the controversy is still ongoing. Climate model data, reanalysis datasets, and observational records show large uncertainty ranges in their trend values, many of them even disagree in important aspects of trend characteristics.

This thesis investigates methods to analyze upper-air climate data. Firstly, an innovative approach to deal with large atmospheric datasets is presented: Interactive visual exploration is shown to be a valuable tool to complement classical statistical methods. It opens new opportunities for data analysis because it does not require prior knowledge of data characteristics, thus enabling the user to come up with new hypothesis about the data. Several datasets from climate models, reanalyses and observations are explored with sophisticated interactive visualization techniques, showing how these methods make it easy to determine potentially unknown patterns and characteristics in the data.

Secondly, Radio Occultation (RO) as a recent upper-air dataset with high accuracy is employed as reference for stratospheric radiosonde and (Advanced) Microwave Sounding Unit ((A)MSU) climatologies. Special care is taken to account for sparse sampling in the radiosonde and RO climatologies. The results show good agreement of radiosondes and RO, while (A)MSU and RO trends are found to differ significantly. The advantages of RO with homogeneously distributed observations, high vertical resolution and accuracy are confirmed, helping to overcome problems of conventional upper-air data. The suitability to serve as reference for other observational records is demonstrated, thus narrowing the large structural uncertainties involved in today's upper-air climate records.

Zusammenfassung

Obwohl die wissenschaftliche Gemeinschaft bereits einen guten Wissensstand über das Klimasystem erreicht hat, bleiben dennoch offene Fragen. Eines dieser Fragen betrifft den Klimawandel der freien Atmosphäre. Die wissenschaftliche Debatte darüber der letzten Jahrzehnte führte zu einer bis heute andauernden Kontroverse. Klimamodelle, Reanalysen und Beobachtungsdaten zeigen große Unsicherheiten in ihren Trendwerten, einige sogar widersprüchliche Trendcharakteristika.

Diese Dissertation untersucht verschiedene Methoden zur Analyse der Atmosphärendaten. Im ersten Teil wird ein innovativer Umgang mit großen atmosphärischen Datensätzen präsentiert: Interaktive visuelle Exploration wird als geeignetes Werkzeug zur Ergänzung klassischer Statistik aufgezeigt. Vorwissen zu Datencharakteristika ist nicht erforderlich, wodurch sich neue Möglichkeiten der Analyse ergeben. Der/die Benutzer/in kann dadurch neue Hypothesen über die Daten entwickeln. Daten von Klimamodellen, Reanalysen und Beobachtungen werden mit fortschrittlichen interaktiven Visualisierungstechniken untersucht. Dabei zeigt sich, wie einfach damit potenziell unbekannte Charakteristika der Datensätze gefunden werden können.

Der zweite Teil der Dissertation verwendet hochgenaue Daten satellitenbasierter Radio Occultation (RO) als Referenz für Radiosonden- und (Advanced) Microwave Sounding Unit ((A)MSU)-Klimatologien in der Stratosphäre. Besondere Sorgfalt gilt den Abtastcharakteristika bei Radiosonden und RO. Die Ergebnisse zeigen gute Übereinstimmung zwischen Radiosonden und RO, während sich (A)MSU und RO Trends signifikant unterscheiden. Die Vorteile von RO mit homogen verteilten Beobachtungen, hoher vertikaler Auflösung und Genauigkeit werden bestätigt und zeigen das Potenzial, Probleme früherer Datensätze zu überwinden. Sie sind damit gut geeignet, als Referenz für andere Beobachtungsdaten zu dienen und damit die problematisch-großen strukturellen Unsicherheiten der herkömmlichen Datensätze einzuschränken.

Acknowledgments

> "What's the use of a house if you haven't got a tolerable planet to put it on?"
>
> *(Henry David Thoreau 1817–1862)*

While writing of a doctoral thesis is done by a single person only (a rule which unfortunately has not always been followed to its full extend by everyone), nevertheless many people were involved in the process of creating this dissertation.

First of all, I am thankful to my supervisors Univ.-Prof. Mag. Dr. Gottfried Kirchengast and Dr. Andrea Steiner. Gottfried's impressive attitude of always doing his best for the Wegener Center and its inhabitants—being it late at night or early in the morning—is certainly motivating, and his experience of great value. Andrea's unlimited support, encouragement and dedication for her work is equally impressing, and I am grateful that I have had the opportunity to participate in her project team.

The Wegener Center has provided for me the frame to get in touch with one of today's most exciting and urgent research topics, and I am happy to have had this opportunity. It is also home to many interesting people—I am grateful for the inspiring and great working atmosphere.

I also want to thank the co-authors of the research publications which are part of this thesis. The cooperation with visualization researchers from the SimVis GmbH, Vienna and from the University of Bergen was rewarding; special thanks go to Johannes Kehrer (who is also the first author of one of the presented publications), Helmut Doleisch, Philipp Muigg, and Helwig Hauser for important discussions. Later work was done in collaboration with the University of Vienna, thanks to Leopold Haimberger and Christina Tavolato for providing radiosonde data and valuable input. Fruitful discussions and input from my co-authors of the Wegener Center, Bettina Lackner, Barbara Scherllin-Pirscher, Ulrich Foelsche, Andrea Steiner, and Gottfried Kirchengast are really appreciated.

I furthermore acknowledge UCAR (Boulder, USA) and GFZ (Potsdam, Germany) for providing RO data, the Wegener Center GPS RO team for the OPS system development, ECMWF (Reading, UK) for access to their global operational analysis, reanalysis and forecast data; and the modeling groups, the Program for Climate Model Diagnosis and Intercomparison (PCMDI) and the WRCP's Working Group on Coupled Modelling (WGCM) for their roles in making available the WRCP CMIP3 multi-model datasets. UAH, RSS, and NESDIS/STAR (all USA) are acknowledged for access to their (A)MSU

records. This work received financial support from the Austrian Science Fund (FWF) research grants INDICATE, TRENDEVAL and BENCHCLIM.

The Wegener Center is an exceptional place to work, also and especially thanks to its people. Special thanks go to my office colleagues Veronika Proschek and Thomas Kabas for being part of Wegener Center's best office. Many thanks for lots of contributions to my scientific and personal life go to Armin Leuprecht, Michael Pock, Barbara Scherllin-Pirscher, Michael Borsche, Thomas Schinko, Wim de Geeter, Bettina Schlager, Sabine Tschürtz, Johannes Fritzer and my colleague in the project team, Bettina Lackner; and many more should be mentioned here. Michael Pock deserves special attribution for providing the LaTeX framework together with invaluable tricks to ease the typesetting of this thesis.

I am more than thankful to Eva for all support received in many ways, and helping me out whenever words were missing—let all the bamboozlement begin!

Finally, I want to thank my parents for making it possible.

Contents

Abstract v

Zusammenfassung vii

Acknowledgments ix

List of Figures xv

List of Tables xix

Acronyms xxi

I Synopsis 1

Introduction 3

1 History of Climate Change 5
1.1 The Past—Natural Climate Change 5
1.2 The Present—Current Climate Change 8
1.3 A Global Experiment—Models and Observations 9
1.4 The Future—Human-Driven Climate Change 12

2 Upper-Air Climate Research 15
2.1 An Ongoing Controversy 15
2.2 Conventional Long-Term Upper-Air Datasets 16
2.2.1 Radiosondes 16
2.2.2 MSU/AMSU 18
2.2.3 Reanalyses 19
2.2.4 Climate Models 20
2.3 Temperature Trends in the Troposphere and Stratosphere 20
2.4 Towards Better Understanding of Atmospheric Change 25

3 Visual Exploration and Comparison of Upper-Air Climate Records 29
3.1 GPS Radio Occultation, a New Potential Reference Climate Record . . . 29
3.1.1 Measurement Principles . . . 29
3.1.2 Characteristics of RO . . . 31
3.1.3 Applications . . . 32
3.1.4 RO Missions . . . 32
3.2 An Innovative Approach: Visual Interactive Exploration . . . 33
3.2.1 Interactive Visual Exploration Methods . . . 33
3.2.2 Research Papers in this Thesis . . . 34
3.3 Utilizing RO as Reference for Conventional Observations . . . 39
3.3.1 GPS RO Reference Data . . . 39
3.3.2 Research Paper in this Thesis . . . 40

4 Conclusions 47

II Published papers 49

Publications Overview 51

A SimVis: An Interactive Visual Field Exploration Tool Applied to Climate Research 53
1 Introduction . . . 54
2 Data . . . 55
3 Method . . . 55
3.1 SimVis–The Simulation Visualization Tool . . . 55
3.2 SimVis Application to Climate Data . . . 57
4 Results . . . 59
5 Conclusions and Outlook . . . 63

B Hypothesis Generation in Climate Research with Interactive Visual Data Exploration 65
1 Introduction . . . 66
2 Climatological Background . . . 67
3 Interactive Visual Data Exploration . . . 70
4 Exploring The Two Climate Datasets . . . 72
4.1 Hypothesis Generation . . . 73
4.2 Parameter Optimization . . . 79
4.3 Analyzing Relations Between Selections . . . 80
4.4 Further Results . . . 82
4.5 Performance Issues . . . 83

5 Conclusion and Future Work 84

C Exploration of Climate Data Using Interactive Visualization 87
1 Introduction 88
2 Interactive Visual Exploration Methods 89
3 Datasets 91
3.1 Reanalysis and Model Trend Data 91
3.2 GPS Radio Occultation Data 93
4 Application to Climate Data 93
4.1 Exploring Reanalysis Data 94
4.2 Exploring Climate Model Data 96
4.3 Exploring GPS Radio Occultation Data 100
5 Conclusions 103

D An assessment of differences in lower stratospheric temperature records from (A)MSU, radiosondes, and GPS radio occultation 105
1 Introduction 106
2 Data 107
2.1 GPS Radio Occultation 108
2.2 (Advanced) Microwave Sounding Unit 109
2.3 Radiosondes 110
2.4 ECMWF 110
3 Method 111
3.1 Setup of comparable data 111
3.2 Sampling error estimation 112
3.3 Computation of TLS anomalies and anomaly differences 114
4 Results 114
4.1 Sampling error 114
4.2 TLS anomalies and anomaly differences 117
5 Summary and conclusions 124

Bibliography 127

List of Figures

I Synopsis

1.1 Ice core proxy data . . . 6
1.2 Carbon Dioxide concentrations ("Keeling curve") . . . 7
1.3 Surface temperature change from the "Copenhagen Diagnosis" . . . 10
1.4 Sea level change from the "Copenhagen Diagnosis" . . . 11
1.5 Comparison of annual global mean surface temperatures from observations and models . . . 12
1.6 Global temperature of the last 1500 yrs and projected global warming from the "Copenhagen Diagnosis" . . . 13

2.1 Radiosonde station coverage for HadAT2 and RATPAC . . . 17
2.2 (A)MSU weighting functions . . . 19
2.3 List of GCMs available at the PCMDI . . . 21
2.4 Vertical temperature profile . . . 22
2.5 Observed upper-air temperature records . . . 25
2.6 Temperature trend maps for MSU/AMSU . . . 26

3.1 Occultation geometry . . . 30
3.2 Example for brushing of regions within a visualization view . . . 36
3.3 Robust stratospheric temperature trends in ECHAM5 . . . 37
3.4 Exploring the CHAMP temperature profile . . . 38
3.5 Parallel coordinates view: Relations between different RO processing systems 39
3.6 Global coverage of RO . . . 41
3.7 Sampling error of radiosondes and RO . . . 42
3.8 Effect of subtracting the sampling error for radiosondes and RO in the Northern Hemisphere . . . 42
3.9 TLS anomaly difference time series for all datasets (2001 to 2010) . . . 43

II Published papers

A SimVis: An Interactive Visual Field Exploration Tool Applied to Climate Research

1 SimVis 3D view . . . 57
2 Exploration of ECHAM5 temperature and refractivity data, selection of high values of SNR . . . 59
3 Exploration of ECHAM5 temperature and refractivity data, selection of specific features . . . 60
4 Exploration of ERA-40 geopotential height data . . . 61
5 Exploration of ERA-40 temperature data . . . 62

B Hypothesis Generation in Climate Research with Interactive Visual Data Exploration

1 Illustration of the vertical thermal structure of the atmosphere . . . 68
2 Process of interactive visual exploration of climate data . . . 73
3 Hypothesis generation using interactive visual exploration . . . 74
4 Hypothesis generation on derived trend in geopotential height fields . . . 77
5 ECHAM5: Explore sensitive regions with respect to climate change . . . 79
6 ECHAM5 temperature: derived parameters computed over 10 years instead of 25 years . . . 81
7 Similarity-based brushing . . . 82
8 Cooling trend brushed . . . 83

C Exploration of Climate Data Using Interactive Visualization

1 Exemplary visual exploration session with SIMVIS . . . 94
2 Inspecting outliers of the geopotential height trend field of ERA-40 . . . 96
3 Interactively removing the southern high latitudes and restricting the analysis to the post-1979 time . . . 96
4 Exploration of the geopotential height field of an ECHAM5 run . . . 97
5 Exploration of the temperature field of the ECHAM5 run . . . 98
6 IPCC regions and ECHAM5 trend significances . . . 99
7 Inspecting the Canada-Greenland-Iceland (CGI) region . . . 100
8 Inspecting a feature in the southern hemisphere subtropics . . . 100
9 Zonal mean monthly-mean temperature profiles from RO . . . 101
10 Relative refractivity differences in the parallel coordinates view . . . 102

D An assessment of differences in lower stratospheric temperature records from (A)MSU, radiosondes, and GPS radio occultation

1 Time frames of datasets used . . . 108
2 Global monthly coverage of RO profiles . . . 109
3 Global coverage of radiosonde launches . . . 111
4 Brightness temperatures (TLS) for two monthly means at 2.5° × 2.5° resolution . . . 113
5 Sampling error of radiosondes and RO . . . 114
6 TLS anomalies before/after subtracting the sampling error . . . 118
7 Evolution of TLS anomalies for radiosondes, RO, and (A)MSU . . . 119
8 TLS anomaly time series for all datasets . . . 120
9 Evolution of TLS anomaly differences of radiosonde and (A)MSU datasets to RO . . . 121
10 TLS anomaly difference time series for all datasets . . . 122
11 Trend values of anomaly differences . . . 123

List of Tables

I Synopsis

2.1 Trends of temperature anomalies 1979 to 2010, Lower Stratosphere 24
2.2 Trends of temperature anomalies 1979 to 2010, Middle Troposphere . . . 24

3.1 Trends of anomaly differences (2001 to 2010, Lower Stratosphere) 44

II Published papers

1 Trends of anomalies 2001 to 2010, Lower Stratosphere 115
2 Trends of anomaly differences 2001 to 2010, Lower Stratosphere 116

Acronyms

Symbols

(A)MSU (Advanced) Microwave Sounding Unit. vii, ix, 18, 43, 47, 105–108, 110, 112, 113, 117, 123–125

CH_4 Methane. 8

CO_2 Carbon Dioxide. 5–8, 12, 21

H_2O Water Vapor. 21

O_3 Ozone. 21

20C3M Climate of the 20^{th} Century Experiment. 20

4D-Var Four-Dimensional Variational Analysis. 19

A

AMSU Advanced Microwave Sounding Unit. xxvii, 15, 17, 18, 22, 23, 39, 40, 43, 108, 109, 112

AR4 IPCC Fourth Assessment Report [Climate Change 2007]. 8, 9, 11–13, 20, 54

C

CFD Computational Fluid Dynamics. 34, 55

CHAMP Challenging Mini-Satellite Payload. 32, 38, 92, 101, 103, 105, 107, 108, 124

COSMIC Constellation Observing System for Meteorology, Ionosphere, and Climate. 32, 107, 108

D

DOI Degree of Interest. 55, 56, 70–72, 74–76, 78, 79, 90, 94, 95

E

ECHAM ECMWF–MPI-M Hamburg [general circulation model]. xxiii

ECHAM5 Fifth-Generation ECMWF–MPI-M Hamburg [general circulation model]. 35–37, 53–56, 58, 61, 63, 65, 69, 72–76, 78–83, 91, 92, 96–98, 103

ECMWF European Centre for Medium-Range Weather Forecasts. xxiv, 16, 19, 35, 40, 41, 54, 103, 110–113, 125

ECV Essential Climate Variable [As defined by GCOS]. 27

EDA Exploratory Data Analysis. 34, 88

ENSO El Niño-Southern Oscillation. 23, 32

EPICA European Project for Ice Coring in Antarctica. 5

ERA ECMWF Reanalysis. xxiv, 17, 19, 40, 110

ERA-40 40-yr ECMWF Reanalysis. 16, 17, 35, 36, 53–55, 58, 61–63, 65, 69, 73, 76, 78–80, 83, 91, 92, 94, 95, 103

F

F3C FORMOSAT-3/COSMIC. 32, 105, 107, 108, 114, 124

FCDR Fundamental Climate Data Record [As defined by GCOS]. 25

FORMOSAT-3 Formosa Satellite Mission-3. 32, 107

G

GCM General Circulation Model. 9, 20, 33, 54, 88, 91

GCOS Global Observing System for Climate. xxiv, 25, 27, 29, 30

GNSS Global Navigation Satellite System. xxiv

GPS Global Positioning System. xxiv, 3, 4, 19, 27, 29–31, 33, 37, 39–42, 47, 51, 52, 92, 101, 103, 107, 108, 125

GPS/MET Global Positioning System/Meteorology [experiment]. 32

GRACE Gravity Recovery and Climate Experiment. 32, 105, 107, 108, 124

GRAS Global Navigation Satellite Systems Receiver for Atmospheric Sounding. 32

GRUAN GCOS Reference Upper-Air Network. 25, 27

H

HadAT Hadley Centre Atmospheric Temperature [A homogenized radiosonde data set provided by UK Met Office]. 17

I

IGRA Integrated Global Radiosonde Archive. 16, 17

IPCC Intergovernmental Panel on Climate Change. xxiii, xxvii, 8, 9, 15, 20, 22, 54, 63, 69, 91, 98

J

JRA25 Japanese 25-year Reanalysis. 19

L

LEO Low Earth Orbit. 29, 32

LS Lower Stratosphere [Region]. xxvii, 18, 22, 23, 40, 42

M

Metop Meteorological Operational [satellite series]. 32

MPI Max Planck Institute. xxv

MPI-M Max Planck Institute for Meteorology. 54

MSU Microwave Sounding Unit. xxiii, xxvi, xxvii, 15, 17–19, 22, 23, 39, 40, 42, 43, 108–112, 117, 124

MT Middle Troposphere [Region]. xxvii, 18, 23

N

NASA National Aeronautics and Space Administration. xxvii

NCAR National Center for Atmospheric Research. 19

NCEP National Centers for Environmental Prediction. 19

NESDIS National Environmental Satellite, Data and Information Service [Part of NOAA]. xxvi, 19, 109, 125

NH Northern Hemisphere. 16, 23, 41–43, 105, 112–114, 117, 123, 124

NOAA National Oceanic and Atmospheric Administration [USA]. xxv–xxvii, 5, 106, 108

O

OPS Occultation Processing System. 108, 110, 125

P

PCMDI Program for Climate Model Diagnosis and Intercomparison [http://www-pcmdi.llnl.gov/]. 20, 63, 103

PICTRL Pre-Industrial Control Experiment. 20

ppm parts per million. 6, 7

R

RAOBCORE Radiosonde Observation Correction using Reanalyses [A homogenized radiosonde data set provided by the University of Vienna]. 17, 23, 41, 43, 110, 114, 117, 123, 124

RATPAC Radiosonde Atmospheric Temperature Products for Assessing Climate [A homogenized radiosonde data set provided by NOAA]. 17

RICH Radiosonde Innovation Composite Homogenization [A homogenized radiosonde data set provided by the University of Vienna]. 17, 23, 43, 110, 114, 117, 123, 124

RMS Root Mean Square. 31

RO Radio Occultation. vii, ix, 3, 4, 19, 27, 29–33, 37–43, 47, 51–54, 63, 92, 93, 100–103, 105, 107, 108, 110–114, 117, 123–125

RSS Remote Sensing Systems [Research company, provider of a version of MSU datasets, California, USA]. 19, 23, 43, 109, 114, 117, 124, 125

RTTOV Radiative Transfer for TOVS. 110–112, 124

S

SAC-C Satélite de Aplicaciones Científicas/Scientific Applications Satellite C. 32, 105, 107, 108, 124

SH Southern Hemisphere. 23, 40, 113, 114, 117, 123, 124

SI Système International d'Unités [International System of Units]. 27, 29, 31

SIMVIS Simulation Visualization [Software Tool]. 34, 35, 51–57, 63, 70–72, 74, 78–80, 83, 88, 90, 92–94, 103

SNR Signal-to-Noise Ratio. 35, 36, 58–63, 72–83, 90, 92, 94, 95, 97–99

SRES Special Report on Emission Scenarios. 20, 54

SSU Stratospheric Sounding Unit. 22

STAR Satellite Applications and Research [Part of NESDIS, provider of a version of MSU datasets]. 19, 23, 43, 109, 112, 114, 117, 123–125

T

TAR IPCC Third Assessment Report [Climate Change 2001]. 9, 11

TIROS Television Infrared Observation Satellite [Launched by NASA]. 18

TLS Temperature Lower Stratosphere [Denotes MSU channel 4 and AMSU channel 9]. 23, 42, 43, 109–114, 117, 123–125

TMT Temperature Middle Troposphere [Denotes MSU channel 2 and AMSU channel 5]. 23

TOVS Tiros Operational Vertical Sounder [Suite of vertical sounding instruments, flying on NOAA polar orbiting satellites]. xxvi, 18

U

UAH University of Alabama at Huntsville [Provider of a version of MSU datasets, Huntsville, USA]. 19, 23, 43, 109, 114, 117, 124, 125

UCAR University Corporation for Atmospheric Research. 103, 108, 125

UG University of Graz. xxvii

UN United Nations. xxvii, 8

UNFCCC United Nations Framework Convention on Climate Change. 8, 9

UT Upper Troposphere [Region]. 18

UTC Coordinated Universal Time. 16, 41, 110, 113, 117

UTLS Upper Troposphere–Lower Stratosphere [Region]. 3, 29, 31–33, 53, 54, 63, 93, 97, 106, 107

W

WEGC Wegener Center for Climate and Global Change [University of Graz]. 108, 125

Part I

Synopsis

Introduction

The rate at which climate changes today is unprecedented in Earth's recent paleoclimatic history. The ecosystems will very likely see drastic changes in the next decades, threatening life in many regions of the Earth, and posing new pressure on global equity and human rights. Although there is today little doubt concerning the long-term warming of the atmosphere in response to human actions, global greenhouse gas emissions are still rising.

Scientists have the obligation to provide the best possible information about changes—both now and in the future—of the climate system. A detailed knowledge is crucial as basis for subsequent political decisions—time is pushing, since recent research indicates that even limiting the global warming to 2 °C is increasingly unlikely to achieve.

The tools used by climate scientists are observations and climate models. Both are needed to gain knowledge of all aspects of the components of the climate system and to provide estimates about possible future changes. While for some parts of the climate system, such as the Earth's surface, knowledge is considered to be advanced, the situation has been more challenging for other parts. In particular, the last two decades have seen a debate about upper-air climate change, and some have even used this controversy to dispute anthropogenic climate change at all.

This thesis deals with the eminent importance of upper-air climate records, focusing on two aspects of today's research: Firstly, the amount of time-dependent, multivariate atmospheric data produced by diverse models and observational systems becomes increasingly large. This significantly complicates analyzing the data with classical statistical methods. In this thesis I introduce sophisticated data exploration methods to facilitate efficient and quick analyses of huge upper-air datasets. Based on these methods it becomes easier to determine potentially unknown patterns and characteristics in these datasets. Going beyond the scope of classical statistics, I show that these exploration methods complement the common data analysis techniques used in geosciences.

Secondly, the lack of observational upper-air records of climate quality makes it difficult to gain knowledge of upper-air trend characteristics. In this thesis I make use of Global Positioning System (GPS) Radio Occultation (RO), a new satellite measurement system with highest precision in the Upper Troposphere–Lower Stratosphere (UTLS), to compare the available upper-air datasets with this potential reference system. This comparative study shows differences between the datasets due to structural uncertainties and helps to quantify the deviations. I focus on the lower stratosphere region and show the importance of taking into account the specific global sampling distribution characteristics of the

observations. This study confirms the advantage of good vertical resolution, high data quality, and the value of additional, independent observations provided by GPS RO.

The thesis is structured into:

Part I (Chapter 1–Chapter 4)

Chapter 1 A short history of the changing climate on Earth is summarized to set the scene, starting with past climate changes, continuing with recent and current developments of climate change, and finishing with an outlook to probable future scenarios.

Chapter 2 The current status of upper-air climate research is outlined. The history of the ongoing controversy regarding upper-air temperature trends is presented, together with a short description of the characteristics of existing long-term upper-air datasets. An update of the current knowledge of upper-air temperature trends is given. Possible ways to achieve better knowledge of upper-air climate are illustrated and set the background for the following chapters.

Chapter 3 The contributions of this thesis to upper-air climate research are explained. The new potential reference climate record GPS RO is presented. Exploratory techniques are summarized and used for analyzing upper-air climate data. GPS RO is then specifically presented as reference for other, conventional upper-air datasets.

Chapter 4 Briefly summarizes the main contributions of this thesis for upper-air climate research.

Part II (Paper A–Paper D) In Part II, the four research publications including the main scientific work of this thesis are presented.

1 History of Climate Change

THE evidence of human-induced climate change is today undisputed. It still remains surprising that humans are able to substantially influence Earth's large climate system at all. Today's scientific consensus is based on research over more than a century. Studies of the last decades emphasize the severity of people's footprints on the planet.

1.1 The Past—Natural Climate Change

It is well known that in Earth's history climate has always changed (Figure 1.1). To better understand the current situation it is educating to study patterns of past climate changes. The climate reacts sensitively to changes in the radiation balance. These changes inevitably lead to altered global mean temperatures, determined by the *climate sensitivity* of the climate system. Climate sensitivity is commonly defined as the global warming that is occurring after doubling equivalent Carbon Dioxide (CO_2) concentration[1] in the atmosphere and waiting for the climate system to reach equilibrium again (Solomon et al. 2007a).

The main driving forces for the changes in radiation balance are variations in the orbital parameters of the Earth, known as *Milankovitch cycles*. This is true for short-term (in geological sense, $<10^6$ yrs) climate variability, whereas in the long term other effects play an important role (continental drifts and varying energy output of the sun being major components). The effects of the Milankovitch cycles on the climate system are strongly influenced by various feedback mechanisms, amongst others the carbon cycle or the ice-albedo feedback. Global temperature changes also have an effect on the CO_2 concentrations through the carbon cycle. This is a positive feedback, increasing global temperatures increases the CO_2 concentration, which in turn increases the temperature further.

The current situation of the climate system starts at another point in the feedback loop: The increase of CO_2 concentration induced by human activities increases the global mean temperature due to the greenhouse effect and abrupt release of massive amounts of carbon from fossil sources—bound to the ecosystem some 100 Myrs ago—imposes a significant impact on the climate system today.

[1] The equivalent CO_2 concentration is the concentration of CO_2 that would cause the same amount of radiative forcing as a given mixture of greenhouse gases

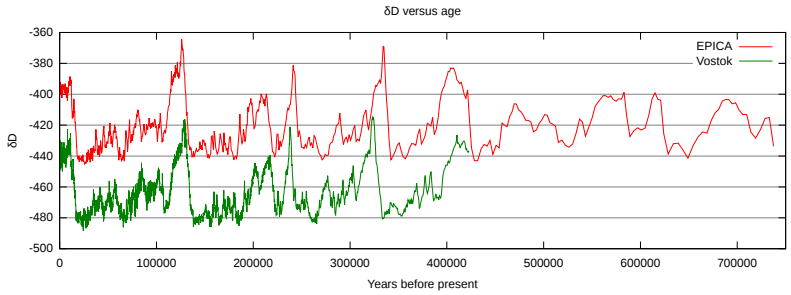

Figure 1.1: Data from EPICA and Vostok showing δ-deuterium, a proxy for temperature, against age. The offset between the EPICA and Vostok cores in δ-deuterium is because Vostok is a colder site, hence has more negative delta. Differences in the apparent age of events are likely to be inaccuracies in converting ice depth to age. The EPICA ice core data span 8 previous glacial cycles (EPICA community members 2004). Retrieved from Wikipedia (http://en.wikipedia.org/wiki/European_Project_for_Ice_Coring_in_Antarctica) on May 17, 2011, with original data from NOAA.

Rapid releases of CO_2 have happened before in Earth's history. In the "Paleocene-Eocene Thermal Maximum", around 55 Myrs ago, such an event brought abrupt warming by several degrees, ocean acidification and a mass extinction. The last stable climate state with CO_2 concentrations comparable to today's level was the Pliocene (about 3 Myrs to 5 Myrs ago). Temperatures at that time are estimated between 2 °C to 3 °C above pre-industrial levels and sea level was at least 15 m to 25 m higher than today (Solomon et al. 2007a). These severe consequences should clearly be a warning for today's society. Paleoclimatology gives some hints on what the political agenda should be today.

Although one could argue that no further knowledge is required, a more detailed picture of possible scenarios for the future is desirable. In a more detailed picture, the climate system becomes increasingly complicated.

The eminent importance of the topic has lead to great efforts by the scientific community to tackle the issue. The effect that some gases, including CO_2, trap heat close to the Earth's surface had been discovered long before concerns about possible impacts of human behavior on the climate system arose. The greenhouse effect was already described in 1824 by Jean Baptiste Joseph Fourier (Fourier 1824), a mathematical physicist nowadays better known for developing the *Fourier Analysis*. Swedish physicist and chemist Svante Arrhenius was the first to estimate climate sensitivity, arriving at a value of 4 °C to 5 °C (Arrhenius 1896). He later suggested that the combustion of coal suffices to prevent Earth from entering a new ice age. He was also exited about the perspective of starting new ages with a "better" and warmer climate.

The CO_2 concentration in that time had not yet risen above what is now called the "pre-industrial" level of 280 parts per million (ppm). Since then, CO_2 concentrations have been continuously rising and the increase of fossil CO_2 emissions accelerated to 3 % to 4 %

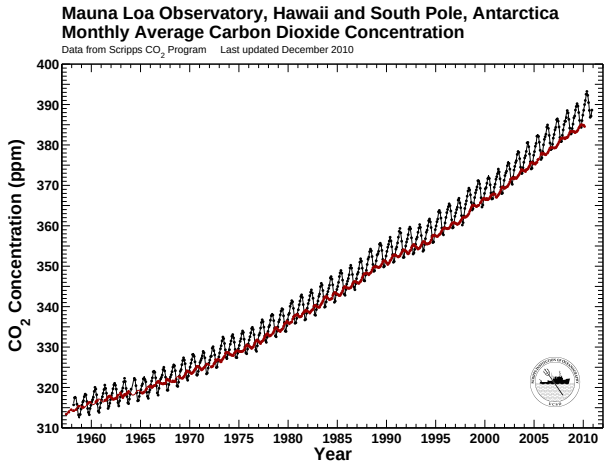

Figure 1.2: "Keeling Curve"; Black Curve: Monthly average atmospheric CO_2 concentration at Mauna Loa Observatory, Hawaii; Red Curve: Monthly average atmospheric CO_2 concentration at the South Pole, Antarctica. The data from Antarctica shows much less inter-annual variability because there exists less "breathing" biosphere in the Southern Hemisphere. Retrieved from the Scripps CO_2 program web-page (http://scrippsco2.ucsd.edu/) on May 4, 2011.

per year in the last decade (Solomon et al. 2007a; Allison et al. 2009).

The curve showing the increase of atmospheric CO_2 concentration counts amongst the most famous ones in science (Figure 1.2). It was initiated by Charles David Keeling who started the first measurements of the CO_2 levels in 1958 at Mauna Loa, Hawaii. The "Keeling Curve" was the first to show observational evidence of increasing CO_2 concentration, and it is still regularly updated (Figure 1.2). It shows a current value of 385 ppm, 105 ppm above its pre-industrial level. As we know from ice core data, this level is higher than any time in the last 800 000 yrs, and possibly even the last 3 Myrs to 20 Myrs (Allison et al. 2009). This is exceptional also because ice core data show that its level stayed close to the pre-industrial level of 280 ppm for 10 000 yrs before.

With the "Keeling curve" available, the increase of CO_2 was already evidenced in those measurements in the 1960's. An official report from the U.S. White House (President's Science Advisory Committee 1965) warned of possible "deleterious climatic changes" caused by increased CO_2 content and detailed possible effects such as melting of the Antarctic ice cap or increased acidity of fresh waters.

This was only one of the early official reports documenting and warning of possible effects of human behavior.[2] Many more were yet to come. Broecker (1975) introduced the term "global warming" in the title of his publication "Climatic Change: Are We on the Brink of a Pronounced Global Warming?" stating that "the atmospheric carbon

[2] Ironically published by the nation with the largest contribution to global warming in the decades to come after the report.

dioxide content will tend to become a significant factor and by early in the next century will have driven the mean planetary temperature beyond the limits experienced during the last 1000 years." The global warming Broecker talked about was first measurable in the 1980's.

1.2 The Present—Current Climate Change

As a result of scientific evidence for global warming, the Intergovernmental Panel on Climate Change (IPCC) was created in 1988. Its initial task as outlined in the corresponding United Nations (UN) General Assembly Resolution was to assemble the state of the art knowledge about climate change.[3] This marked the begin of a series of IPCC assessment reports, the first released in 1990 and the latest (IPCC Fourth Assessment Report (AR4)) in 2007. The first of these was the basis for an international treaty signed in 1992, the United Nations Framework Convention on Climate Change (UNFCCC) with the goal of reducing global warming.[4] Currently there are 195 parties to the UNFCCC, but despite all efforts very little has been achieved by now.

Carbon Dioxide is not the only greenhouse gas of concern. Methane (CH_4) is of particular importance, too. This potent greenhouse gas is emitted by agriculture and by natural reservoirs (e.g. permafrost). Paleoclimatology indicates that large releases of CH_4 caused major climatological changes in Earth's history (e.g., Norris and Rohl 1999). There are several carbon sources in the climate system which most probably contributed to a large extend to those changes. The northern hemisphere permafrost stores around 1672 GtC—twice the amount of carbon contained in the atmosphere (Allison et al. 2009), and it continues to melt. Another significant source of CH_4 is stored as hydrates in the deep ocean. The total amount stored is still unknown, but estimated to be 500 GtC to 64 000 GtC (Hester and Brewer 2009). Destabilization of these hydrates and release of CH_4 into the atmosphere would have catastrophic impacts on the climate. Recent simulations indicate that the hydrates are indeed able to destabilize in the next decades and that this will have an effect on ocean acidification, but that the impact on global warming would be small in the next 100 yrs (Biastoch et al. 2011). Since the release of these captured amounts of carbon is a positive feedback in the climate system, it is easy to judge the proposed impact on future generations on Earth.

The release of captured carbon is one process amplified by global warming (and, in turn, then amplifying global warming itself). There also exist carbon reservoirs in the climate system constantly absorbing carbon. These carbon sinks (terrestrial biosphere and the oceans) together have absorbed half of the total emissions of CO_2. This is part of the natural carbon cycle. At present, the oceans are the largest CO_2 sink, but this might change in the future. When oceans turn into carbon sources, global warming will

[3] http://ipcc.ch
[4] http://unfccc.int

be amplified further. New studies show that the efficiency of natural carbon uptake has already decreased (Allison et al. 2009).

The result of failing to achieve UNFCCC's goals can be seen in observational records. Each of the last 10 yrs (2001–2010) has been among the 11 warmest since instrumental records began. Allison et al. (2009) state surface trend values for the 25-year trend as (0.187 ± 0.052) K per decade for the period ending 2008 (Figure 1.3). Sea levels have risen faster than projected in the IPCC Third Assessment Report (TAR) and AR4 (Figure 1.4), threatening the densely populated coastal regions. Ocean acidification and de-oxygenation continue and are potentially lethal to large parts of the marine ecosystem in the near future.

1.3 A Global Experiment—Models and Observations

The scientific foundation of the IPCC assessment reports rely on both observations and numerical simulations. Climate models are the only tool to simulate the response of the climate system to forcings. These simulations take the role of physical "experiments". As such, they try to incorporate as many of the internal dynamics of the climate system as possible. The experiment is then performed by adjusting the various external forcing parameters. The main natural external forcings are changes in solar output and the impact of volcanic eruptions. The main anthropogenic forces perturbing the radiative balance of the Earth are changes in the concentration of greenhouse gases, aerosols including indirect effects such as cloudiness, and land-use changes affecting the albedo (Karl et al. 2006; Solomon et al. 2007a).

Owing to the complexity of the climate system, the only way to verify (or falsify) the outcome of the simulations is the ongoing real-time experiment, i.e. the observational records. The confidence in climate models for simulating global climate at large scales is considerable today, because they are able to simulate important features of all parts of the climate system (atmosphere, cryosphere, ocean and surface). This has been shown in short-term comparisons (i.e. weather forecasts) and can also be verified in aspects of seasonal variability. They are also successful in reproducing past climate conditions. Although a great number of different climate models exists today (developed independently to a large extend, although founded on the same basic physical principles), the models succeed in predicting atmospheric temperature trends consistently. In short, the models predict a warming of the surface and troposphere when concentration of greenhouse gases rises, and they specifically predict an "amplification" of this trend in the tropical troposphere (Solomon et al. 2007a). The "amplification" feature is not an outcome of modern sophisticated General Circulation Models (GCMs), but was already simulated in the 1975 paper by Manabe and Wetherald (1975).

Nevertheless, there are still known (and potentially unknown) deficiencies in the models, some of them of considerable importance. These deficiencies include feedback mechanisms

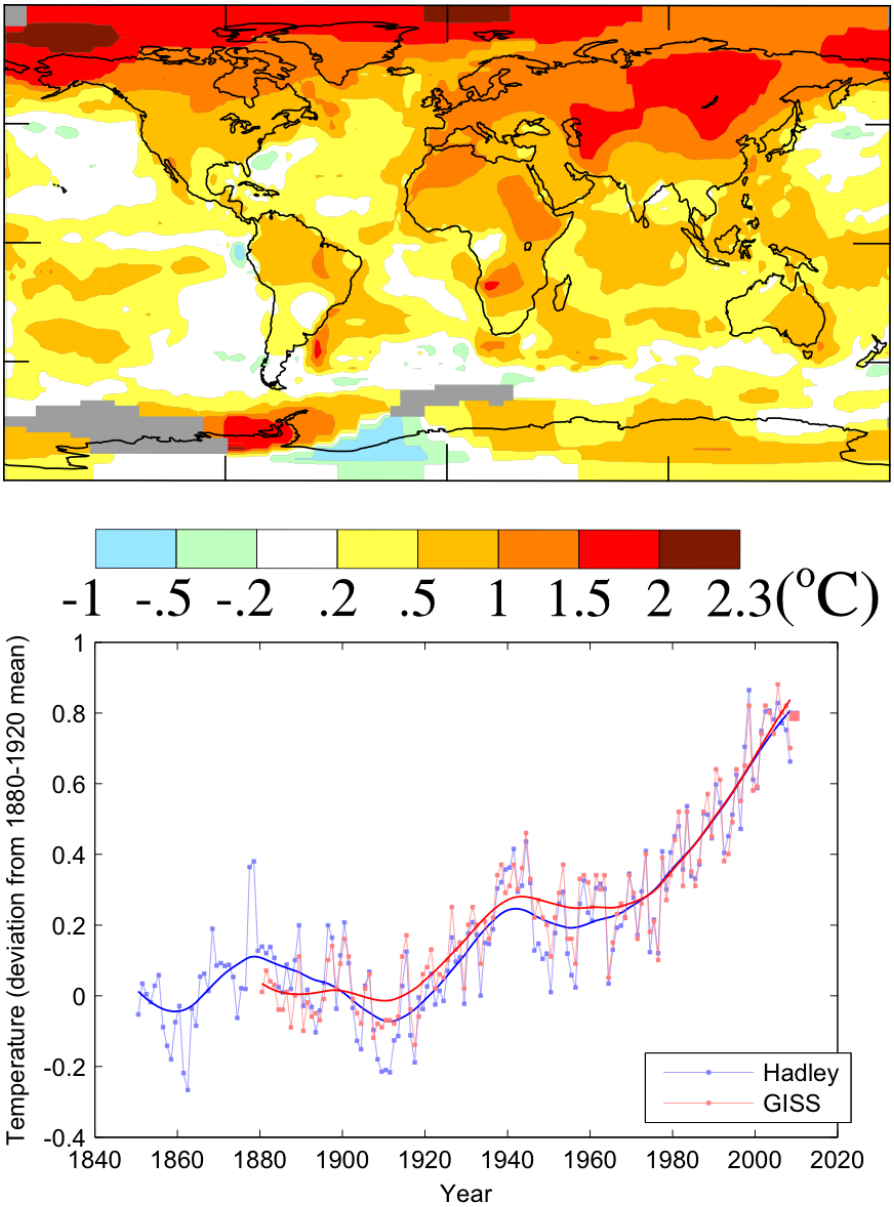

Figure 1.3: Surface temperature change from the "Copenhagen Diagnosis". (top) Mean temperature change for 2001–2007 relative to 1951–1980 (NASA/GISS); (bottom) Global average temperature 1850–2009 relative to 1880–1920 (NASA/GISS and Hadley).

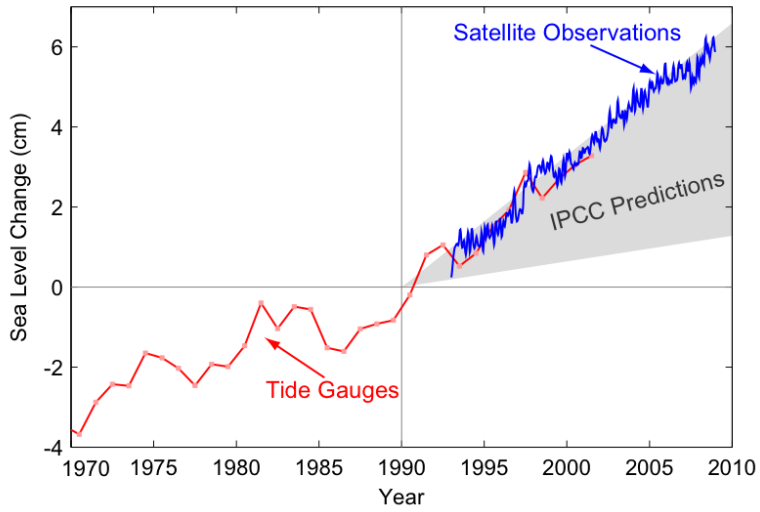

Figure 1.4: Sea level change from the "Copenhagen Diagnosis". Red curve: Tide gauge data, Blue curve: satellite data. Gray area: Projections of the IPCC Third Assessment Report (TAR).

such as water vapor feedback or indirect aerosol effects such as representation of clouds, precipitation events or other small-scale variations (Solomon et al. 2007a). Even though most of them only touch small-scale effects, they might act on larger-scale variations as well. Only detailed verification of the model output leads to improvements of the simulations and ultimately to better understanding and predictability of the climate system's behavior.

Unfortunately, observational records of sufficient quality are only partially available. This is one reason why studies often concentrate on one part of the climate system, the Earth's surface—the existing observational record of the surface goes back to approximately 1850 with sufficient stations available to allow a detailed assessment of the climate change on the surface.

Rahmstorf et al. (2007) compared surface observations to model projections, and an updated version of the global mean surface temperature changes since 1973 is shown in Figure 1.5. Temperature trends are well inside the TAR projections, and comparisons with AR4 projections show similar agreement.[5]

Assessing climate change is more difficult for other parts of the climate system, especially for the upper-air atmosphere. Few sources of observational data are available there. This is unfortunate, since that region includes many of the driving components of the net radiation balance, and it provides valuable information about the causes of observed

[5] See http://www.realclimate.org/index.php/archives/2011/01/2010-updates-to-model-data-comparisons/

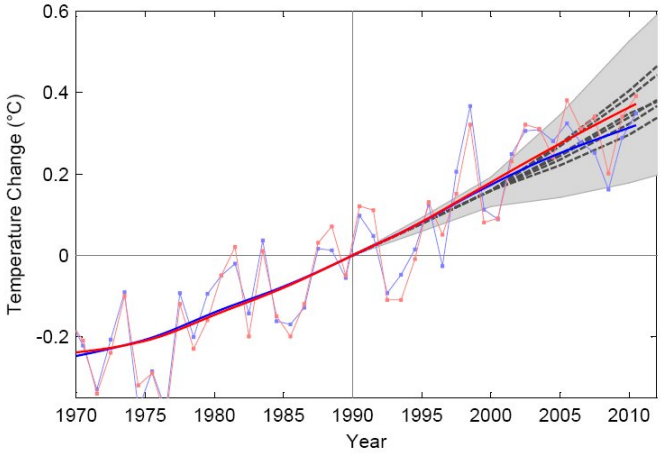

Figure 1.5: Comparison of annual global mean surface temperatures from observations and model projections. Red curve: NASA GISS; Blue curve: Hadley Centre/Climatic Research Unit. Dashed lines and gray range are temperature projections of the IPCC Third Assessment Report (TAR). Non-linear trend lines with an 15 yrs smoothing are also shown. Data are deviations from the trend line value in 1990. Retrieved from http://www.pik-potsdam.de/~stefan/update_science2007.html/ on May 4, 2011.

changes.

This crucial source of information derives from the effects of various types of forcings on temperature being dependent on the height range (Karl et al. 2006). For example, an increase in concentration of greenhouse gases such as CO_2 is expected to cause warming at the surface and in the troposphere and cooling in the stratosphere. An increased solar output on the other hand causes warming at the surface as well as in the troposphere and stratosphere. Other forcings also have their typical fingerprint in the vertical thermal structure of the atmosphere. Therefore, a precise knowledge of relative changes in the troposphere and stratosphere is an important source of information about the cause of changes. It can help to distinguish between natural and anthropogenic influences on the climate system.

1.4 The Future—Human-Driven Climate Change

Humans are changing the climate of Earth and have started the epoch of the *Anthropocene* (Zalasiewicz et al. 2010). The projected changes in this century are tremendous: Latest estimates of global mean temperatures for the year 2100 range from 2 °C to 7 °C above pre-industrial levels (Figure 1.6). The large range of projections is mainly due to the unknown evolution of future emissions. In a business-as-usual scenario for the next decades to come, global temperatures are estimated to reach 4 °C to 7 °C by 2100. Even

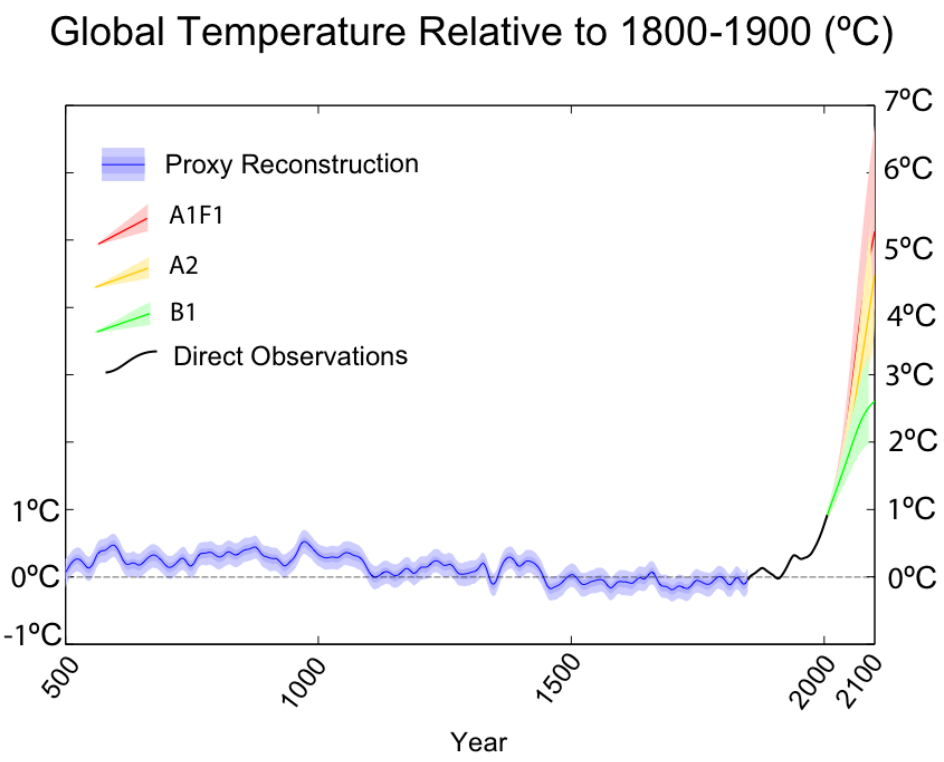

Figure 1.6: Reconstructed global surface temperatures and projected temperatures until 2100, an updated figure from the AR4 by the "Copenhagen Diagnosis". Temperatures are relative to 1800–1900, and the projections correspond to different emission scenarios from the AR4, cf. Subsection 2.2.4.

if mankind accomplishes to rapidly cut emissions by 2020, global mean warming is estimated to reach 2 °C to 3 °C by the end of the century (Allison et al. 2009). Only 2 °C warming already carries a large risk of having severe consequences for the climate system and human beings. Recent research indicates that sea-level rise is likely to be two to three times higher than projected by the AR4 and might reach 1 m to 2 m by 2100 (Vermeer and Rahmstorf 2009). Extreme events, such as temperature extremes, heavy precipitation or drought continue to increase and pose a serious threat to the inhabitants of many regions on Earth (Solomon et al. 2007a). The projections for this century therefore trigger serious concerns.

The rate of change is highly unusual, and the need for detailed knowledge about what to expect is urgent. Remaining uncertainties in the climate models and observational systems thus need to be addressed to prepare for the near future.

2 Upper-Air Climate Research

DETAILED knowledge of upper-air trends of climate variables is limited. Longer-term observations for the upper-air are available only from radiosondes (since 1958) and Microwave Sounding Unit (MSU)/Advanced Microwave Sounding Unit (AMSU) (since 1979). Both of these very different instrument types suffer from typical deficiencies and problems when it comes to the requirements of climate records. These requirements specifically include long-term stability and global coverage, amongst others. The calibration of time series containing data from changing instrumentation as it is the case for both radiosondes and MSU/AMSU is a challenging task. This is especially true for upper-air records where only two longer-term records are available, and where a reference record is missing. The need for additional datasets to reduce the structural uncertainties intrinsic to a low number of independent data sets (Thorne et al. 2005) is recognized by different institutions (Karl et al. 2006; GCOS 2010)

2.1 An Ongoing Controversy

These limitations have lead to a controversy regarding upper-air temperature trends in the last two decades. Since the publication of an analysis of MSU satellite data in 1990 (Spencer and Christy 1990), claiming that the warming of the troposphere shown by climate models might be wrong, there has been great effort by scientists to understand this supposed inconsistency (for a detailed review on the history of this controversy, see Thorne et al. 2011). Even the last report of the Intergovernmental Panel on Climate Change (IPCC) in 2007 (Solomon et al. 2007a) stated remaining uncertainties in temperature trends in the tropical troposphere, where the observational datasets of that time showed less warming than expected.

A possible implication of an actual discrepancy between climate models and reality as presented by observations might be that projections of future temperature changes are wrong. Douglass et al. (2008) claimed that tropical temperature trends were indeed inconsistent with model trends, and concluded that "If these results continue to be supported, then future projections of temperature change, as depicted in the present suite of climate models, are likely too high." These conclusions were used by so-called "climate skeptics" to assert that the "hypothesis" of anthropogenic greenhouse warming was falsified. Later these claims were refuted by Santer et al. (2008), identifying serious flaws in the methodology used in Douglass et al. (2008) and using newer radiosonde and satellite datasets.

As Santer et al. (2008); Thorne et al. (2011) state, there is no longer evidence of disagreement between models and observations regarding the vertical structure of temperature trends from surface to the troposphere. This statement relies on the usage of recent versions of all involved datasets. They conclude that the primary reason for the controversy was lacking knowledge of structural uncertainties involved in creating a climate record from only few datasets. They also formulate several key lessons learned from the history of this controversy. Among them is the importance of assessing the structural uncertainty inherent to the information, and that reference observations are required to allow calibration of data.

The increasing agreement between models and observations is certainly good news. Nevertheless, it does not mean that issues concerning the reliability of climate models and observational data are resolved. This improvement relies on better understanding of error ranges of measurements (structural uncertainties) and on improved homogenization methods for the available observational datasets. The observational uncertainties in these datasets are still substantial. These large uncertainties make it difficult to precisely determine upper-air trends from observations and using them to verify the output of climate models and to better understand climate change above the surface layer.

2.2 Conventional Long-Term Upper-Air Datasets

All existing conventional upper-air observing systems were originally intended to support weather forecasting, and were not developed for climate monitoring. Immediate consequences of this fact are that demanding intercalibration and homogenization procedures are required to use the data for climate applications such as trend studies.

2.2.1 Radiosondes

The longest existing observational record is from radiosondes, going back to the 1950s. Today exists a global network of about 1500 radiosonde stations collected in the Integrated Global Radiosonde Archive (IGRA)[1] and 40-yr ECMWF Reanalysis (ERA-40) radiosonde archive, mainly concentrated over Northern Hemisphere (NH) land masses, and substantially less coverage away from NH mid-latitudes. Radiosonde balloons are typically released once or twice a day (0 UTC and 12 UTC). The observations are in-situ measurements as the instruments are carried on a balloon through the atmosphere.

There are instruments of several different manufacturers used, each of them with specific characteristics, and some of them with minor quality and suitability for climate applications. Over the time period of operation, many changes in instrumentation and observation practices have occurred, many of them poorly documented. Creating a climate record out of raw data is therefore a demanding task, involving expert assumptions.

[1] http://www.ncdc.noaa.gov/oa/climate/igra/

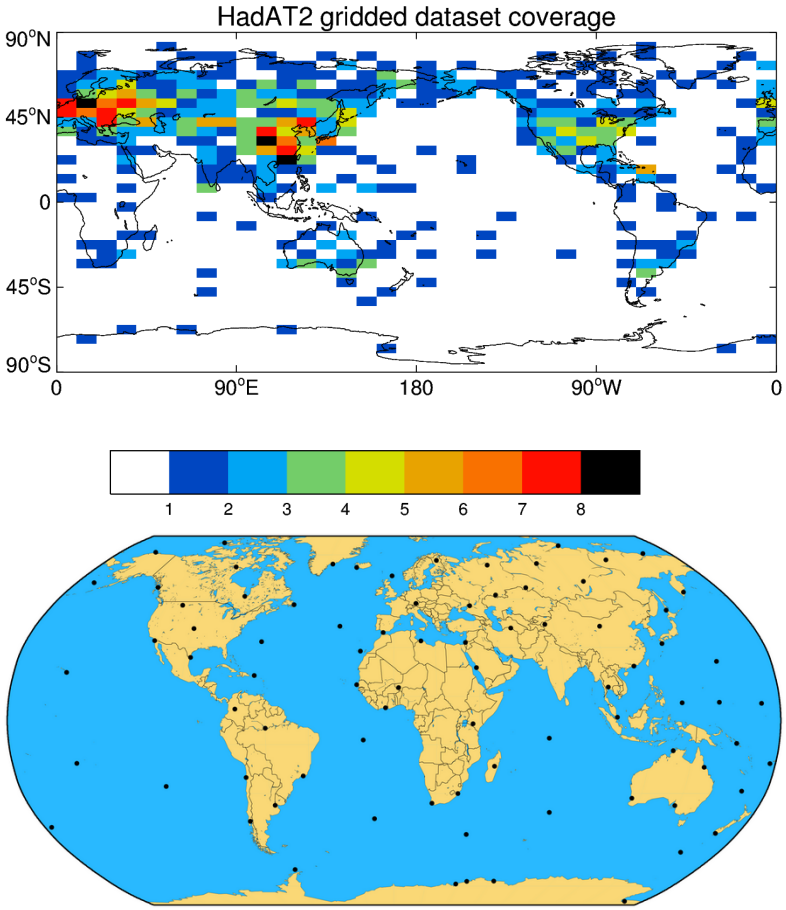

Figure 2.1: Maximum station coverage for each gridbox in HadAT2 (Top; Available at http://www.hadobs.org/) and the distribution of the 85 stations in RATPAC (Bottom; Available at http://www.ncdc.noaa.gov/oa/climate/ratpac/).

This results in structural uncertainties (Thorne et al. 2005), which are hard to estimate without a number of additional, independent measurements.

Several groups have created homogenized, adjusted radiosonde datasets, some of them using only a selected sub-set of stations of higher quality, others using a larger number of stations to collect as much data as possible. The Radiosonde Atmospheric Temperature Products for Assessing Climate (RATPAC) dataset is based on a limited network of only 85 stations (Free et al. 2005), whereas the Hadley Centre Atmospheric Temperature (HadAT) dataset uses a much larger number of stations (Thorne et al. 2005), cf. Figure 2.1. Sherwood et al. (2008) use a statistical model to identify artificial shifts and natural fluctuations in the global radiosonde data.

Two recent homogenized radiosonde datasets are provided by the University of Vienna:

Radiosonde Observation Correction using Reanalyses (RAOBCORE) (Haimberger 2007) and Radiosonde Innovation Composite Homogenization (RICH) (Haimberger et al. 2008), both using data from the IGRA and ERA-40 archive. RAOBCORE employs a novel homogenization approach: Differences of radiosonde time series to ERA-Interim reanalyses (Dee et al. 2009) are sensitive to changes in radiosonde biases and therefore used to detect breakpoints and to adjust the breakpoints in a next step. RAOBCORE itself, strictly speaking, is not independent of satellite data, because ERA-Interim data contain MSU/AMSU information. RICH on the other hand incorporates only neighboring stations for the actual homogenization, and uses the breakpoint information provided by RAOBCORE. This qualifies RICH as an entirely independent dataset (Haimberger et al. 2008).

2.2.2 MSU/AMSU

The Microwave Sounding Unit (MSU) type of instrument measures layer-average brightness temperatures[2] by measuring microwave emissions of oxygen molecules, proportional to temperature (Spencer and Christy 1990). Due to the nadir geometry of the observations, the vertical resolution is coarse, and the delivered temperatures are single values describing a rather thick bulk of the atmosphere. Tuning the frequency samples different layers of the atmosphere, as shown by weighting functions describing the vertical weight distribution (Figure 2.2). Horizontal resolution on the other hand is very good, and implies a major advantage over the uneven distribution of radiosonde stations. In contrast to in-situ measurement systems with many different instruments operating at the same time to form the time series, satellite data only come from one instrument at a given time. Any problem or bias of the instrument at a certain time can therefore easily introduce biases in the time series, and can be hard to discover.

Starting with continuous microwave measurements in late 1978, they are the only near-global upper-air observation system spanning multiple decades. The first MSU instrument was part of Tiros Operational Vertical Sounder (TOVS) flying on the Television Infrared Observation Satellite (TIROS) spacecraft. The MSU instrument was later (in 1998) upgraded to AMSU, incorporating more operational channels, among other improvements. In total, 13 different satellites have contributed to the time series. The last satellite carrying a MSU instrument on board was decommissioned in 2004.

The Middle Troposphere is sampled by channel 2 (MSU) and 5 (AMSU), the Lower Stratosphere by channel 4 and 9, respectively. The corresponding channels for MSU and AMSU are intentionally very similar, to ensure a continuing time series.

The coarse vertical resolution is a disadvantage for climate applications, since trend patterns change significantly around the tropopause, whose height is latitude- and time-dependent. The Middle Troposphere (MT) channels contain contributions of the Lower Stratosphere (LS), and the LS channel contributions of the Upper Troposphere (UT).

[2] The brightness temperature is the temperature a black body with the same intensity as observed from the real gray body would have.

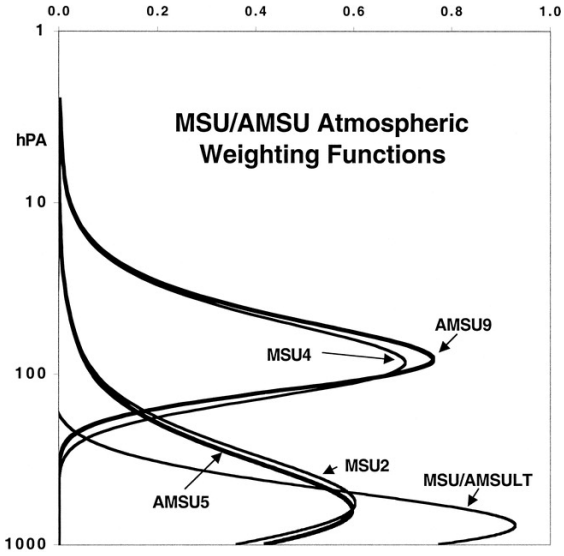

Figure 2.2: (A)MSU weighting functions, describing the contribution of vertical atmospheric layers to the specified (A)MSU channel. Christy et al. (2003), Figure 1.

Continuous long-term records are produced by several groups, adjusting the time varying biases. The most important among these biases are: diurnal drifting (changes in the equatorial crossing times), orbit decay, calibration shifts, and instrument changes (Christy et al. 2006).

Adjusted time series for MSU come from University of Alabama at Huntsville (UAH) (Christy et al. 2003), Remote Sensing Systems (RSS) (Mears and Wentz 2009b), and from National Environmental Satellite, Data and Information Service (NESDIS) Satellite Applications and Research (STAR) (Zou et al. 2009), all applying their own homogenization schemes.

2.2.3 Reanalyses

Reanalysis data are based on as much observational data as available. These data then are assimilated into global weather forecasting systems. For the whole time period of the produced reanalysis dataset, the assimilation model is fixed, thus avoiding data inhomogeneities due to changes in the processing. The resulting reanalysis records have continuous spatial and temporal sampling, posing a distinct advantage over observational systems. Several authors have reported erroneous trend findings from reanalysis datasets (e.g., Christy et al. 2006; Randel et al. 2009), concluding that trends derived from reanalyses are not always reliable, but latest or future reanalyses may be well suited for trend studies. The three main reanalysis datasets available are the National Centers for Environmental Prediction (NCEP)/National Center for Atmospheric Research (NCAR)

reanalysis (Kalnay et al. 1996; Kistler et al. 2001), the Japanese 25-year Reanalysis (JRA25) (Onogi et al. 2007), and the reanalysis products of the European Centre for Medium-Range Weather Forecasts (ECMWF), with the latest being ERA-Interim (Uppala et al. 2004; Dee et al. 2009). ERA-Interim covers the time period from 1989 until now, using a Four-Dimensional Variational Analysis (4D-Var) scheme in near-real time. It has already started to benefit from the inclusion of Global Positioning System (GPS) Radio Occultation (RO) data (Section 3.1), whose fine vertical resolution results in a reduction of errors in the mean vertical temperature structures (Simmons et al. 2006; Uppala et al. 2008).

2.2.4 Climate Models

There exists a wide range of numerical models with varying degree of complexity. General Circulation Models (GCMs) are the most complete, three-dimensional representations of the real climate system. They usually comprise not only the atmosphere, but also other parts of the climate system (cryosphere, oceans, land surface) and their interactions and feedback mechanisms. The Program for Climate Model Diagnosis and Intercomparison (PCMDI) collects many of the available GCM datasets to analyze and to support modeling studies initiated by the IPCC. The large number of models is depicted in the summary of data available at PCMDI in Figure 2.3.

For the IPCC Fourth Assessment Report (AR4) a range of experiments based on various forcings was implemented. Apart from experiments with pre-industrial greenhouse gas levels (Pre-Industrial Control Experiment (PICTRL)) and modeling the climate of the last century (Climate of the 20^{th} Century Experiment (20C3M)), experiments including future climate projections according to a set of scenarios described in the Special Report on Emission Scenarios (SRES) (Nakícenović et al. 2000) were carried out. The SRES describes four different "scenario families": A1—more integrated world, rapid economic growth, and rapid introduction of new technologies; A2—high population growth and regionally orientated economic development; B1—low population growth, rapid economic changes towards an information economy, more integrated world; B2—emphasis on local solutions and environmental protection. The A1 family includes subsets based on different possible paths concerning changes in energy technologies: A1FI (fossil fuel intensive), A1B (balanced), and A1T (predominantly non-fossil fuel). These different scenarios for a possible future lead to different emission paths, spanning a wide range of uncertainties.

2.3 Temperature Trends in the Troposphere and Stratosphere

Observed climate trends for the surface temperature are stated as $(0.187 \pm 0.052)\,\mathrm{K}$ per decade in recent publications (Section 1.2). At the surface, horizontal variations are

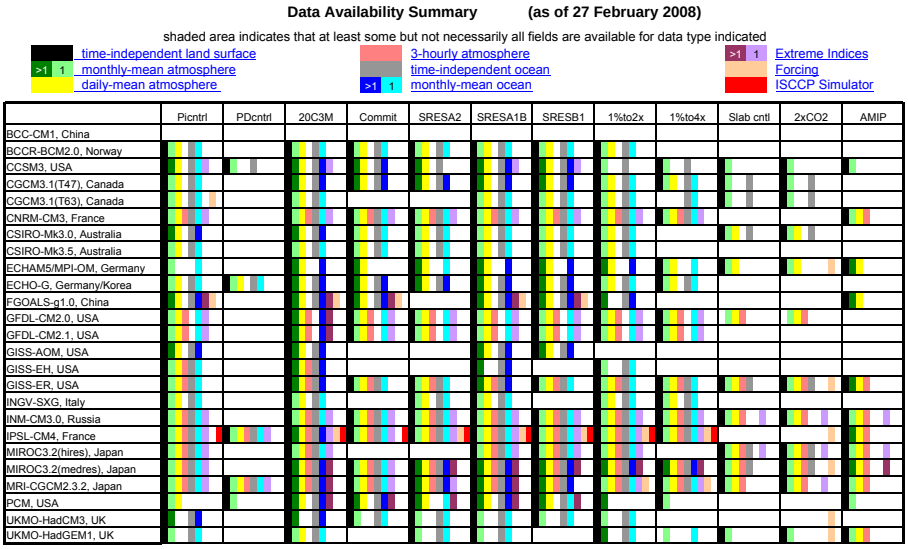

Figure 2.3: List of GCMs available at the PCMDI. Available at http://www-pcmdi.llnl.gov/.

strong due to vastly different properties of surface types (ocean, land masses, ice cover, vegetation etc.). The globally averaged value stated above is therefore only a coarse description of surface trends. Above the surface layer, these variations quickly smooth out. Surface trend values for various climatological parameters can easily be found in literature. On the other hand, the uncertainties in trends in the atmosphere above the lowest layers make it more difficult to state actual upper-air trend values.

The vertical temperature profile above the surface (Figure 2.4) reflects a balance of various processes in the atmospheric system (Karl et al. 2006). In the troposphere, ranging from the surface up to the tropopause at 8 km to 16 km (depending on the latitude), temperatures are generally decreasing with height, depending strongly on the atmospheric humidity. The detailed vertical structure in the troposphere results from balancing radiative processes involving greenhouse gases, clouds, and aerosols. Even more important is the role of strong vertical motions, leading to the transfer of heat throughout the troposphere. These moist convective processes pose an important difference to the stratosphere. The stratosphere exhibits only weak vertical motions. There, in the vertical range from the tropopause up to ≈50 km, the thermal profile is mainly influenced by radiative processes involving greenhouse gases, especially Carbon Dioxide (CO_2), Ozone (O_3), and Water Vapor (H_2O) (Baldwin et al. 2007). The net result is an increase of temperature with height in the stratosphere. In the boundary between stratosphere and troposphere (i.e. the tropopause), temperature varies little with height.

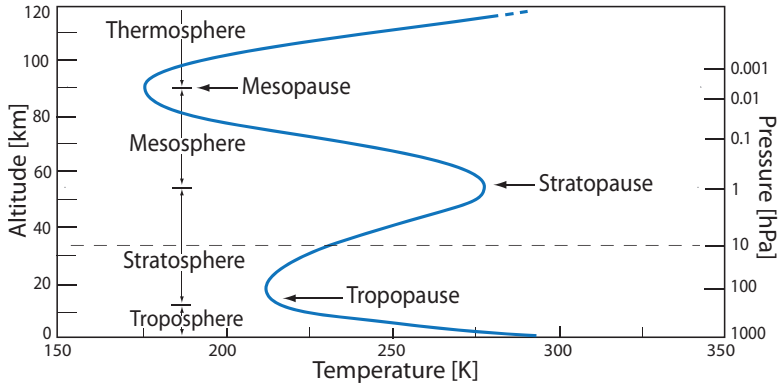

Figure 2.4: Vertical temperature profile, reflecting a balance of various processes in the atmospheric system. Illustration adapted by Kehrer et al. (2008) from Melbourne et al. (1994).

These height-dependent variations of physical effects mean that temperature trends at the surface can be expected to differ from trends higher up in the atmosphere (Laštovička et al. 2006). Although linked, surface, tropospheric, and stratospheric temperatures are separate physical entities. Observations and models show warming at the surface and in the troposphere, and cooling in the stratosphere since beginning of upper-air measurements in the late 1950s. Tropospheric warming can be linked to increases in greenhouse gases (amongst other influences), and stratospheric cooling is probably mainly driven by ozone depletion (Shine et al. 2003).

Whether or not warming is greater in the troposphere than at the surface is not yet clear. The uncertainties involved in both models and observations do not allow a definite answer to this question. At least in the tropics, "amplification" (changes in the troposphere are amplified relative to those at the surface) is expected from physical principles: Latent heat is released as air rises and condenses, and this effect is important in particular in the moist tropics (Karl et al. 2006; Thorne et al. 2011). Precise understanding of stratospheric trends is also missing, mostly due to large uncertainties concerning the homogeneity of observational data (Randel et al. 2009).

The IPCC (Trenberth et al. 2007) reports tropospheric warming of 0.12 K to 0.19 K per decade since 1979. They note that there likely is slightly greater warming in the troposphere than at the surface (the latter trend value stated to be more than 0.16 K per decade from 1979 to 2005). According to Trenberth et al. (2007), lower stratospheric trends are in qualitative agreement between radiosondes and satellite measurements, and data suggest a cooling of 0.3 K to 0.6 K per decade since 1979. Karl et al. (2006) explain that "largest differences between datasets are in the stratosphere" and that "it is very likely that the discrepancy between satellite and RS trends arises primarily from uncorrected errors in the RS data". Randel et al. (2009) present an update of observed stratospheric temperature trends. They include two MSU/AMSU and one Stratospheric

Sounding Unit (SSU) satellite dataset as well as six different homogenized radiosonde datasets. Their analysis reveals that the LS has cooled at a rate of ≈0.5 K per decade between 1979 and 2007. They also say that in the global mean, the LS has not cooled since 1995. Cooling since 1979 has occurred in two downward steps coinciding with the end of the transient warming associated with two major volcanic eruptions during that time period, El Chichón (Mexico) in 1982 and Pinatubo (Philippines) in 1991. For the pre-satellite years with upper-air data available (1958 to 1978), they stress that there is a large range of temperature trend results due to the poor data quality of that time. There is evidence that many radiosonde datasets are biased cold in the stratosphere and show insufficient warming in the troposphere (Randel and Wu 2006; Haimberger et al. 2008; Titchner et al. 2009; Thorne et al. 2011).

An update of observed lower atmospheric temperature trends to the time period 1979 to 2010 is shown in Figure 2.5. It includes the newest long-term datasets available at the time of writing: Two radiosonde datasets, RAOBCOREv1.4 and RICH; and three MSU/AMSU datasets, UAHv5.4, RSSv3.3, and STARv2.0. Corresponding trend values are summarized in Table 2.1 for the LS and in Table 2.2 for the MT. The trend is calculated using least-squares fitting of linear trends. Trend values for the LS are in the range of −0.3 K to −0.5 K per decade globally, consistent with the above-stated results. In the tropics values are quite similar to the global mean, although they are expected to show weaker cooling there, due to the fact that the MSU LS channel peaks at ≈17 km, hence including tropospheric warming in the tropics.

As can be seen in Figure 2.5 (Top), the statement in Randel et al. (2009) that the LS has not cooled since 1995 seems to be still valid in the longer time series. The trends are not linear mainly because of the influence of major volcanic eruptions, visible in Figure 2.5 (depicted with vertical lines) and causing stratospheric warming. The large variability over the considered time range further complicates trend studies. Linear trend fitting is therefore not the best suited statistical tool to characterize LS trend behavior. A proper trend analysis to assess climatological trends needs to take care of transient effects such as the warming following volcanic eruptions or other irregular long-term fluctuations such as El Niño-Southern Oscillation (ENSO) (Santer et al. 2000, 2001; Free and Seidel 2006). The trend values presented here should therefore be treated with caution. While the climatological interpretability is limited, the comparison of the different datasets is still valuable since all observations are subject to the same natural fluctuations.

Middle Troposphere temperatures (Figure 2.5 (Bottom) and Table 2.2) show warming of the globally-averaged and tropical troposphere. While the overall characteristics of the datasets used is consistent, there are substantial differences in the detailed behavior. Trends range from 0.05 K to 0.15 K per decade globally and in the tropics. Note that the MSU MT channel includes parts of the stratosphere (10 % to 15 %), which makes interpretation of trend values more difficult. Trends derived from STAR show more warming in the MT than all other datasets, UAH shows the least, and RSS is similar to the two radiosonde datasets (RAOBCORE and RICH).

Table 2.1: Linear trends of temperature anomalies in the Lower Stratosphere (LS) for the time period 1979 to 2010. The ± value defines the 95% confidence intervals for the trends. The anomalies are relative to the monthly average of 2002 to 2010.

Datasets	Trend (K/10 years)
20.0°S to 20.0°N	
RAOBCORE	-0.332 ± 0.072
RICH	-0.452 ± 0.072
RSS	-0.294 ± 0.074
STAR	-0.354 ± 0.074
UAH	-0.345 ± 0.073
90.0°S to 90.0°N	
RAOBCORE	-0.386 ± 0.041
RICH	-0.461 ± 0.042
RSS	-0.308 ± 0.036
STAR	-0.328 ± 0.036
UAH	-0.391 ± 0.036

Table 2.2: Linear trends of temperature anomalies in the Middle Troposphere (MT) for the time period 1979 to 2010. The ± value defines the 95% confidence intervals for the trends. The anomalies are relative to the monthly average of 2002 to 2010.

Datasets	Trend (K/10 years)
20.0°S to 20.0°N	
RAOBCORE	$+0.080 \pm 0.027$
RICH	$+0.105 \pm 0.029$
RSS	$+0.117 \pm 0.032$
STAR	$+0.144 \pm 0.032$
UAH	$+0.048 \pm 0.031$
90.0°S to 90.0°N	
RAOBCORE	$+0.094 \pm 0.018$
RICH	$+0.090 \pm 0.019$
RSS	$+0.093 \pm 0.020$
STAR	$+0.143 \pm 0.020$
UAH	$+0.053 \pm 0.019$

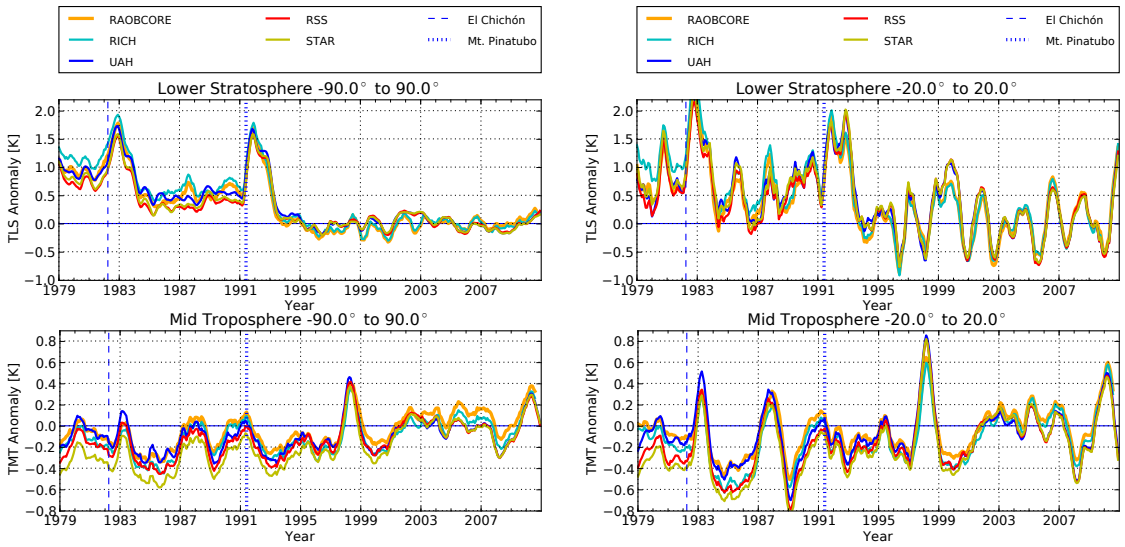

Figure 2.5: Layer-average temperature anomalies for two radiosonde (RAOBCORE and RICH) and three MSU/AMSU (UAH, RSS, and STAR) datasets. (Top) Lower stratospheric channel (TLS); (Bottom) Middle tropospheric channel (TMT) of MSU/AMSU. For the radiosonde datasets, MSU-equivalent temperature anomalies were provided. (Left) Global average and (Right) tropical zonal-mean temperatures. The original monthly data is smoothed using a 7-month running-average. The anomalies are expressed relative to the monthly average of 2002 to 2010. The two major volcanic eruptions for this time period are indicated.

A finer spatial resolution of temperature trends for MSU/AMSU observations is shown in Figure 2.6 for the MT and LS. The trend values presented on these maps might be misleading, because maps in general are not specifically well suited to examine trends. Spatial averaging reduces the statistical uncertainties involved in any real observational system with limited spatial sampling. Nevertheless, the maps provide basic information about spatial patterns of trends (e.g. land-sea, SH/NH differences) and in particular about differences between the various MSU/AMSU datasets.

2.4 Towards Better Understanding of Atmospheric Change

There has been considerable progress in upper-air climate science in the last two decades. The problematic controversy could partly be resolved by more thoroughly accounting for uncertainties in the observational datasets. This certainly also implies that the controversy will continue, because the involved uncertainty ranges are still large. For a better understanding of atmospheric climate, the need for detailed analysis of observations and model data is obvious.

To resolve the issues concerning the reliability of lower atmospheric climate data it

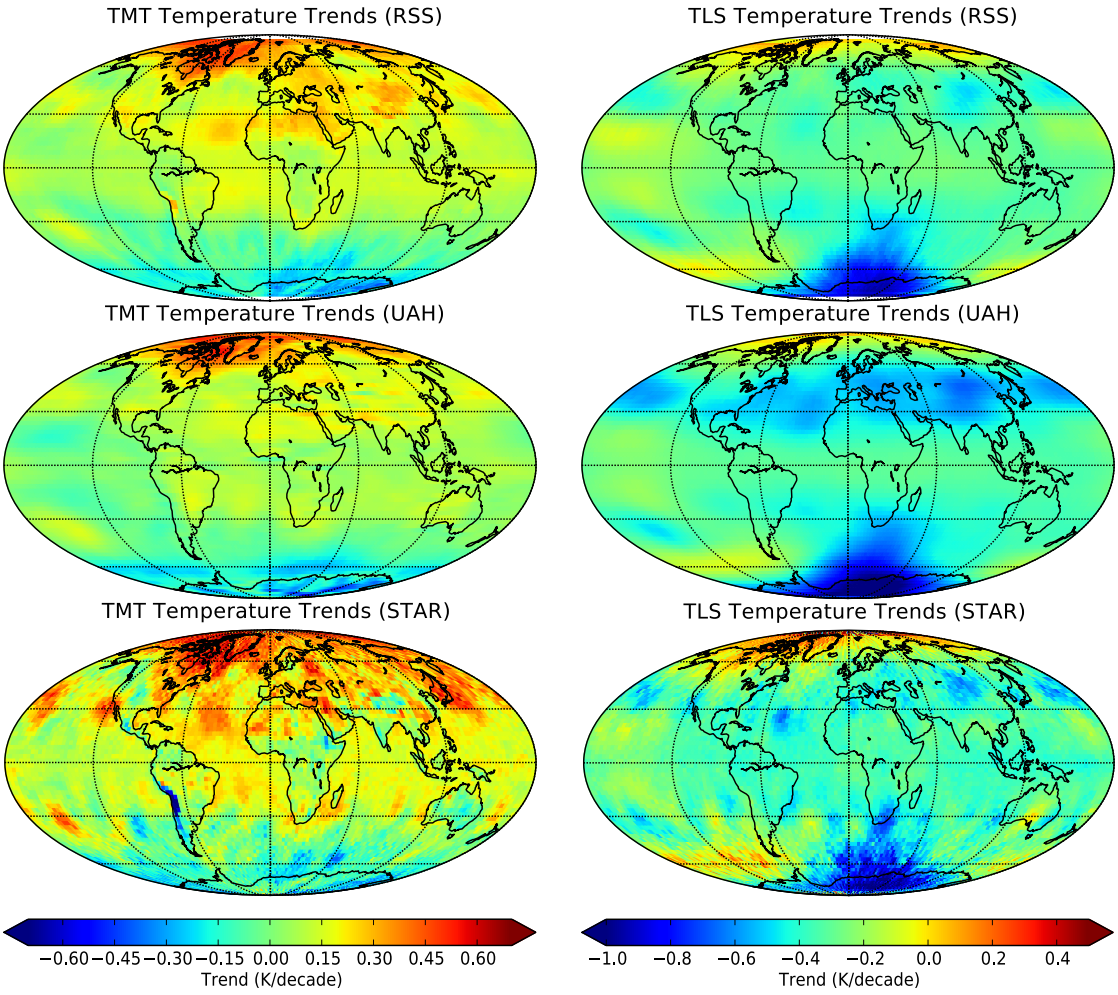

Figure 2.6: Temperature trends in K per decade for the time period 1979 to 2010. Shown are layer-average temperatures from (Top) RSS, (Center) UAH, (Bottom) STAR; (Left) Middle tropospheric channel (TMT), (Right) Lower stratospheric channel (TLS).

is essential to reduce the structural uncertainties involved. Karl et al. (2006) state this requirement in their first "primary recommendation" to improve the understanding of observed changes: "The independent development of data sets and analyzes [...] will help to quantify structural uncertainty". The implementation plan for Global Observing System for Climate (GCOS) also states the need for more upper-air measurement systems for climate monitoring purposes. In the GCOS guidelines, requirements for records of climate quality are defined. The shortcomings of previous observational systems (as described above) are addressed there. According to the GCOS guidelines, a Fundamental Climate Data Record (FCDR) is defined as a "long-term record, involving a series of instruments, with potentially changing measurement approaches, but with overlaps and calibrations sufficient to allow the generation of homogeneous products providing a measure of the intended variable that is accurate and stable enough for climate monitoring" (GCOS 2010). Part of GCOS is the implementation of the GCOS Reference Upper-Air Network (GRUAN) which is designed to provide the currently missing reference system (Immler et al. 2010). It shall consist of a network of high-quality radiosondes and other ground-based measurement systems. This network could both provide contributions to climate research of the upper-air as well as calibrate satellite observation systems.

Generally, fundamental aspects of reference observations include that they are traceable to standards of the Système International d'Unités (SI) (Ohring 2007; Immler et al. 2010). The majority of today's measurement systems do not fulfill this requirement (Immler et al. 2010). This leads to the problem that the available datasets cannot be combined to one reliable long-term record. GRUAN is one ground-based approach to serve as a reference, and Ohring (2007) calls for a set of satellite benchmark missions to be able to create irrefutable climate records and to calibrate other satellites. The implementation plan for GCOS emphasizes that GPS RO measurements provide such benchmark observation, supplementing GRUAN for the Essential Climate Variable (ECV) upper-air temperature.

GPS RO is a new, independent observational system (Kursinski et al. 1997). It fulfills the above-stated requirement of traceability to standards of SI. There is legitimate hope that RO is able to overcome the problems of other upper-air observations, and that its properties make it well qualified to assess the quality of these observations, going beyond the role of being a mere "supplement".

3 Visual Exploration and Comparison of Upper-Air Climate Records

While driving forces in the climate system are today well known and there is little doubt about the range of changes Earth will be facing in the next decades, a more detailed assessment of these changes is still urgently needed (as outlined in Chapter 1 and Chapter 2). One of the topics under debate in today's climate research is concerned with changes in upper-air climate. The work in this thesis is motivated by the need for deeper insight into the upper-air part of the climate system, an insight which should ultimately resolve remaining discrepancies. The main contributions of this thesis to upper-air climate research are: a) To present an innovative approach to analyze and explore atmospheric data; and b) To assess the quality of conventional upper-air measurements using Global Positioning System (GPS) Radio Occultation (RO), a recent observational system of reference quality.

3.1 GPS Radio Occultation, a New Potential Reference Climate Record

One major obstacle for better understanding upper-air climate change has been the lack of a potential reference dataset (Section 2.4). Reference measurements can provide both an independent source of observational data of its own as well as calibration of other, already existing systems. The past decade had been the first where such a potential reference satellite system was in orbit. GPS RO is an active limb sounding technique and it has been demonstrated that it can be considered of potential reference quality (Leroy et al. 2006, 2008; Steiner et al. 2009a). It aims to fulfill the requirements stated by the Global Observing System for Climate (GCOS) guidelines (GCOS 2010), delivering high-quality observations in the Upper Troposphere–Lower Stratosphere (UTLS), traceability to Système International d'Unités (SI) standards, and global coverage and high vertical resolution.

3.1.1 Measurement Principles

RO is an active remote sensing technology. It uses electromagnetic signals transmitted by GPS satellites, which are refracted by the atmosphere and received by Low Earth

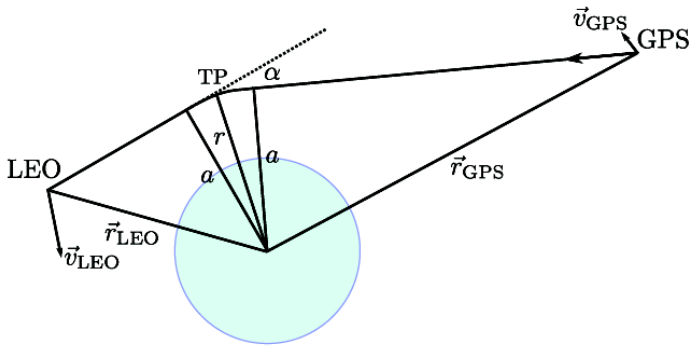

Figure 3.1: The Radio Occultation geometry of a setting RO event. Relative movements of both GPS and LEO satellites lead to a scanning of the electromagnetic signal through the atmosphere. Illustration taken from Pirscher (2010).

Orbit (LEO) satellites. Due to the relative movement of the two satellites, the signal scans through the atmosphere, resulting in vertical profiles of atmospheric parameters.

The basic measured quantity are phase changes of the transmitted GPS signals. GPS satellites broadcast at two frequencies at equivalent wavelengths of 0.19 m (L1 signal) and 0.24 m (L2 signal). Through precise time and orbit information for both transmitter and receiver, available as main products of the GPS network, the delay of the signals due to atmospheric and ionospheric influences can be determined. Potential timing errors can be corrected by relating the measurements to additional GPS satellites and/or ground stations, if required. Thus the measurement can be traced back to the fundamental quantity "time", fulfilling one of the most important GCOS requirements.

To retrieve the atmospheric parameters of interest an *inverse problem* needs to be solved, a typical procedure in remote sensing. In the case of RO, the observed raw excess phase $\Delta\varphi$ is first converted into profiles of bending angles α as a function of the impact parameter a (cf. Figure 3.1). The bending angle α is the integrated incremental bending along the path ray. It has the form of an Abel integral and can be inverted to yield the basic atmospheric quantity measured by RO, the refractive index n:

$$n(r_1) = \exp\left[-\frac{1}{\pi}\int_{a_1}^{\infty}\frac{\alpha(a)}{\sqrt{a^2-a_1^2}}\mathrm{d}a\right], \tag{3.1}$$

where a_1 is the impact parameter for a particular ray and r_1 is the radius of the corresponding tangent point, $a_1 = n(r_1)r_1$.

The refractive index n is close to unity, and for practical reason it is more common in atmospheric sciences to use the refractivity N, simply defined as

$$N(h) = (n(h) - 1) \cdot 10^6, \tag{3.2}$$

where h is the height above the Earth's ellipsoid. The refractivity N is related to other atmospheric parameters of interest by the Smith-Weintraub relation (Smith and Weintraub 1953), valid at microwave wavelengths:

$$N = 77.6\frac{p}{T} + 3.73 \times 10^5 \frac{e}{T^2} - 4.03 \times 10^7 \frac{n_\mathrm{e}}{f^2} + 1.4W, \tag{3.3}$$

where p is the atmospheric pressure (hPa), T the temperature (K), e the partial pressure of water vapor (hPa), n_e the electron density (m^{-3}), f the transmitter frequency (Hz), and W is the mass of condensed water in the atmosphere ($\mathrm{g\,m}^{-3}$). The terms of this equation represent the influence of the dry atmosphere ($\propto p/T$), the moist atmosphere (second term), the ionosphere and of liquid water and ice content in the atmosphere. The last term containing the contribution of condensed water can usually be neglected in RO applications, and after correcting the ionospheric influence using a combination of the two GPS frequencies, only the first and the second term remain important. In the UTLS, where moist content is low, the moist term is also usually neglected in RO retrievals, highly simplifying the retrieval. The remaining dry term is directly proportional to air density ρ, which is transformed to pressure via the hydrostatic equation, and then to temperature using the ideal gas law. The important constraint in this derivation is the limitation to dry air conditions (Scherllin-Pirscher et al. 2011b). The parameters retrieved by the RO processing chain (T_dry and p_dry, if neglecting the wet term) are therefore strictly speaking no physical parameters, although the difference to physical temperature and pressure can be small, depending on height and latitude. For a thorough discussion of the RO retrieval chain see, e.g., Pirscher (2010).

3.1.2 Characteristics of RO

The measurement technique outlined in Subsection 3.1.1 has the following properties:

Long-term Stability This crucial requirement for climate studies is fulfilled by RO observations, because every measurement can be traced back to the precise determination of time, which is achieved by stable atomic clocks. The time measurements related to a RO event are sufficiently stable over the occultation duration, and they will be the same on every satellite employed. This guarantees traceability to the SI unit "second", and therefore reproducibility and long-term stability (Leroy et al. 2006).

Resolution and Accuracy A major advantage over conventional satellite upper-air observation systems is the good vertical resolution of RO measurements. The resolution ranges from about 0.5 km in the troposphere to 1.5 km in the stratosphere (Kursinski et al. 1997). On the other hand, the horizontal resolution is comparatively low with about 300 km. For climate applications, a high vertical resolution is important because of the distinct vertical thermal structure of the atmosphere.

A range of studies have been conducted to assess the error characteristics of RO measurements (e.g., Kursinski et al. 1997; Rocken et al. 1997; Steiner and Kirchengast 2005; Foelsche et al. 2008b; Ho et al. 2009b; Foelsche et al. 2011; Scherllin-Pirscher et al. 2011a,b). In the UTLS, temperature can be retrieved with high accuracy (<1 K), refractivity Root Mean Square (RMS) errors are found to be <0.5 %. The statistical observational error becomes negligible when averaging over many profiles as it is done in zonal-mean climatologies.

Global Coverage The quality of global coverage depends both on the inclination and the number of receiving satellites. For a single LEO satellite in the near-polar orbit, around 250 occultations per day can be expected. This number can rise considerably if more receiving satellites are in orbit; ongoing RO missions with six satellites provide up to 2500 occultation events per day. The sampling error due to finite sampling of continuous fields is estimated to be smaller than 0.3 K in the UTLS in monthly-mean 10° zonal-mean climatologies.

3.1.3 Applications

The last decade has already seen a range of studies using RO data for a variety of climatological applications. Among them are first validations of RO data with other datasets (e.g., Schrøder et al. 2003; Kuo et al. 2005; Gobiet et al. 2007; Ho et al. 2007; Steiner et al. 2007), investigation of the tropopause region (e.g., Schmidt et al. 2004; Gobiet et al. 2005; Schmidt et al. 2005b; Borsche et al. 2007), the El Niño-Southern Oscillation (ENSO) (e.g., Lackner 2010), atmospheric waves (e.g., Steiner and Kirchengast 2000; Tsuda et al. 2000; Pirscher et al. 2010), and the impact of RO on weather forecasting (e.g., Healy et al. 2005). First trend studies based on the RO record have already been conducted (e.g., Leroy et al. 2008; Steiner et al. 2009a; Schmidt et al. 2010). For an up-to-date overview of RO applications see Steiner et al. (2011).

3.1.4 RO Missions

The first proof-of-concept mission was established with Global Positioning System/Meteorology (GPS/MET) in 1995. GPS/MET was successful in demonstrating the feasibility of the technique, although only few months of observations are available (Ware et al. 1996). First continuous observations were delivered by Challenging Mini-Satellite Payload (CHAMP) (Wickert et al. 2001), with RO profiles available from September 2001 to early October 2008. Satélite de Aplicaciones Científicas/Scientific Applications Satellite C (SAC-C) (Hajj et al. 2004) and Gravity Recovery and Climate Experiment (GRACE) (Wickert et al. 2005) are two more single-satellite missions, complementing CHAMP data and continuing to provide data up to now. The first multi-satellite mission was FORMOSAT-3/COSMIC (F3C), constituted of six receiving satellites launched in 2006, and

is still ongoing, delivering up to 2500 profiles every day. The Meteorological Operational (Metop)/Global Navigation Satellite Systems Receiver for Atmospheric Sounding (GRAS) mission started in 2006 and is planned to be continued at least until 2020.

3.2 An Innovative Approach: Visual Interactive Exploration

The availability of new upper-air measurements and improved data homogenization techniques have lead to an improved state of knowledge about the UTLS. The therewith associated better agreement between expectations (driven by model output) and measurements directs the attention of research to applications of these data.

Here we take the advent of the new potential benchmark observational system RO as motivation to investigate an innovative approach to analyze the existing large set of atmospheric data, and to specifically search for global climate change indicators in the data with special focus on the UTLS. The sub-range UTLS in the vertical atmospheric structure is chosen because of its sensitivity to climate change and the accessibility of this region by RO measurements. In the course of research, the unique qualification of the exploration approach for quickly understanding data characteristics and for generating hypotheses without prior knowledge of the data emerged.

3.2.1 Interactive Visual Exploration Methods

The global coverage of the growing amount of available datasets, coming from General Circulation Models (GCMs), from satellite and radiosonde observations, and from reanalysis products (Section 2.2), leads to an enormous total amount of data produced. The quickly increasing amount of climate data poses problems for data analysis—quite paradoxically, since today's climate research faces the problem of structural uncertainties being too high in upper-air observational datasets just because there is a lack of sufficient number of independent datasets. Still, the number and complexity of climate models is increasing fast (see Figure 2.3), the spatial and temporal resolution of reanalysis and model data is also increasing, new observational missions are operational (e.g., GPS RO), and more observations are still needed. There is no end in sight: The number of specific climate change publications has seen exponential growth over the last two decades (Grieneisen and Zhang 2011), indicating the interest in the research topic.

The resulting large, multivariate, and time-dependent datasets need to be analyzed. Traditionally, geophysics uses the tools provided by classical statistics (Wilks 2006). While these tools are very appropriate for quantitative analysis, the sheer amount of today's data provides new challenges. This becomes obvious when realizing that classical statistics usually need a *hypothesis* beforehand to work. Such a hypothesis can be of many kinds, and there will be virtually always such assumptions at the beginning of a

statistical analysis. In other words, the scientist usually *knows* what he/she is looking for, and uses classical statistics to verify his/her hypothesis. While this method provides meaningful quantitative analysis, it is less suited to come up with new hypothesis without prior knowledge or to search for unexpected features in the data. Classical statistical methods thus, while being very powerful, contain the risk of having a view on data which is too focused on certain sub-domains. This might lead to overlooking potentially interesting features.

The general concept of identifying useful patterns in large datasets is called "data mining" (Fayyad et al. 1996; Friedman 1997; Goebel and Gruenwald 1999). In this context, interactive visual exploration has proved to be a powerful tool for Exploratory Data Analysis (EDA), which is one important data mining task (Tukey 1977). The interaction with the data, as opposed to static visual representation of results, opens the opportunity to *discover* features in the datasets which had not been anticipated. Nearly no previous knowledge about the data is required. Interactive visual exploration can hence facilitate the iterative and interactive browsing through the parameter space. The ability of the human vision to detect visual patterns is used to extract useful information. The patterns that attract the attention of the user can interactively be selected and iteratively explored in more detail.

The concepts of EDA, although discussed in information and visualization science for decades, are hardly used in geosciences. This might be the case because they are unknown to the geophysical community, or simply because adequate tools are missing (Nocke 2007; Nocke et al. 2008; Kehrer 2011). In this thesis the approach is applied to climate datasets to evaluate the benefit of using interactive visual exploration for atmospheric scientists. I introduce the concept of an exploratory approach to large atmospheric datasets and show the advantages of this approach for quick access to data characteristics, for easy detection of data deficiencies, and for the potential of exploration to encounter the danger of missing important pieces of information in large datasets. Exploration techniques are well suited for these tasks. Its special value for improving the understanding of upper-air climate lies both in its quick access to data characteristics as well as in its ability to uncover unexpected features in the datasets.

The work relating to visualization was done in collaboration with and with support from visualization researchers and culminated in the publication of three research papers. In the following, the specific contributions of the related publications to be found in Part II are discussed.

3.2.2 Research Papers in this Thesis

General concepts of visualization are introduced in the first publication (Paper A, Ladstädter et al. 2009). Simulation Visualization (SIMVIS), a software tool originally developed by the VRVis Research Center in Vienna, Austria is presented and applied to model and reanalysis data. SIMVIS was originally developed for the visualization

and analysis of multivariate data resulting from Computational Fluid Dynamics (CFD) simulations (Doleisch et al. 2005). Several key concepts of interactive visualizations are implemented in this software package:

Interactive Feature-Based Visualization and Brushing One major concept of exploratory techniques is the ability to concentrate on subsets (*features*) of the data. This key ingredient helps to reduce the complexity of the data, enabling the user to handle even very large datasets. The *feature-based* visualization approach as employed by SIMVIS uses a *brushing* mechanism to select features of interest. Brushing means that the user interactively selects points of interest directly within a visualization view, for example by defining a selection rectangle with the mouse in a two-parameter space. See Figure 3.2 for an example, here the user applied an inverse selection (rectangle) to the southern high latitude range of the parameter "geopotential height trend", effectively expressing interest in all latitudinal regions except the southern high latitudes.

Linked Multiple Views SIMVIS allows multiple open views, showing different aspects of the same dataset. The concept of feature-based visualization gains power in that the selection of features by the user in one view is translated to the other views. Further selections can be applied in each view and are propagated immediately to all other views (Doleisch et al. 2004b). Several types of view are available: scatterplot, histogram, spatial 3D view, curve view and others. Brushing and linking between the views is an efficient way to apply constraints on the data interactively and immediately see the results in all views (Baldonado et al. 2000). When applied iteratively, this becomes a powerful concept to explore a (potentially unknown) huge dataset. SIMVIS allows interactivity even when large datasets are loaded into computer memory.

Focus and Context Visualization To distinguish selected from unselected data items, SIMVIS uses a *Focus and Context* visualization concept. Data items which are selected in one of the views are shown in an emphasized way and said to be "in focus", while the context is drawn in a reduced style. This concept is employed in all available views and helps the user to easily identify relevant data.

These concepts are then applied to climate datasets in Paper A as proof-of-concept and to explain the methodology. Seasonal-mean (June to August) fields for the Fifth-Generation ECMWF–MPI-M Hamburg (ECHAM5) climate model dataset and the 40-yr ECMWF Reanalysis (ERA-40) dataset are used as representative climate datasets (cf. Section 2.2). Gridded temperature, refractivity, and geopotential height parameters on pressure levels ranging from 1000 hPa to 10 hPa are considered. While it is possible to simply explore the datasets as they are, more insight can be gained if exploration includes features of special interest. In the case of climate datasets, this often are trend characteristics.

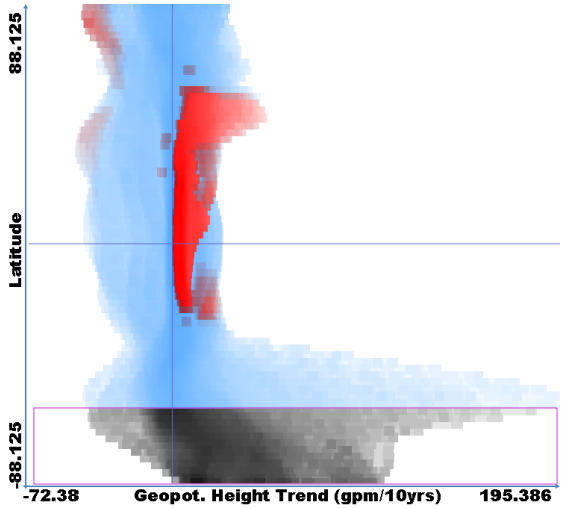

Figure 3.2: Example for brushing of regions within a visualization view. The inverse selection (rectangle) deselects the southern high latitudes range and keeps the remaining latitude ranges selected. The user can change this selection interactively on-screen. Deselected regions are marked in black.

SIMVIS allows the user to select every available parameter of the dataset as the source of a "derived" parameter, using a set of pre-defined mathematical operations. Suitable derived parameters are the linear trend and the Signal-to-Noise Ratio (SNR), the latter defined as the ratio of the trend to the detrended standard deviation. The detailed description of the method can be found in Paper A, Subsection 3.2.

Features of the datasets are then explored in an exemplary interactive session. There it is shown that it is easy to find out characteristics of the data, even if they were unknown before. The exploration sessions show that temperature trends in ECHAM5 are positive in the troposphere and negative in the stratosphere, and a simple feature selection immediately shows that remaining negative trends in the 150 hPa and 200 hPa pressure levels only stem from northern high latitudes. ERA-40 reveals large differences in data quality between the early years of the reanalysis and the post-satellite era. It can be seen that different aspects of the varying quality are easily explored. The visual representation also indicates that stratospheric temperature trends in ECHAM5 are especially robust (see Figure 3.3), even though it is noted that a more detailed classical statistical analysis is needed.

The aspect of generating new hypotheses using interactive visual data exploration of climatological datasets is highlighted from the point of view of visualization scientists in Kehrer et al. (Paper B, 2008). The power of the exploratory concept is investigated, including that no prior knowledge about the data is required to rapidly come up with hypotheses. The work builds on previous research carried out in Paper A, using similar

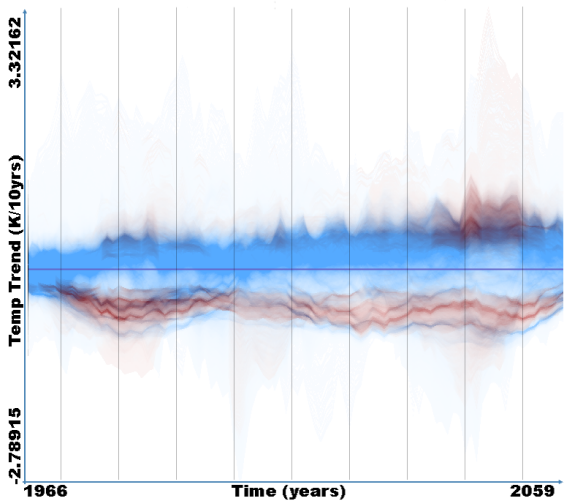

Figure 3.3: ECHAM5 temperature trends, with high values of SNR selected in another view. The selected data appears in red in this view and stem from the stratosphere.

datasets. The quick generation of hypothesis is explained and several exemplary hypothesis are identified. It is investigated whether visual exploration can help in the search for sensitive indicators of atmospheric climate change, or even support such investigations in a new, unique way. Among the created hypotheses relating to this background, robust indicator regions with respect to climate change are identified in the lower stratosphere for ECHAM5 temperatures, and in the tropical lower to middle troposphere for the ERA-40 geopotential height field. More sophisticated ways of brushing, e.g. the similarity-based brush selecting curves with similar shape are presented.

A further interesting output of Paper B is that an unexpected negative trend feature visually emerged at surface pressure levels while exploring the ECHAM5 dataset in search for climate change indicators, strengthening the proposition of "discovering the unexpected". Further narrowing the selection to this new feature is remarkably easy, which is intrinsic to the innovative approach taken. It turns out that the feature stems from a narrow area mainly located at the Tibetan Plateau. It can be expected that this feature—which might be considered as prototypical for unexpected characteristics in climatological datasets—would have been overlooked in classical statistical procedures.

Ladstädter et al. (Paper C, 2010) further elaborates on the potential of visual exploration techniques to enhance the conventional analysis methods in atmospheric sciences. A possible workflow is proposed, utilizing the complementary characteristics of visual exploration. In addition to the model and reanalysis data already utilized in former studies (Paper A and B), GPS RO observational data are analyzed. Exploring RO datasets from different data processing centers, differences between the output from these centers can easily be detected.

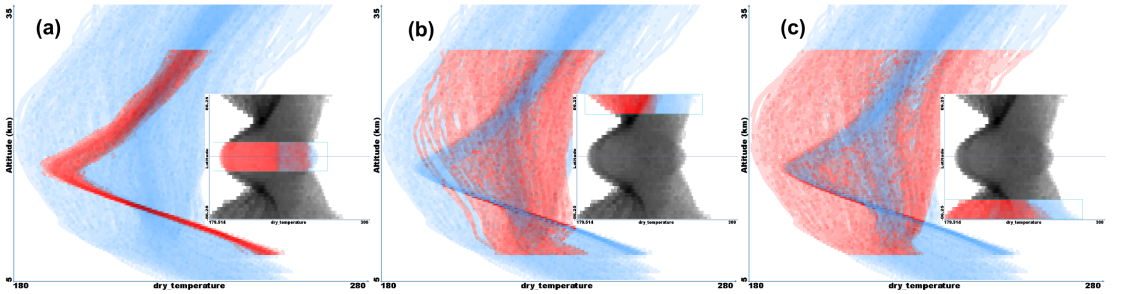

Figure 3.4: Zonal-mean monthly-mean temperature profiles from CHAMP. The interactive selection (shown in the respective inset) of latitude ranges has an immediate effect on the shown temperature profile, with selected data shown in red.

The main advantages of both visual exploration and classical statistics are complementary and can be combined: Visual exploration, while not good in rigorous statistical conclusion, can be used to interactively and iteratively explore the data and generate hypotheses about the data without prior knowledge necessary. Classical statistical methods can then quantitatively confirm (or refute) the hypothesis. Paper C shows examples for this workflow, visually selecting areas reacting sensitively to climate change (see Paper B), and using classical statistical trend testing to evaluate the outcome. The study confirms the usefulness of this approach, and stresses the complementary nature of visual exploration in the field of atmospheric sciences.

The interactive approach is found to be useful also in the context of observational satellite data: It is easy to get a quick overview over the basic data characteristics, as exemplary shown in Figure 3.4, where the user chooses to brush different areas in the latitude parameter. The temperature profile, shown in another open view, is updated immediately as the user moves the selection rectangle with the mouse.

For the comparison of RO datasets from different processing centers, a parallel coordinates view is a sophisticated and adequate visualization tool. The parallel coordinates view shows a set of parameters on parallel coordinates placed next to each other (Figure 3.5). Corresponding points on the parallel axes are connected via line segments. The view is well suited to show interdependencies between the parameters. In Figure 3.5, northern high latitudes are brushed for demonstration purposes (left coordinate). Four coordinates, representing differences of the number of profiles contributing to refractivity climatologies from four different RO processing systems to the mean of all processing systems, show without any further analysis a visual correlation between two of them lying above the blue zero line and two lying below.

Model, reanalysis, and observational upper-air datasets have been successfully analyzed in Paper A, B, and C using a novel interactive visualization technique, presenting an opportunity for new insight into the large atmospheric climate datasets.

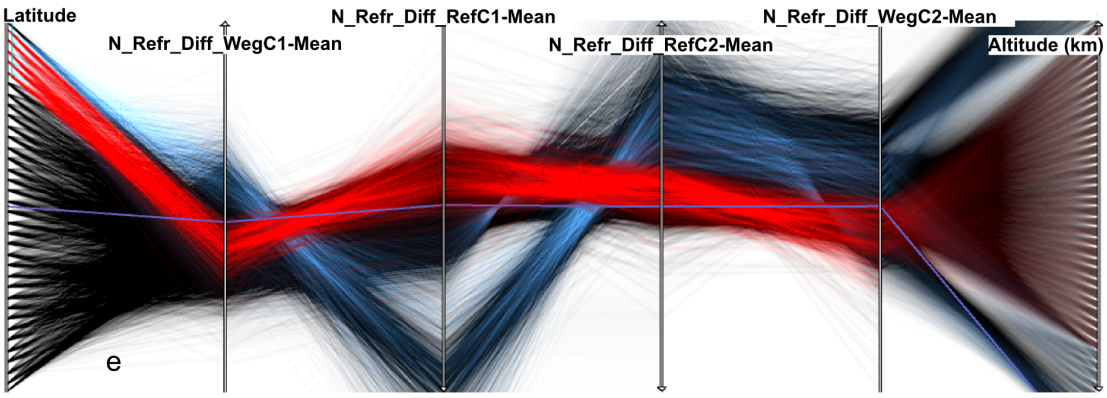

Figure 3.5: Relations between different RO processing systems (WegC1, RefC1, RefC2, WegC2) revealed by the parallel coordinates view. Northern high latitudes are brushed (left coordinate), data selected in all views appear in red and data selected only in this view in blue (there is a further selection in another view, not shown, limiting the height range).

3.3 Utilizing RO as Reference for Conventional Observations

The innovative exploration techniques elaborated in Section 3.2 emerged as valuable complement to classical statistical methods when analyzing atmospheric datasets, helping in deepening the insight into upper-air climate. They facilitate the understanding of large climate datasets. The amount of data available is only one obstacle for better understanding atmospheric climate, another significant one—widely discussed in the last decades—is the lack of potential reference datasets. These reference datasets are important to advance research of the upper-air part of the climate system, to be able to calibrate conventional observations, and to validate climate model output.

3.3.1 GPS RO Reference Data

Such a potential reference system has been implemented in the last decade (Section 3.1). The (continuous) data record from GPS RO missions now covers nearly 10 years. First validation studies have been conducted previously (Subsection 3.1.3). Extensive studies of RO data quality and error ranges (Subsection 3.1.2) strengthen the view that RO is indeed qualified as a source of reference observations.

This thesis uses RO data as reference for comparison with recent radiosonde and Microwave Sounding Unit (MSU)/Advanced Microwave Sounding Unit (AMSU) datasets. For the first time sparse sampling is accounted for in the comparison of upper-air climatologies showing the importance and impact of doing so. Having a new independent source of upper-air data is certainly a step forward in fulfilling some of the requirements

stated in Section 2.4.

Several previous studies compared RO data to radiosonde and MSU/AMSU. Schrøder et al. (2003); Steiner et al. (2007, 2009b) compared MSU/AMSU zonal-averaged climatologies and Ho et al. (2007) collocated small-scale bins. Regarding radiosondes, Kuo et al. (2005); He et al. (2009); Sun et al. (2010) compared radiosonde profiles with collocated RO soundings.

3.3.2 Research Paper in this Thesis

In Ladstädter et al. (Paper D, 2011) it is shown how conventional observational systems compare with GPS RO in the Lower Stratosphere (LS) region. The comparison is based on zonal-mean climatologies and in this respect differs from previous studies for radiosondes. Special care is taken to properly account for the specific sampling characteristics of the datasets. Anomaly difference time series are compared in order to isolate the differences due to structural uncertainties.

Sampling Characteristics Instead of collocating radiosonde and RO profiles, the distinct sampling characteristics of both measurement techniques are explicitly accounted for. When aiming to compare records from various observational records, it is important to keep in mind that none of them reproduces "reality" due to their limited, finite sampling of the atmosphere. Depending on their respective global coverage, the error made by discrete sampling (the "sampling error") can be more or less substantial. This problem is less pronounced for satellite-based measurements than for fixed ground-based techniques. For MSU/AMSU, it is virtually non-existing, because the employed nadir-measurement geometry results in a very good horizontal resolution. The limb-sounding technique of GPS RO results in coarser horizontal resolution, but global coverage is still sufficient for single-satellite and good for multi-satellite missions (Figure 3.6). Comparing to other atmospheric fields (e.g. ECMWF analyis fields or ERA-Interim), the error made by discrete sampling can be estimated and accounted for (Foelsche et al. 2008b; Scherllin-Pirscher et al. 2011b).

On the other hand, the ground-based radiosonde stations are not distributed uniformly over the globe (see Figure 2.1). Several large regions of the Earth (Southern Hemisphere (SH), tropics, oceans) are sparsely represented. A comparison of zonal averages involving datasets with such different sampling characteristics is not valid. Previous studies therefore collocated single RO profiles with matching radiosonde launches to guarantee a comparison of the same atmospheric patterns in both records. In Paper D, sampling errors are treated consistently in both GPS RO and radiosonde data, allowing the comparison of zonal-mean climatologies of all three upper-air observational systems.

For GPS RO, the sampling error is estimated using European Centre for Medium-Range Weather Forecasts (ECMWF) analysis fields as a approximation for a global "true" atmospheric field. The error made by finite sampling is estimated by considering two

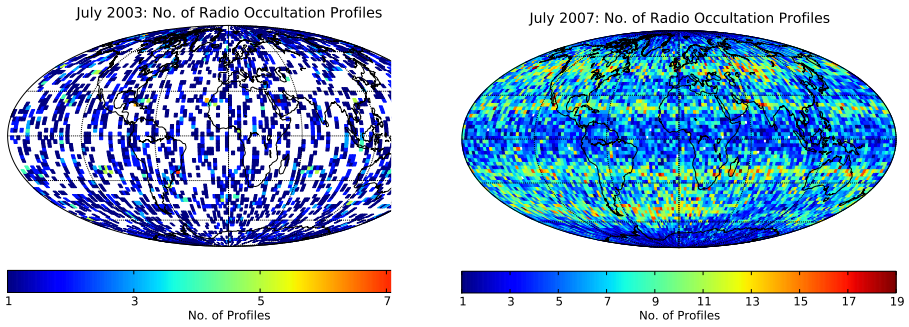

Figure 3.6: Global monthly coverage of RO profiles for July 2003 (left) single-satellite (CHAMP) and for July 2007 (right) multi-satellite data (CHAMP, COSMIC, GRACE-A). Number of profiles in $2.5° \times 2.5°$ bins are shown

fields: 1) collocated (to RO profiles, in space and time) ECMWF profiles are averaged to monthly means and latitudinal bands, representing the atmospheric state at the times and locations of RO measurements as seen by the reference field and 2) the full ECMWF analysis field containing all four time layers is equally averaged. The *sampling error* of RO is then defined as the difference of the full reference field and the collocated field. The so-estimated sampling error is finally subtracted from the RO climatologies. The originating data is not part of the sampling error estimate, only the temporal and spatial characteristics plays a role. For RO, the sampling error is generally very small ($<$0.2 K) although it can be larger at high latitudes, and much smaller for multi-satellite missions.

In Paper D, an equivalent approach consistent to the one explained above is applied to radiosonde data. It utilizes the advantageous fact that all radiosonde launches take place either at 0 UTC or 12 UTC. For both times there exist ECMWF analysis fields. Together with the fact that radiosonde launches always occur at the same place, it is possible to collocate monthly mean radiosonde data (binned in $2.5° \times 2.5°$ resolution) to ECMWF fields, both in space (taking only bins where there exist valid radiosonde data) and time (either 0 UTC or 12 UTC). As it is done in the case of RO, the sampling error is then defined as the difference of the collocated ECMWF reference field to the "true" ECMWF field, where all time layers and the full horizontal resolution is incorporated in the mean. In a final step the sampling error is subtracted from the radiosonde data, yielding a radiosonde climatology field adjusted by its spatial and temporal errors. For regions with very sparse sampling and large atmospheric variability, this method will be less successful in improving the dataset quality, but for most regions the approach seems to substantially improve the atmospheric representation as given in climatological means.

The resulting sampling errors for the radiosonde stations used in the Radiosonde Observation Correction using Reanalyses (RAOBCORE) datasets and for GPS RO are shown in Figure 3.7. The periodic sampling error structure in the Northern Hemisphere (NH) winter for radiosondes is an interesting feature, implying that the radiosonde network

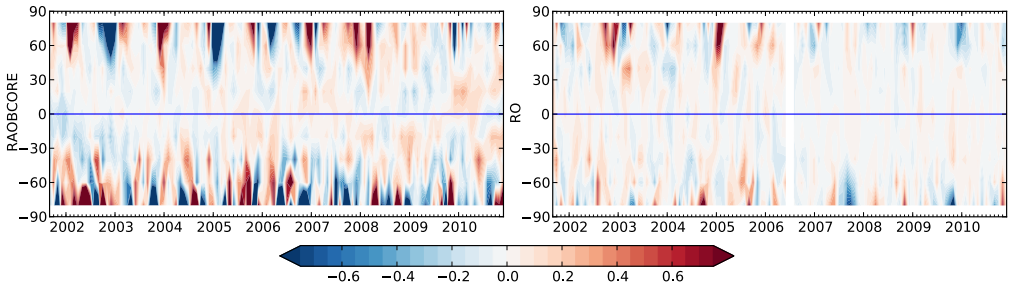

Figure 3.7: Sampling error of radiosondes (left) and RO (right). Shown are latitudinal bands in 20° resolution.

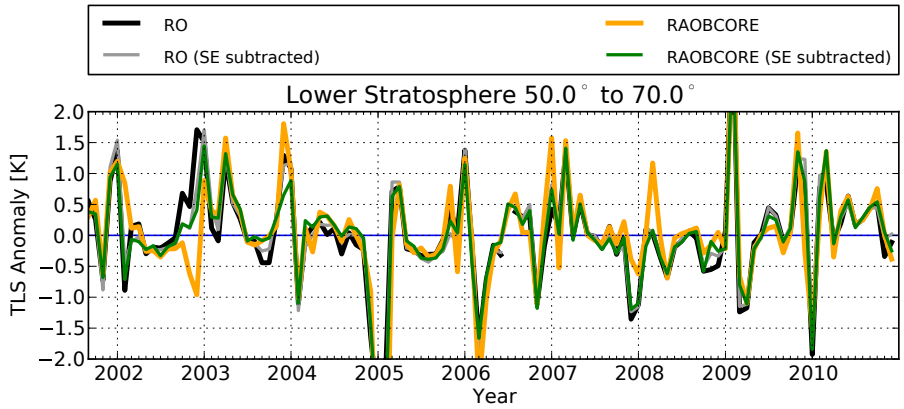

Figure 3.8: Effect of subtracting the sampling error of radiosondes (orange/green) and RO (black/gray) in the NH. Shown is the TLS before and after subtracting the respective sampling error.

largely misses the atmospheric variability in winter. An important outcome of Paper D is therefore that it is essential to consider the sampling error for radiosondes to produce meaningful zonal-mean climatologies, which is confirmed by the comparison with RO temperature anomalies in the study.

The effect of subtracting the sampling error from GPS RO and radiosonde climatologies is shown in Figure 3.8 for the zonal band 50°N to 70°N for MSU-equivalent TLS. The large effect in NH winter is clearly visible—after subtracting the sampling error, the radiosonde TLS is much closer to the RO record, indicating a substantial improvement.

Comparing Anomaly Differences Structural uncertainty arises as a result of the choice of approach to observe the atmosphere (Thorne et al. 2005). Differences in measurement systems and in homogenization techniques to arrive at final climate records add a systematic bias to each dataset. Assessing the differences between several *independent* datasets enables to get a feeling for the magnitude of these biases. Paper D uses six

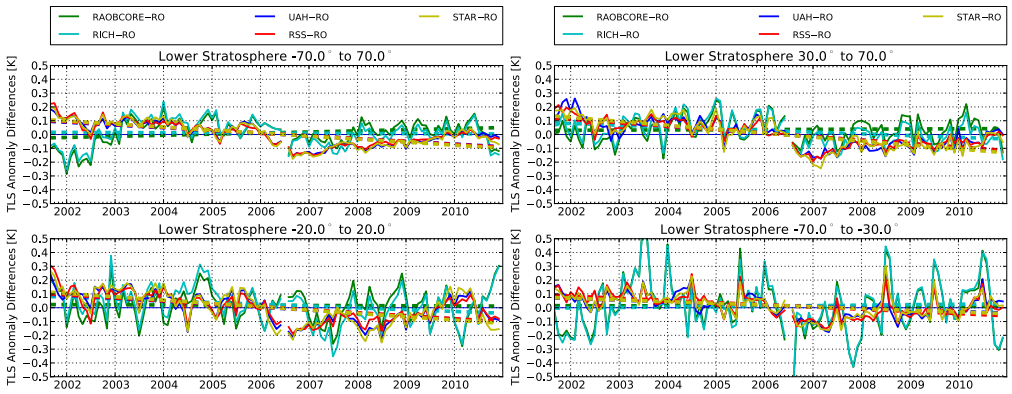

Figure 3.9: TLS anomaly difference time series for all datasets (Sep. 2001 to Dec. 2010). The linear regression lines are shown as dashed lines.

different datasets, three independent types of observations, to analyze if substantial differences between Lower Stratosphere (LS) datasets still remain in the newest versions, with special focus on comparing to the potential reference GPS RO.

In this comparative study, the datasets to be compared represent the same variable, since they are all observations of the same atmospheric region (as opposed to comparing observations with data or observations at different regions). The statistically correct method to asses differences between correlated data series is to compare difference time series (Wigley 2006). Differencing of two correlated variables removes the variability common to both datasets, isolating those differences due to the structural uncertainties involved. Removing the differences due to varying spatial coverage by subtracting the sampling error for each dataset separately, as described above, furthermore focuses the comparison to the differences in their measurement techniques.

To get rid of seasonal influences in the data records, monthly anomalies are used. The time series of anomaly differences are then analyzed with linear regression analysis, to assess the significance of the trend differences. The results are summarized in Figure 3.9 together with the trend analysis in Table 3.1.

The results show very small differences of RAOBCORE to RO in all considered regions, and good agreement of the second radiosonde dataset (RICH) globally. Radiosonde Innovation Composite Homogenization (RICH) depends on neighboring stations for homogenization as outlined in Subsection 2.2.1, which is a plausible explanation of the worse agreement at least in the tropics, where radiosonde coverage is sparse. While RICH shows larger differences to RO than RAOBCORE in the tropics and NH, its anomalies still agree better with RO than (Advanced) Microwave Sounding Unit ((A)MSU) data. Without taking into account the sampling error, the trend of anomaly differences and the confidence interval between RAOBCORE and RO is around twice as large in the NH (not shown). MSU/AMSU and RO are found to differ significantly (at a 95 % level) in all considered regions.

Table 3.1: Trends of TLS anomaly differences (Sep. 2001 to Dec. 2010). The ± value defines the 95% confidence intervals for the trends. Trend values which are significantly different from 0 at the 90% and 95% level are marked by a single and double asterisk, respectively.

Datasets	Trend (K/10.0 years)	$\text{StdDev}_{\text{Residuals}}$(K)
	70.0°S to 70.0°N	
RAOBCORE–RO	$+0.080 \pm 0.061^{**}$	0.09
RICH–RO	-0.013 ± 0.065	0.10
UAH–RO	$-0.198 \pm 0.042^{**}$	0.06
RSS–RO	$-0.206 \pm 0.043^{**}$	0.06
STAR–RO	$-0.220 \pm 0.045^{**}$	0.07
	20.0°S to 20.0°N	
RAOBCORE–RO	-0.012 ± 0.083	0.12
RICH–RO	$-0.129 \pm 0.089^{**}$	0.13
UAH–RO	$-0.216 \pm 0.061^{**}$	0.09
RSS–RO	$-0.215 \pm 0.058^{**}$	0.08
STAR–RO	$-0.242 \pm 0.071^{**}$	0.10
	30.0°N to 70.0°N	
RAOBCORE–RO	$+0.014 \pm 0.061$	0.09
RICH–RO	$-0.125 \pm 0.063^{**}$	0.09
UAH–RO	$-0.256 \pm 0.051^{**}$	0.07
RSS–RO	$-0.252 \pm 0.045^{**}$	0.06
STAR–RO	$-0.286 \pm 0.054^{**}$	0.08
	70.0°S to 30.0°S	
RAOBCORE–RO	-0.006 ± 0.139	0.20
RICH–RO	$+0.034 \pm 0.139$	0.20
UAH–RO	$-0.118 \pm 0.055^{**}$	0.08
RSS–RO	$-0.159 \pm 0.052^{**}$	0.08
STAR–RO	$-0.124 \pm 0.056^{**}$	0.08

The study shows the importance of taking into account sampling characteristics of radiosonde data, even in regions where coverage is generally very good (e.g., Northern Hemisphere). Considering the specifics of the datasets, agreement between radiosonde and RO is good, indicating that remaining differences between (A)MSU and RO mainly stem from (A)MSU data.

4 Conclusions

TREMENDOUS efforts in the scientific community have lead to remarkable knowledge of the processes involved in the climate system of the Earth. While this knowledge strengthens the confidence in future projections of climate changes on Earth, there are still many open questions left. Since today's changes in the climate system happen very fast compared to similar events in Earth's history, a detailed knowledge is urgently needed to guide society and policy-makers in their decisions and to better prepare for the future.

One of these open questions is concerned with upper-air climate change. Important details of how upper-air climate reacts under the influence of increasing anthropogenic greenhouse gas concentrations are still under debate. The conventional existing observations were never intended to provide records of climate quality, and existing upper-air data from observations, climate models and reanalyses show large uncertainty ranges in their trend values, many of them even disagree in important aspects.

The synopsis and in particular the scientific publications presented in this thesis intend to help analyzing the current situation. An innovative approach to deal with large atmospheric datasets is presented: Interactive visual exploration is shown to be a valuable tool to complement classical statistical methods. It opens new opportunities for data analysis because it does not require prior knowledge of data characteristics, thus enabling the user to come up with new hypotheses about the data. The methodology originates in the general field of data mining, concerned with identifying useful patterns in large datasets. Interactive visual exploration is well suited to iteratively and interactively browse a multi-dimensional parameter space, thus assisting in a) quickly understanding the data characteristics; b) identifying deficiencies in the data; c) easily focusing on subsets of the data containing interesting information; and d) coming up with new hypotheses which can then be tested by classical statistical methods.

In Paper A, the basic concepts and a suitable software framework for interactive visual exploration are introduced and applied to model and reanalysis datasets. In Paper B, the methodology is discussed from the point of view of visualization scientists, with special focus on the aspect of generating new hypotheses using interactive visual exploration. Paper C combines the complementary potential of visual exploration and classical statistics, and applies the concepts to model data, reanalysis data and Global Positioning System (GPS) Radio Occultation (RO) satellite data.

For further insight into upper-air climate change, GPS RO satellite data then are used to compare the conventional upper-air observational systems with these new high-accuracy measurements in Paper D. The capability of GPS RO for climate monitoring

has been assessed in a range of studies before; in this thesis the dataset is employed as reference for stratospheric radiosonde and (Advanced) Microwave Sounding Unit ((A)MSU) climatologies. Special care is taken to account for sparse sampling in the radiosonde and GPS RO climatologies, allowing for the first time a comparison of such zonal-mean climatologies. Significant differences between the datasets are found and analyzed. The advantages of homogeneously distributed observations with high vertical resolution and accuracy are discussed. The importance of an independent reference observational system such as GPS RO for other upper-air datasets is thus evident. GPS RO has the potential to overcome problems of former generations of upper-air datasets.

Part II

Published papers

Publications Overview

THREE first-author research papers and one second-author paper presented in this part contain the main scientific outcome of this thesis.

Paper A Interactive visual exploration is introduced as a novel approach to gain information of large multi-dimensional climate datasets. Simulation Visualization (SIMVIS) is presented as suitable software framework for visual exploration.

Contribution: This work was done in collaboration with the SimVis GmbH, Vienna, Austria. They provided the software framework (SIMVIS) and supported its use, also by providing incremental updates. J. Kehrer, who is also first author of Paper B, provided an extension to SIMVIS to improve the representation of time series. I wrote the manuscript and performed the analysis, both with valuable input from the co-authors.

Citation: F. Ladstädter et al. (2009). "SimVis: An Interactive Visual Field Exploration Tool Applied to Climate Research." In: *New Horizons in Occultation Research: Studies in Atmosphere and Climate*. Ed. by A. K. Steiner et al. Berlin Heidelberg: Springer, pp. 235–245. DOI: 10.1007/978-3-642-00321-9_19

Paper B This work focuses on demonstrating how visual exploration is able to rapidly generate hypotheses about unknown climate datasets, using new visualization and interaction techniques available in SIMVIS.

Contribution: First author of this publication is J. Kehrer from the University of Bergen, Norway. He wrote most of the manuscript and was the principal researcher for the part of research dealing with visualization. Support for the visualization again came from SimVis GmbH, Vienna, Austria, who provided the software framework. I was the principal researcher for the part dealing with climate research, I contributed parts of the manuscript and figures, and provided support for climate science and feedback for the manuscript, together with other co-authors.

Citation: J. Kehrer et al. (2008). "Hypothesis Generation in Climate Research with Interactive Visual Data Exploration." In: *IEEE Transactions on Visualization and Computer Graphics* 14.6, pp. 1579–1586. DOI: 10.1109/TVCG.2008.139

Paper C Visual exploration techniques are applied to various upper-air climate datasets, including GPS RO. The complementary potential of visual exploration and classical statistics is analyzed. The direct and interactive access to data characteristics is

shown to support the process of analyzing large atmospheric datasets in a fast and effective way, and with the potential to spot features of the data which might have been overlooked in classical statistics.

Contribution: This work was done in collaboration with the SimVis GmbH, Vienna, Austria, and the University of Bergen, Norway. I was the principal researcher, wrote the manuscript and did the analysis. The co-authors provided support for the software platform SIMVIS, as well as valuable input for the analysis and the manuscript.

Citation: F. Ladstädter et al. (2010). "Exploration of Climate Data Using Interactive Visualization." In: *J. Atmos. Ocean. Tech.* 27.4, pp. 667–679. DOI: 10.1175/2009JTECHA1374.1

Paper D Conventional upper-air climate datasets are compared to GPS RO in the stratosphere, showing the potential of GPS RO to act as reference climate dataset. Sampling characteristics for radiosondes and GPS RO are accounted for in the respective climatologies.

Contribution: I wrote the manuscript and performed the analysis. The University of Vienna provided appropriate radiosonde datasets for the analysis. The co-authors provided valuable support and input for the analysis and the manuscript text.

Citation: F. Ladstädter et al. (2011). "An assessment of differences in lower stratospheric temperature records from (A)MSU, radiosondes, and GPS radio occultation." In: *Atmos. Meas. Tech.* 4, pp. 1965–1977. DOI: 10.5194/amt-4-1965-2011

PAPER A

SimVis: An Interactive Visual Field Exploration Tool Applied to Climate Research

F. Ladstädter[1], A.K. Steiner[1], B.C. Lackner[1], G. Kirchengast[1], P. Muigg[2], J. Kehrer[2], and H. Doleisch[2]

[1]Wegener Center for Climate and Global Change (WEGC) and Institute for Geophysics, Astrophysics, and Meteorology/Inst. of Physics (IGAM/IP), University of Graz, Austria
[2]VRVis Research Center, Vienna, Austria

ABSTRACT

CLIMATE research often deals with large multi-dimensional fields describing the state of the atmosphere. A novel approach to gain information about these large data sets has become feasible only recently using 4D visualization techniques. The Simulation Visualization (SIMVIS) software tool, developed by the VRVis Research Center (Vienna, Austria), uses such techniques to provide access to the data interactively and to explore and analyze large three-dimensional time-dependent fields. Non-trivial visualization approaches are applied to provide a responsive and useful interactive experience for the user. In this study we used SIMVIS for the investigation of climate research data sets. An ECHAM5 climate model run and the ERA-40 reanalysis data sets were explored, with the ultimate goal to identify parameters and regions reacting most sensitive to climate change, representing robust indicators. The focus lies on the Upper Troposphere–Lower Stratosphere (UTLS) region, in view of

This article was published in *New Horizons in Occultation Research: Studies in Atmosphere and Climate.* Ed. by A. K. Steiner, B. Pirscher, U. Foelsche, and G. Kirchengast. Berlin Heidelberg: Springer, 2009, pp. 235–245. DOI: 10.1007/978-3-642-00321-9_19

future applications of the findings to Radio Occultation (RO) climatologies. First results showing the capability of SIMVIS to deal with climate data, including trend time series and spatial distributions of RO parameters are presented.

1 Introduction

Since the Upper Troposphere–Lower Stratosphere region reacts sensitively to climate change, the variations of its fundamental parameters such as temperature, geopotential height of pressure levels, and refractivity are promising candidates for monitoring the climate. All these key parameters are provided by RO observations with high quality in the UTLS and have high potential for climate analysis and monitoring (e.g., Leroy et al. 2006; Steiner et al. 2007; Foelsche et al. 2008b,a, 2009) and shall be explored to find the most favorable indicators for monitoring global atmospheric change. Due to the limited time period of available acro data (available on a continuous basis only since September 2001) the parameters are explored in both reanalysis and General Circulation Model (GCM) data first. Climate models such as the Fifth-Generation ECMWF–MPI-M Hamburg (ECHAM5) of the Max Planck Institute for Meteorology (MPI-M) Hamburg provide long-term climate scenarios and are used over the time frame 1961 to 2064. Reanalysis data, e.g., the 40-yr ECMWF Reanalysis (ERA-40) data set of the European Centre for Medium-Range Weather Forecasts (ECMWF), are used from 1961 onwards, with special focus on the time period after 1979 when satellite data were assimilated.

Complementary to classical trend testing methods to find the indicators of choice (Lackner et al. 2009), a novel approach to visually explore the climate data sets is used in this study. The interactive visual analysis tool SIMVIS (Doleisch et al. 2003; Kehrer 2007) has been developed with special focus on dealing with large data sets, which makes it particularly well applicable to the data fields occurring in climate research. In SIMVIS, different aspects of the whole data set can be concurrently analyzed in multiple linked views. The sophisticated feature specification tools of SIMVIS provide a way to interactively select regions of interest (the so-called *features*) in time and space. These techniques are used to gain an overview over all data sets, to easily reveal deficiencies in the data, and to localize regions of trends with high signal-to-noise ratio. No prior knowledge of the fields needs to be presumed, and no subset needs to be preselected, since the data can be explored as a whole at once. Interesting features can be specified while interactively exploring the field. These characteristics can be regarded as the main advantages compared to classical statistical methods.

Section 2 gives a brief description of the data sets used in this study. In Sect. 3 the SIMVIS software tool is presented and its application to climate data is explained. The results of the data set exploration are shown in Sect. 4, and conclusions are drawn in Sect. 5.

2 Data

The data sets explored are an ECHAM5 Special Report on Emission Scenarios (SRES) A2 simulation (MPI-M Hamburg, Roeckner et al. (2003)) for the 4th Assessment Report of the Intergovernmental Panel of Climate Change (IPCC AR4) for the time period 1961 to 2064 and ERA-40 (obtained from the ECMWF data server, Simmons and Gibson (2000)) for the time period 1961 to 2002, respectively. Regarding the ECHAM5 A2 run starting 2001, the ECHAM5 IPCC 20th century run complemented the data before 2001.

The native resolutions were $1.875° \times 1.875°$ on 16 pressure levels for ECHAM5 and $2.5° \times 2.5°$ on 23 pressure levels for ERA-40, respectively. To obtain easy comparability, the data were regridded to a common $2.5° \times 2.5°$ grid in latitude and longitude and to 18 pressure levels ranging from 1000 hPa to 10 hPa. Due to the limited representation of the 10 hPa level in ECHAM5 (Cordero and de Forster 2006), this upper boundary model level is not used in this study, and the highest level effectively interpreted becomes the 20 hPa level for ECHAM5.

In this study we concentrate on seasonal (northern) summer means (JJA), exploring the parameters temperature and refractivity from the ECHAM5 A2 run and geopotential height and temperature from ERA-40, respectively. Decadal averages and trends were generally used, i.e., 1966 to 2059 effective time span for ECHAM5 and 1966 to 1997 for ERA-40, respectively.

3 Method

To apply the feature-based visualization technique of SIMVIS to climate data, additional derived parameters were investigated. In this section the elements and terminology of SIMVIS are presented, followed by a description of how to apply those key elements to the climate data sets.

3.1 SimVis–The Simulation Visualization Tool

SIMVIS is a research software framework that was developed for the interactive visualization and analysis of complex (4D, multi-variate) data resulting from Computational Fluid Dynamics (CFD) simulations, e.g., the injection and combustion processes in car engines (Doleisch et al. 2005; Schmidt et al. 2005a). The key elements of this software framework such as *interactive feature specification and visualization*, *brushing*, *linked views*, *focus+context visualization*, *derived data*, or different types of *views*, are described in the following.

Feature-Based Visualization and Brushing

SIMVIS uses a *feature-based visualization* approach. This type of visualization is characterized by the possibility to focus on especially interesting subsets of the data, the so-called *features*. To give to the user the opportunity to interactively select features becomes increasingly important when dealing with larger data sets. In SIMVIS the user can specify features by a *brushing* mechanism in different views such as scatterplots and histograms. Brushing simply means to select data points directly on the screen (e.g., using the mouse), thus assigning a *Degree of Interest (DOI)* attribute to each data point. The DOI can be either 0 or 1 in the case of a discrete feature classification. In SIMVIS also fractional values of the DOI are possible, representing a "fuzzy" selection (Doleisch and Hauser 2002).

In the different views the user can select data attributes (variables) of interest (e.g., the temperature), which either stem directly from the imported data set or are derived attributes (e.g., the temperature trend).

Linked Views

Another important concept is the use of multiple, linked views. Different aspects of the data set are shown in several views side by side. Brushing in one view is immediately propagated to all other views (Doleisch 2004). Thus changing the selection in one of the views is immediately reflected in all other views, using a different coloring scheme for the selected data points. Visualizing different attributes (e.g., climate state variables or diagnostic variables derived from them) in the views easily reveals correlations as well as other distinctive features between the data attributes.

Focus+Context Visualization, 3D View

The 3D view is a core component of the visualization system and allows the user to orientate both in space and time (if time-dependent data is available). SIMVIS uses a *focus+context (F+C)* visualization (Hauser 2005): according to the DOI value, each data item is either drawn in an emphasized way (being *in focus*) or in a reduced style (e.g., transparent gray in the 3D view). This distinction is consistent through the linking in all views, but plays an especially important role in the 3D view (Fig. 1). The user can easily distinguish between the relevant data with high degree of interest (colored) and the context (in gray) in which it is located.

Derived Data

In order not to limit the user only to the data attributes (variables) already available in the imported data set itself, SIMVIS provides the possibility to perform certain mathematical operations on the existing attributes. This concept is very flexible and easily extendable

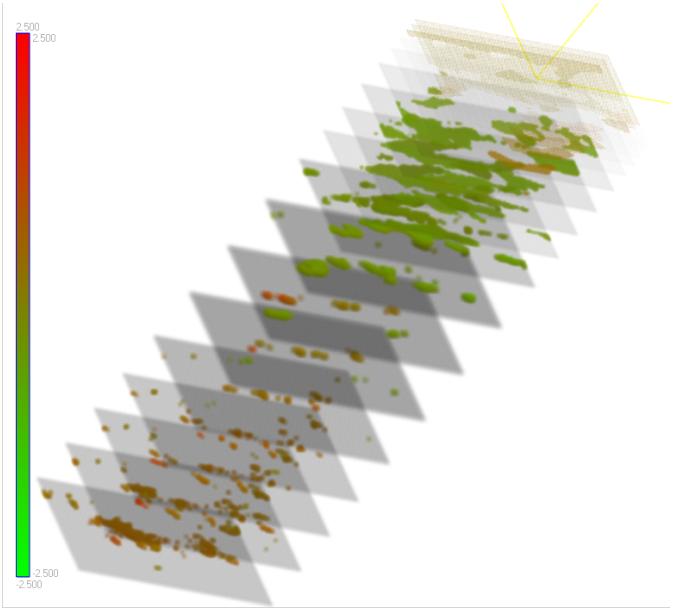

Figure 1: SIMVIS 3D view. Shown is the trend in refractivity in the ECHAM5 data set for the year 2044 (seasonal summer means), for all pressure levels ("sheets") from 1000 hPa to 20 hPa; each "sheet" itself is a latitude-vs.-longitude slice. Data points with high values of the signal-to-noise ratio (see Sect. 3.2) are selected ("in focus") and colored.

in the SIMVIS system. Currently available formulae include, for example, temporal and spatial gradients, data smoothing, elementary algebraic expressions, and normalizations.

Types of Views

There are several types of views available in SIMVIS, the most important ones being scatterplot, histogram, curve, and 3D view. In scatterplot and histogram views selections can be made via the brushing mechanism explained above. The curve view (Kehrer 2007; Muigg et al. 2008) shows the variation in time of each data point, drawn on top of each other. In this view, advanced brushing mechanisms can be applied, such as selecting all curves going through a certain volume in time and parameter space. The 3D view is a *passive* view (i.e., no selections can be made here) displaying the specified features using F+C visualization. Here, interaction in space and time as well as viewing perspective changes are available.

3.2 SimVis Application to Climate Data

To apply the techniques of feature-based visualization to climate data sets, we need to think about what to consider as features of special interest. The basic parameters

available such as temperature, refractivity, and geopotential height have rather well-known dependencies between each other, so additional insight is anticipated mainly from investigating newly derived parameters.

Two derived parameters are considered: The linear trend calculated as a moving 10-years-difference and the Signal-to-Noise Ratio (SNR) defined as the ratio of the trend to the detrended standard deviation. To detect and explore regions sensitive to climate change in time and space, the features of interest are composed of high values for the linear trend while maintaining a high SNR. To obtain these features the following parameters are generated:

- Smoothed Data y^{av}: To generate the linear trend the data y is first smoothed using a moving arithmetic average with an averaging timeframe of 11 years.
- Linear Trend b: The linear trend per year b_i (where i denotes the center year of the current timeframe) is calculated as a moving 10-years difference between the data of year $i+5$ and year $i-5$ (Eq. 1). Due to the exponential character of the refractivity with height, the relative trend (in %) is generated in this case in relation to the first value of the current timeframe (Eq. 2).

$$b_i = \frac{1}{10}(y^{\mathrm{av}}_{i+5} - y^{\mathrm{av}}_{i-5}) \tag{1}$$

$$b^{\mathrm{rel}}_i = \frac{100}{y^{\mathrm{av}}_{i-5}}\frac{1}{10}(y^{\mathrm{av}}_{i+5} - y^{\mathrm{av}}_{i-5}). \tag{2}$$

- Linear Trend Fit Curve y^{FIT}: The trend fit curve for each 11-years timeframe is calculated using the above difference b_i as the slope:

$$y^{\mathrm{FIT}}_{ij} = y^{\mathrm{av}}_{i-5} + [j-(i-5)]\, b_i, \tag{3}$$

  where i is the center year of the current 11-years timeframe and j runs from $i-5$ to $i+5$.

- Detrended Standard Deviation s: The fitted trend curve is removed from the original data y to obtain the detrended standard deviation for the current timeframe:

$$s_i = \left[\frac{1}{11-2}\sum_{j=i-5}^{i+5}\left(y_j - y^{\mathrm{FIT}}_{ij}\right)^2\right]^{\frac{1}{2}}. \tag{4}$$

- Signal-to-Noise Ratio (SNR): Finally, the signal-to-noise ratio is defined as the ratio of the trend to the standard deviation:

$$\mathrm{SNR}_i = \frac{b_i}{s_i}. \tag{5}$$

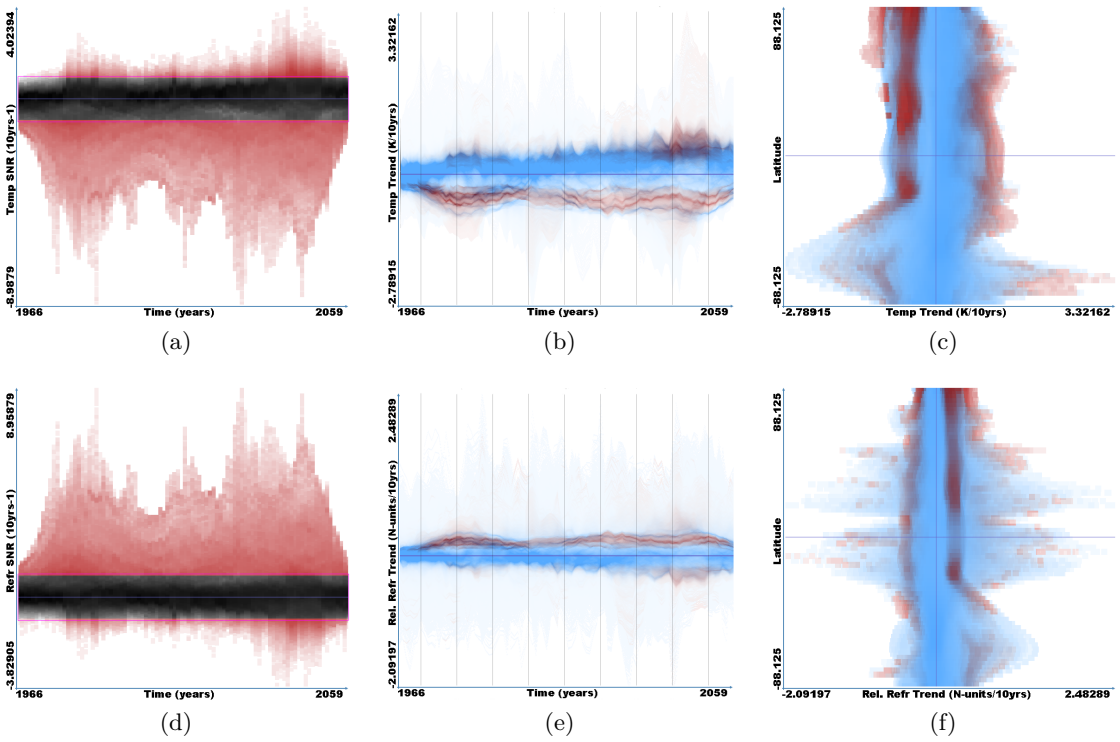

Figure 2: ECHAM5 A2, temperature (in K) in (a)–(c) and refractivity (in N-units) in (d)–(f): Selection of high values of SNR in (a)/(d), the corresponding pattern in the trend variation over time in (b)/(e), and the trend distribution vs. latitude in (c)/(f) are depicted. $|\text{SNR}| \geq 1$ shown in red.

4 Results

A selection of screenshots showing different aspects of the data using the derived parameters described in Sect. 3.2 (trends/10 years and SNR/10 years, respectively) is presented in Figs. 2 and 3 for the ECHAM5 model and in Figs. 4 and 5 for the ERA-40 reanalysis data, respectively. The color intensity depicts the density of the value in the whole data set. Features selected in several views are depicted in red, features selected only in the current view are shown in blue, and context information in black.

The distribution of the signal-to-noise ratio for each time-step for temperature and refractivity is shown in Figs. 2a and 2d, respectively. Selected are values of the $|\text{SNR}| \geq 1$. This selection is carried out directly in the scatterplot using the brushing mechanism described in Sect. 3.1. Any change in this selection (or in any of the subsequently described ones) is immediately propagated into all other views. In Figs. 2b and 2e, the variation of the linear trend (relative trend for the refractivity) over time is shown using

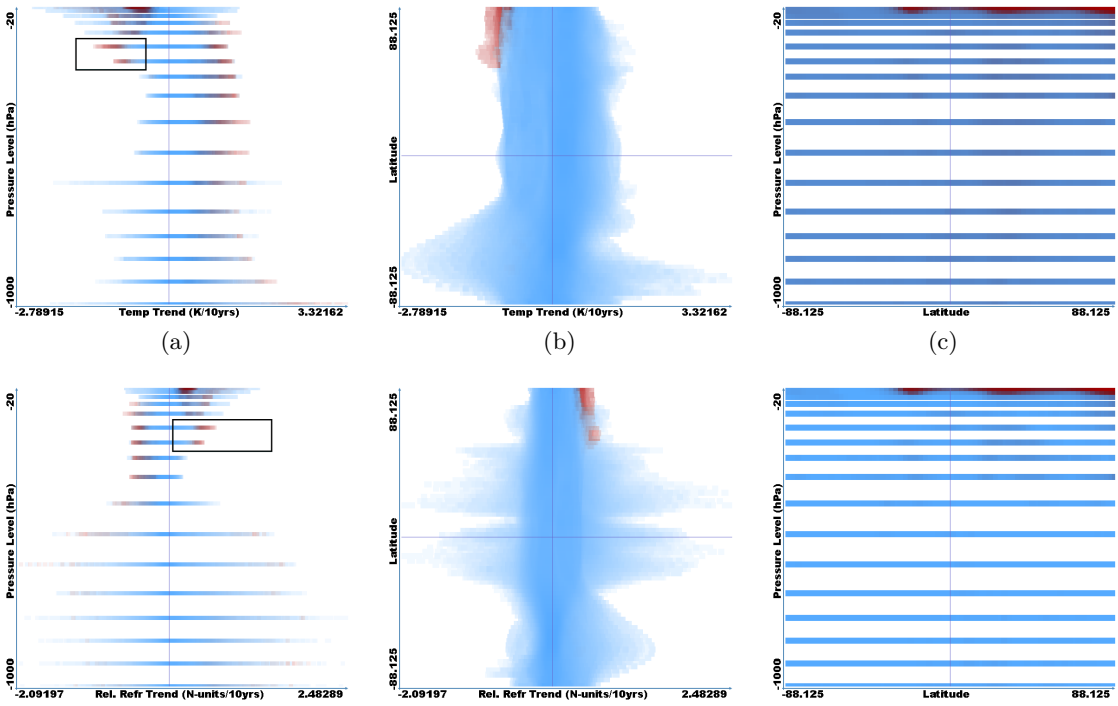

Figure 3: ECHAM5 A2, temperature (in K) represented in (a)–(c) and refractivity (in N-units) in (d)–(f): Selection of one specific feature ((a)/(d), denoted by rectangle box) and the corresponding trend distribution versus latitude in (b)/(e); overview latitude vs. pressure level plot, again without rectangle box selection in (c)/(f), $|\text{SNR}| \geq 1$ shown in red.

the curve view. The additional constraint of selecting high SNR values reflects in the red colored curves. The inversely proportional behavior of temperature and refractivity is clearly observed. Note that the negative temperature (positive refractivity) trend with high significance (high SNR) is prominent over the whole time period, compared to the positive temperature (negative refractivity) trend with high significance only visible in later time periods.

The trend distribution with latitude in Figs. 2c and 2f shows, among other things, that points with high trend values are often also associated with comparably low SNR values (in blue).

The height distribution in Figs. 3a and 3d shows that positive temperature (negative refractivity) trends stem from the troposphere, and that the negative temperature (positive refractivity) trends stem from the upper pressure levels corresponding to the lower stratosphere region, as expected. The SNR-selected data points are marked in red again. Specific selection (rectangle box) is now imposed for negative temperature

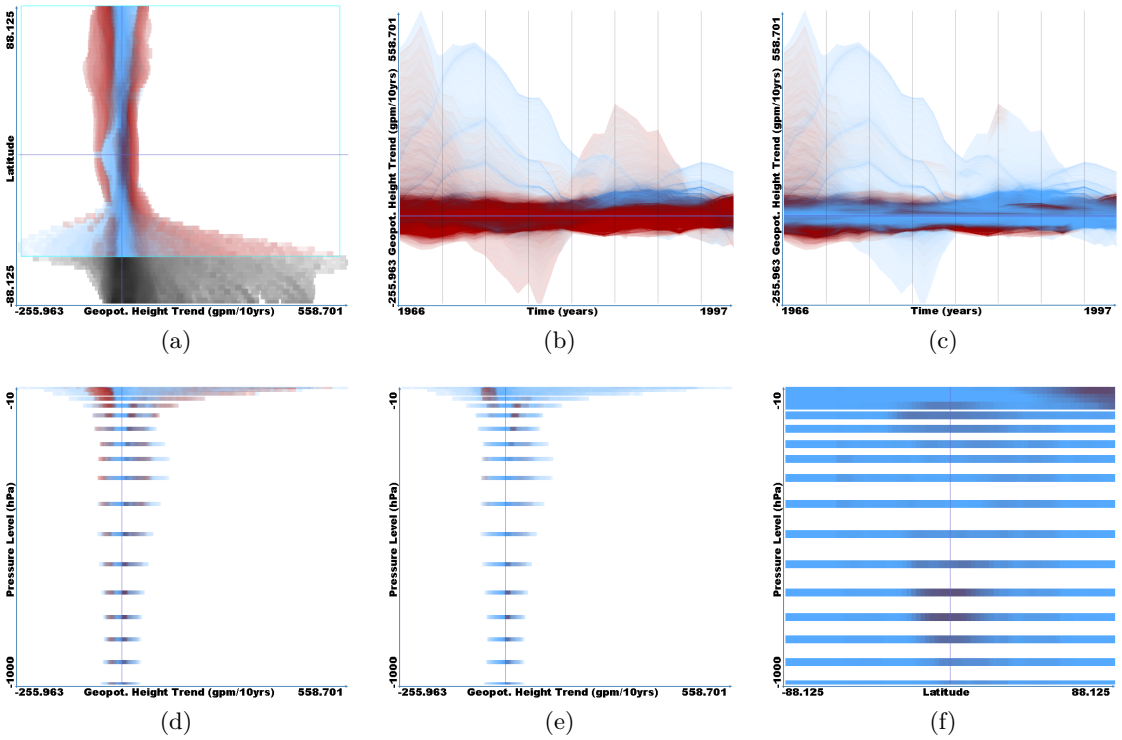

Figure 4: ERA-40, geopotential height trend (in gpm/10 years): Exclusion of southern high latitudes in black, high SNR in red in (a); resulting trend variation over time, selected latitudes in red in (b); additional selection of $|\mathrm{SNR}| \geq 1$ in (c) and (d); additionally restriction to post-1979 time period in (e) and (f).

(positive refractivity) trends at the 150 hPa and 200 hPa levels. With this new selection applied, the red-colored trend distribution with latitude changes from Figs. 2c/2f to what is shown in Figs. 3b/3e. It can be observed that the significant trend features stem only from northern high latitudes, where they are well inside the stratosphere, as expected.

An overview of the spatial distribution of data points with $|\mathrm{SNR}| \geq 1$ (without rectangle box selection) is gained in the plots 3c and 3f, where pressure levels versus latitude are plotted. Values with high SNR are in particular found at the topmost levels (20 hPa to 30 hPa) in the ECHAM5 model run, corresponding to robust negative temperature (positive refractivity) trends in the lower stratosphere observable over the whole investigated time period (see Figs. 2b/2e). Note that at low levels with weaker $|\mathrm{SNR}| \geq 1$ presence, the red color dots are effectively "buried" in the predominant blue color dots (visible on the screen, though).

For the ERA-40 reanalysis the distribution of the geopotential height trend with latitude in Fig. 4a (again $|\mathrm{SNR}| \geq 1$ in red) shows high trend variation in southern high latitudes,

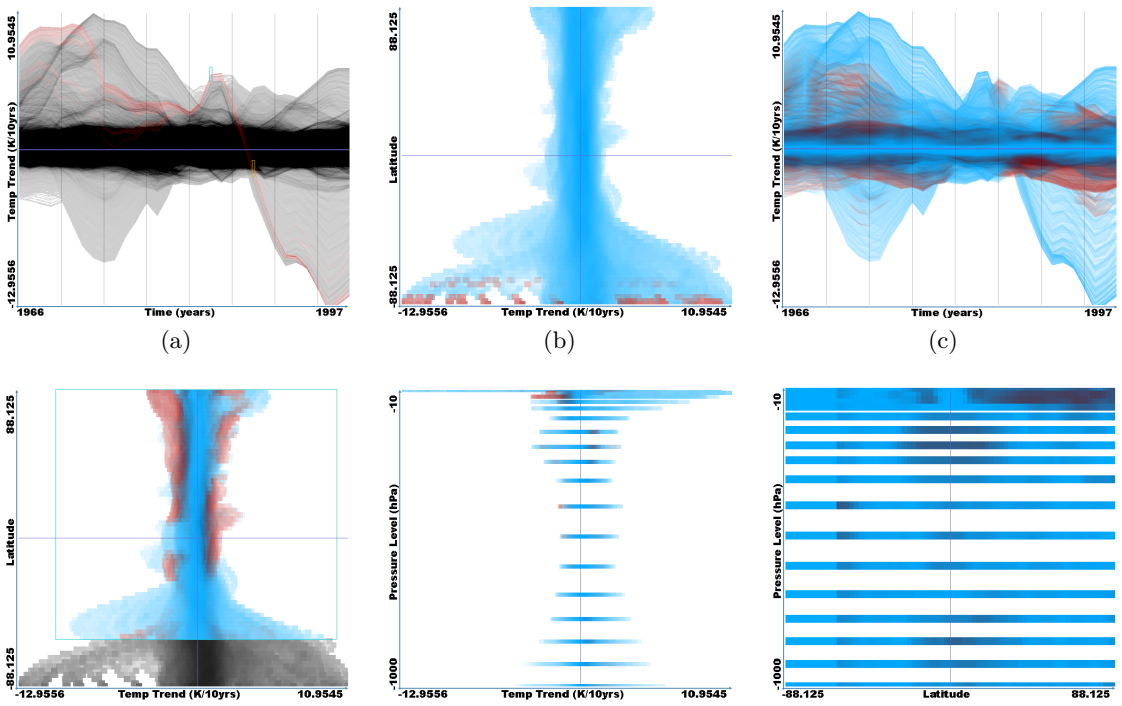

Figure 5: ERA-40, temperature trend (in K/10 years); selection of a confined trend curve ensemble in red in (a); corresponding latitude vs. trend distribution in (b); exclusion of southern high latitudes and $|\text{SNR}| \geq 1$ values in (c); restrict additionally to post-1979 in (d)–(f).

which is a spurious feature according to Santer et al. (2004). The selection was restricted to data over 90°N to 60°S accordingly. The resulting time variation of the geopotential height trend shown in Fig. 4b (only the latitude selection applies here) now has most outliers removed, with the remaining data points in red. Applying the selection of $|\text{SNR}| \geq 1$ values again further improves the result (Fig. 4c), with some outliers still present in the early years of the data set. The same selections apply for the plot in Fig. 4d, still showing a somewhat ambiguous distribution with pressure levels. Restricting to the post-1979 era when satellite data were assimilated (Uppala et al. 2004) displays a better-contrasted height distribution in Fig. 4e. The pressure levels versus latitude plot (Fig. 4f) is based on all selections described above and presents best SNR for the lower stratosphere at northern high latitudes (negative trends, see Fig. 4e) and the lower tropical troposphere (positive trends, partly up to the lower stratosphere), respectively.

High variation of the ERA-40 temperature trends in time is observed in Fig. 5a. Some of the temperature trend curves showing the highest variation over time are selected in the curve view (red) and analyzed further. The corresponding latitude distribution of the

trend in Fig. 5b reveals that it is a spurious feature since it stems from the southern high latitudes. Restricting to 90°N to 60°S and selecting $|\mathrm{SNR}| \geq 1$ (deselecting the curve ensemble before) leads to the trend variation in Fig. 5c. Limiting the time period to the post-1979 era further removes highly variable trends and yields the spatial distributions depicted in Figs. 5d to 5f. As seen in Fig. 5f, high SNR (in red) appears in the lower stratosphere region at northern high latitudes for negative trends and in the tropical upper troposphere for positive trends (again, the latter feature is better visible on the screen).

5 Conclusions and Outlook

Using data sets from the ECHAM5 model and the ERA-40 reanalysis we analyzed atmospheric parameters accessible to RO measurements with focus on the UTLS region. We presented the investigation of these large climate data fields using a novel visualization method. The interactive visual field exploration tool SIMVIS enables the exploration of the whole data set at once and interesting features can be interactively selected by the user.

The utility of this method was demonstrated on the basis of the localization of trends with high SNR in space and in time. Temperature and refractivity from the ECHAM5 model run show robust and sensitive trends in the lower stratosphere region over the whole investigated time period, with considerable contributions from the upper troposphere. Deficiencies in the ERA-40 reanalysis, analyzed in geopotential height and temperature, at southern high latitudes and in early years of the pre-satellite era could be detected. Regions of high SNR reside in the lower stratosphere at northern high latitudes and in the tropical lower troposphere. Ongoing work focuses on the application of the findings to RO observations, the intercomparison of multiple climate model fields, and detailed classical statistical analysis in domains of interest.

Acknowledgement We acknowledge the IPCC climate modeling groups for providing their data for analysis, the Program for Climate Model Diagnosis and Intercomparison (PCMDI) for collecting and archiving the model output, and the JSC/CLIVAR Working Group on Coupled Modelling (WGCM) for organizing the model data analysis activity. The multi-model data archive is supported by the Office of Science, U.S. Department of Energy. This work was funded by the Austrian Science Fund (FWF) Project INDICATE P18733-N10.

PAPER B

Hypothesis Generation in Climate Research with Interactive Visual Data Exploration

Johannes Kehrer,[1] Florian Ladstädter,[2] Philipp Muigg,[3]
Helmut Doleisch,[3] Andrea Steiner,[2] and Helwig Hauser[1]

[1]Department of Informatics, University of Bergen, Norway
[2]Wegener Center for Climate and Global Change (WegCenter) and Institute for Geophysics, Astrophysics, and Meteorology (IGAM), University of Graz, Austria
[2]VRVis Research Center and SimVis GmbH, Vienna, Austria

ABSTRACT

One of the most prominent topics in climate research is the investigation, detection, and allocation of climate change. In this paper, we aim at identifying regions in the atmosphere (e.g., certain height layers) which can act as sensitive and robust indicators for climate change. We demonstrate how interactive visual data exploration of large amounts of multi-variate and time-dependent climate data enables the steered generation of promising hypotheses for subsequent statistical evaluation. The use of new visualization and interaction technology—in the context of a coordinated multiple views framework—allows not only to identify these promising hypotheses, but also to efficiently narrow down parameters that are required in the process of computational data analysis. Two datasets, namely an ECHAM5 climate model run and the ERA-40 reanalysis incorporating observational data, are

This article was published in *IEEE Transactions on Visualization and Computer Graphics*, 14.6 (2008), pp. 1579–1586. DOI: 10.1109/TVCG.2008.139. The work was also presented by the main author at VisWeek 2008, Oct. 19–24, Columbus Ohio, US. An error in equation 2 has been corrected here.

investigated. Higher-order information such as linear trends or signal-to-noise ratio is derived and interactively explored in order to detect and explore those regions which react most sensitively to climate change. As one conclusion from this study, we identify an excellent potential for usefully generalizing our approach to other, similar application cases.

1 Introduction

We can see that climate change has become a broadly discussed topic—politics, business, and also the general public engage with climate issues in parallel to the work of scientists. Of course, it is prediction which is the most important related aspect—but similar to weather research it is difficult to come up with deterministic results. In this study, we investigate whether we can identify particular subsets in climate data—both in time and space—that potentially represent sensitive and robust *indicators* of atmospheric climate change which possibly have strong predictive power with respect to the long-term development of our Earth's climate. We work with two representative datasets to draw our conclusions.

Improved measurement records (e.g., satellite observations) as well as extensive simulations commonly result in large, time-dependent, and multi-variate datasets which are difficult to manage. Visualization has proved to be very useful for gaining insight into such large and complex data. Three main classes of use cases or application goals can be identified (Schumann and Müller 2000), namely (1) visual exploration; (2) interactive visual analysis or confirmative visualization; and (3) presentation (or dissemination).

In our case, we utilize interactive visualization primarily for the early, more explorative steps (compare also to Tukey (1977)). Comparable to the "discover the unexpected"™, as coined by Thomas and Cook (2006), we aim at rapidly identifying *promising hypotheses* that afterwards are checked in an analytical, confirmative process (in our cases mostly handled by statistics). Generally, we think that it is easier for visualization to unfold its maximal utility in the context of undirected exploration (as compared to the analysis of clearly specified application questions)—and that, even though we have seen a number of cases where visualization facilitated interactive analysis very effectively (Doleisch et al. 2004a; Laramee et al. 2005; Rübel et al. 2006).

While *computational approaches* such as statistics conveniently provide good means to accurately—and also quantitatively(!)—check specifically formulated hypotheses, it is generally quite challenging to actually derive these specific application questions. Intuition of experts—based on experiences and knowledge gained from many years—leads to promising hypotheses as well as scientific trial-and-error approaches. The emerged availability of powerful visualization technology now turns into substantial support for this important step in scientific work. Instead of cumbersomely searching within many dimensions and extensive content, we effectively shed light onto complex relations within

multi-variate data by interactive visual exploration. By looking at the data (and the implicit relations within the data) and by integrating domain knowledge, the user is able to efficiently narrow down on interesting aspects of the data, which is usually achieved in an *iterative process* of repeated visualization and interaction steps. Subsequent analysis is thereby fed with well-informed hypotheses, thus resulting in a streamlined overall process with fewer large-cycle iterations.

In addition to the important step of identifying hypotheses in the first place, it also turns out to be important to identify the right *parameter settings* and/or *boundary conditions* for the statistical analysis, especially if there are multiple parameters that influence the process. It is one characteristic of modern scientific methodology that it is now possible to vary many more parameters than ever before. While this is useful for a more varied and more detailed analysis, it also generates the significant challenge of managing all this variability. Since parameters also often influence each other, meaning that we usually cannot utilize separability to efficiently identify optimal parameters (one by one), we again welcome support as offered by interactive visualization to act in a more informed, direct way.

In this paper, we demonstrate how interactive visual exploration is used to identify certain regions in space and time which are sensitive to climate change. Even though we successfully used the here employed visualization technology in conjunction with all three types of application questions (confirmation, exploration, presentation), we focus on hypothesis generation in this paper. For analysis, the identified regions are then statistically evaluated. Visual exploration is also used to narrow down the parameter ranges that affect the computational analysis. The entire datasets can be explored at once without the need to preselect certain subsets, as this is done, e.g., in classical trend testing (Lackner et al. 2009).

The remainder of this paper is organized as follows: section 2 gives a brief introduction to the here investigated questions of climate research. In section 3 the employed visualization technology is described. Several concrete details of this application are presented and discussed in Sec. 4. Finally, the paper is concluded in section 5.

2 Climatological Background

Climate research is concerned with the analysis of the climate system—composed of the atmosphere (compare to Fig. 1), the hydrosphere, cryosphere, lithosphere, and the biosphere—, its variability and its long-term behavior (Wallace and Hobbs 2006). The currently most prominent topic in climate research is the investigation of *climate change*, its detection and attribution, whether naturally or anthropogenically induced.

For this purpose, we are interested in determining characteristic spatial and temporal *climate signals* which can be attributed to some cause such as, for example, anthropogenic forcing. These signals are compared with the climate noise to assess the *significance*

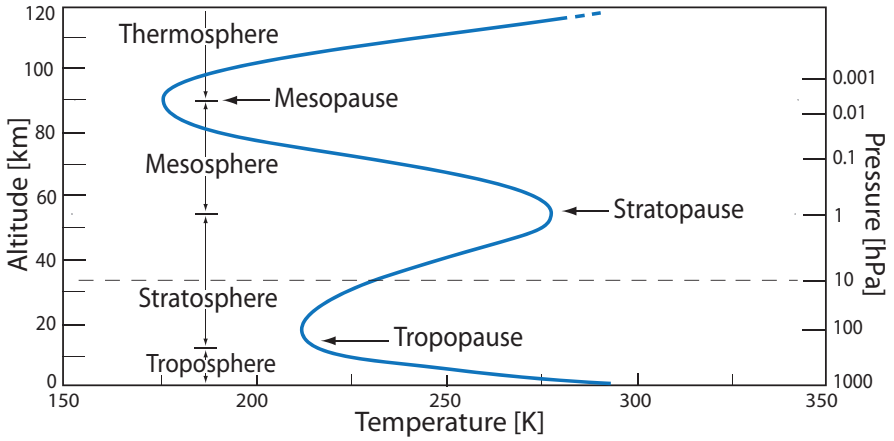

Figure 1: Illustration of the vertical thermal structure of the atmosphere, reflecting a balance between radiative, convective and dynamical heating and cooling processes of the surface-atmosphere system. Different layers of the standard atmosphere are shown (illustration adapted from Melbourne et al. (1994)). Changes in the upper troposphere-lower stratosphere region have strong impact on the Earth's climate system (Wallace and Hobbs 2006).

of the findings. The signal should deviate substantially from the noise to be of use for detecting climate change.

It is not yet completely clear, which physical variable describing the state of the atmosphere is best suited as a sensible parameter for detecting climate change. Previous work mostly concentrates on the surface temperature, not at the least because of the availability of long-term records. With the advent of radiosonde and satellite-based measurements as well as global climate modeling in the last decades, data for upper air atmospheric variables are also available (Solomon et al. 2007b). Key *climate parameters* such as temperature, pressure, humidity, or geopotential height can be accessed and are among the candidates to provide a sensitive indicator for atmospheric climate change (Foelsche et al. 2008a; Karl et al. 2006).

In the context of climate research, large multi-variate data fields are commonly investigated. Usually these fields describe the physical state of the atmosphere and can stem from various sources, such as global climate models, reanalysis data (meteorological observations assimilated into a numerical weather prediction model), or measurement records from a single instrument (e.g., satellite data). For climate models, these gridded data can easily constitute a resolution of $1.875° \times 1.875°$ in latitude and longitude, on 16 pressure levels (leading to a grid with about 300K cells), e.g., repeated on 100 time steps.[1]

[1] Note, however, that the datasets used in this study consist of 180K cells given at 108 and 42 time steps, respectively, corresponding to a horizontal resolution of 2.5°x2.5° and 18 pressure levels up to 10hPa (as indicated in Fig. 1).

When it comes to analyzing the data, it is challenging for scientists and practitioners to get a grip on these large time-dependent three-dimensional fields. The common way to gain information is to use classical *statistical methods* such as linear trend regression, multi-variate data analysis, or pattern analysis, to name only three (Wilks 2006). These methods usually require prior knowledge about the data to narrow down the scope of the analysis (e.g., parameters, boundary conditions).

In this study we focus on the temperature and the geopotential height as interesting key atmospheric variables in climate research. While the temperature is easily comprehensible out of every-day experience, the geopotential height deserves a short elaboration: In meteorology and climatology the common measure of height is not the geometric but the geopotential height z, which can be seen as the geometric elevation above sea level corrected by Earth's gravitation:

$$z := 1/g_N \int_0^h g(\phi, h')dh' \tag{1}$$

where g_N is the standard gravity at sea level, ϕ is the latitude, and h is the geometric elevation. The correction is quite small (less than 1% for $h = 50$km), but using z instead of h is the more natural measure in the application: Using in-situ or remote-sensing measurements of the atmosphere, for example, commonly provides the temperature, pressure and humidity, but not the geometric height. Using the barometric formula (relating the pressure with the height), the geopotential height can be derived directly out of these parameters (Wallace and Hobbs 2006). Measuring geopotential heights of constant pressure surfaces has therefore become a common approach in climate science, also because the thermal expansion raises the height of the constant pressure surfaces, providing a key parameter to detect climate change.

We consider the temperature field of one ECHAM5 climate model simulation run[2] (Roeckner et al. 2003) of the A2 scenario simulations for the Intergovernmental Panel on Climate Change (IPCC) 4$^{\text{th}}$ Assessment Report for the time period 1961 to 2064, as well as the geopotential height field of the ERA-40 reanalysis dataset[3] (Simmons and Gibson 2000) for the time period 1961 to 2002, respectively. Since the ECHAM5 A2 scenario simulation starts in the year 2001, it is complemented using the ECHAM5 IPCC 20$^{\text{th}}$ century run before 2001. Using seasonal (northern) summer means (June-July-August) in this example provides us with data without the influence of the seasonal cycle, yielding clear climate signals.

Given this background, we investigate the following *application questions* in this study. We use visual exploration to:

- rapidly generate promising hypothesis, i.e., identify certain regions in space and time which potentially are sensitive to climate change. Thereby we can efficiently

[2] Max-Planck-Institute for Meteorology (MPI-M) Hamburg, Germany.
[3] European Centre for Medium-Range Weather Forecasts, Reading, U.K.

narrow down the parameters and/or boundary conditions for subsequent statistical analysis;

- assess the influence of smoothing parameters and trend time-frames on the findings;
- analyze the relations between certain interesting subsets of data in multiple dimensions.

The here employed modern visualization approach provides us with the unique ability to achieve these tasks faster, and also without the usually needed a priori knowledge about the datasets (i.e., to get support in data exploration).

3 Interactive Visual Data Exploration

The interactive exploration of the climate data in this application has been carried out in a framework employing a coordinated multiple views setup (Doleisch et al. 2003). The area of coordinated and multiple views has been steadily developing over the past fifteen years. A good overview is given by Roberts (2004). A comprehensive overview on visual data mining and visualization techniques with respect to climate data is given by Nocke (2007).

Interactive visual analysis enables users to get into a *visual dialog* with the climate data. The procedure that is usually employed is the following: first an interactive visualization according to user input is generated. This helps the user to gain knowledge about the data, especially in the case of very large and complex datasets. This knowledge often leads to new questions and/or hypotheses, which can be explored and analyzed in more detail in an iterative process. Through interaction the previous visualization results are modified step by step to gain more knowledge and insight into the data. For this process it is crucial, that the tools supporting this knowledge gaining process must be fully interactive and flexible, allowing to query the data in many different ways, even for large datasets.

In this application study we have used and extended the SIMVIS framework (Doleisch et al. 2003). In contrast to many of the previously published coordinated multiple views prototypes, SIMVIS is targeted at interactive PC-based handling of large datasets. The previous development of this technology was targeted at the analysis of 3D time-dependent flow simulation data especially in the automotive field (Doleisch et al. 2004a), but has recently been extended to also cope with various other data types, e.g., measured 3D weather radar data.

In SIMVIS, multiple linked views are used to concurrently show, explore, and analyze different aspects of multi-field data. The different views that are used next to each other include 3D views of volumetric data (grids, also over time), but also several types of attribute views, e.g., 2D scatterplots and histograms. Interactive feature specification

is usually performed in these attribute views. The user chooses to visually represent selected data attributes in such a view, thereby gaining insight into the selected relations within the data. Then, the interesting subsets of the data are interactively brushed directly on the screen (compare also to the XmdvTool (Ward 1994)). The result of such a brushing operation is reintegrated within the data in the form of a synthetic data attribute $DOI_j \in [0,1]$ (*Degree of Interest (DOI)*), compare to Furnas (1986)). This DOI attribution is used in the 3D views of the analysis setup to visually discriminate the interactively specified features from the rest of the data in a focus+context visualization style which is consistent in all (linked) views (Hauser 2005).

In the SIMVIS system, *smooth brushing* (Doleisch and Hauser 2002) (enabling fractional DOI values) as well as the logical combination of brushes for the specification of *complex features* (Doleisch et al. 2003) are supported. A smooth brush results in a trapezoidal DOI function around the main region of interest in the attribute views. Brush attributes and their composition are explicitly represented in the system and can be interactively adjusted through the integration of a fully flexible derived data concept, a data calculator module with a respective graphical user interface—in this study we will benefit from this feature to derive meaningful parameters with respect to climate change. These new attributes can be derived from existing ones and thereafter are available for full investigation in all linked views. Due to the explicit representation of brush attributes as well as all view settings, analysis sessions can be saved and reapplied to other datasets through the use of a *feature definition language* (Doleisch et al. 2003). This enables an easier and faster comparison of different climate simulation runs, for example.

New Extensions to the SimVis Framework

In this study we extended the SIMVIS technology to also work with large climate simulation results, where especially the time-dependent behavior of different attributes is of interest.

To deal with overdrawing and visual cluttering when depicting large amounts of data we developed a *four-level focus+context* visualization (Muigg et al. 2008), with the context information for orientation and also three different levels of focus in every attribute view. The different focus levels result from logical combinations of features, which are specified by the user in a hierarchical scheme based on individual selections. When several colors representing different focus levels are blended together (based on their respective smooth DOI values), it is crucial to have as little color mixing as possible (i.e., avoid the introduction of additional tints). This enables a more straightforward interpretation of the colors and the understanding of corresponding semantics and interrelations of the data. Moreover, the user is enabled to enhance the contrast of the DOI attribution in a view to place emphasis on regions with only a few important data items that otherwise are occluded by large amounts of context data. Therefore, the DOI values used in our color compositing scheme can be enhanced, i.e., $\overline{DOI}_j = DOI_j^{\gamma}$, where γ can be altered by the user within $[0,1]$. Alternatively, the maximum DOI value per screen pixel can

be displayed opaquely on top, allowing to focus only on the features regardless of the relative importance with respect to the overall data.

For the improved visual analysis of the time-dependent climate data, we extended the existing framework with a *function graphs view*, where we depict a scalar function over time for each voxel/cell of a volumetric and time-dependent dataset (Muigg et al. 2008). In our scenario, this can lead to a dense visualization consisting of hundreds of thousands or even millions of function graphs, which are given at a relatively low number of time steps (e.g., 100). Using customizable transfer functions, the number of function graphs passing through each pixel is mapped to the pixel's luminance, which allows a straightforward interpretation of data trends, prominent (visual) structures within the data, and outliers (Johansson et al. 2005; Novotný and Hauser 2006). We use data aggregation (*frequency binmaps* (Novotný and Hauser 2006) which have been extended to incorporate also DOI information) and image space methods to retain the responsiveness even when interacting with such large datasets.

Enhanced brushing techniques were integrated in order to cope with the temporal nature of the data. Time series are classified according to their *similarity* to a user-defined pattern, which can be directly sketched as a polyline by specifying an arbitrary number of control points. Several measurements were incorporated to quantify similarity, including the sum of absolute differences between the gradients (first derivative estimated as forward or central differences) of the function graphs and the target function. The aggregation of differences per time series is then compared to one threshold (for binary classification) or alternatively two thresholds (again with a smooth transition area between focus and context) to obtain fuzzy DOI values.

4 Exploring The Two Climate Datasets

In this section, we demonstrate the interactive visual data exploration in the field of climate research. We use the extended SIMVIS framework to deal with the application questions as introduced in Sec. 2. Our main goal is to rapidly identify promising hypotheses, i.e., certain regions in the atmosphere which are potentially robust indicators for climate change. The emerged hypotheses are then further investigated using statistical analysis (Lackner et al. 2009), and we are able to present some preliminary results already here.

The respective process is illustrated in Fig. 2. Since it is rather difficult to identify the regions sensitive to climate change within the original data, we first derive meaningful parameters. In our case *linear trends* are calculated on smoothed data as moving differences over N years, and the corresponding *Signal-to-Noise Ratio (SNR)* are derived to determine the significance of the respective trends. The computation of these parameters is detailed in Sec. 4.2, and can be performed and altered directly within SIMVIS.[4] The

[4]The derived data, for instance, for the ECHAM5 climate model results in a 2.38 GB dataset, which can

Figure 2: Interactive visual exploration of climate data: Meaningful climate parameters are derived from the original data which are explored interactively in order to form hypotheses. Statistical analysis confirms or rejects the hypotheses. The results from analysis are generally visualized for illustration. In this pipeline each step can also reflect back on previous steps for efficient information drill down.

sensitive areas in space and time for which the anticipated signal emerges out of the climate noise background can be selected and visualized in all available attributes and views.

In an interactive visual exploration process the promising hypotheses can then be rapidly identified (e.g., certain height/pressure layers given at certain latitudes over a certain timespan). The hypotheses can then be confirmed or rejected using classical *least-squares-fitting* of a linear trend over a fixed timespan and pre-defined geographical region (Lackner et al. 2009). The results from statistics can be further explored and illustrated using confirmative visualization. The parameters affecting each step in our scenario (e.g., the timespan over which the linear trend is computed, the parameters affecting the visualization, or the boundary conditions for the statistical analysis) can be altered and narrowed down efficiently in this process. This leads to more insight and deep information drill-down.

4.1 Hypothesis Generation

In order to quickly come up with new hypotheses, which are otherwise difficult to generate, we first have to consider the features which characterize those atmospheric regions in space and time, which are supposed to be sensitive to climate change. These can be determined by a high absolute SNR, where the derived climate signal (i.e., linear trend) exceeds the natural climate variability. In the following, the temperature field of an ECHAM5 climate model run (A2 scenario), and the ERA-40 geopotential height field will be explored.

The ability to browse the whole field without prior knowledge of its characteristics (as usually required when using computational analysis) is advantageous here. By exploring the data as well as derived attributes with interactive visualization, possible field deficiencies (for example common in certain latitude regions for some reanalysis data) can be efficiently detected and consequently taken into account. Without knowing

be interactively explored and also saved to and loaded from the hard disk.

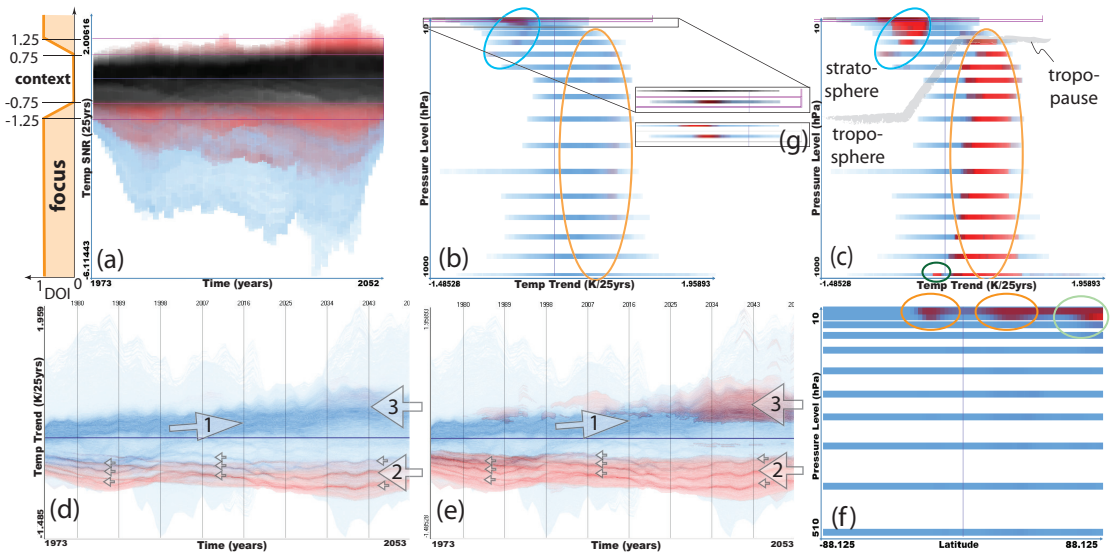

Figure 3: Hypothesis generation using interactive visual exploration of derived temperature parameters in the ECHAM5 climate model. Features selected in multiple linked view are highlighted in red (focus), features only selected in the current view (2^{nd} level focus) depicted in blue, and context information in black (more details in the text).

in advance what the expectations in the data are, interesting features or patterns can be found by browsing interactively through the field. The findings narrow down the scope for a later, more specialized treatment using statistical tools, which then are applied to gain quantitative results.

ECHAM5 climate model run

We examine the temperature field in an ECHAM5 climate model run, where the derived parameters are computed based on a 25 year moving timeframe ($N = 25$). In Fig. 3a the SNR values of the derived linear temperature trends (y-axis) over the time domain from 1973 to 2052 (x-axis) are shown in a scatterplot. We are interested in regions where the derived climate signal has a high significance (i.e., high absolute SNR values), however, there is no sharp boundary which separates data of significance (focus) from the context. So we take advantage of the smooth brushing (Doleisch and Hauser 2002) capability of SIMVIS assigning fuzzy degree-of-interest (DOI) values. Using a smooth NOT-brush (violet rectangle in Fig. 3a) we exclude the data elements with a relatively low SNR from our selection, i.e., a DOI of 0 (context) is assigned to SNR values within $[-0.75, 0.75]$, a DOI value of 1 (focus) where $|SNR| \geq 1.25$, and a DOI from $]0, 1[$ to SNR values from the transition between focus and context (see the illustration on the left of Fig. 3a).

As a next step we investigate the corresponding feature with respect to the height. The

2D scatterplot in Fig. 3b shows derived temperature trend values (x-axis) with respect to pressure levels (y-axis). In the visualization, the averaged DOI values (with respect to the number of data points) are accumulated and highlighted in red according to the DOI. We can see a high significance (represented as pure red) in the topmost layers of the simulation, which may be an indicator region (see inset Fig. 3g). However, according to the literature the ECHAM5 data has known deficiencies in its highest pressure levels (Cordero and de Forster 2006). Therefore, we completely exclude the highest 10 hPa level and partly exclude the 20 hPa layer using a smooth NOT-brush[5] (shown in Fig. 3b, also in the magnification above Fig. 3g). A negative temperature trend with high significance is still highlighted in the remaining highest pressure levels (indicated by a blue ellipse in Figs. 3b and 3c). This cooling trend located in the lower stratosphere is supposed to be of high significance with respect to climate change (and thus part of one here generated hypothesis).

We also investigate regions with only few important data points (i.e., possibly weaker indicators). Therefore, the maximum instead of the average of the DOI values are shown in Fig. 3c. Here, a positive (warming) temperature trend is highlighted in most pressure levels of the troposphere (orange ellipse). Since this feature is barely visible in Fig. 3b it is supposed to be a less robust indicator for climate change compared to the prominent cooling trend in the lower stratosphere (blue ellipse). In figure 3c also the tropopause is visible.[6]

Figures 3d and 3e show the variation of the derived temperature trend over time (1973–2052) in the new function graphs view. The DOI values are enhanced in Fig. 3e in order to make the features more visible. The main part of the positive trend curves rises slightly (see the large amount of blue curves close to the zero line, indicated by arrow 1) and is mainly located in the troposphere. Note that only those parts of the curves in Fig. 3e (arrow 3) are highlighted where the respective SNR at the corresponding time step is relatively high. The emphasized warming trend is supposed to be a less robust climate change indicator since it is only visible when the feature representation is enhanced. On the other hand, one can see that the *negative temperature trend* is very prominent and robust over the whole visible time period (arrow 2)—three traces of curves emerge visually[7] (indicated also by the small arrows). We come back to this later in Sec. 4.3. Therefore the cooling trend stemming from the lower stratosphere is supposed to be a more robust indicator for climate change considering the whole investigated timespan.

[5] As a result, high negative SNR values in the lower part of Fig. 3a no longer belong to the overall feature and are therefore depicted in blue.

[6] The tropopause is the boundary between the troposphere and the stratosphere. It is higher in the tropics (up to about 17 km) and lower at the poles (up to about 8 km), which is also visible in Fig. 3c.

[7] Brushing one of these traces reveals that each trace corresponds to one specific pressure level in the stratosphere (the lower one to the 10 hPa, the middle one to the 20 hPa, and the upper one to the 30 hPa pressure layer). This feature is an artifact resulting from the resolution of the simulation grid, since the ECHAM5 dataset is computed on discrete pressure levels.

An overview of the spatial location of the sensitive regions with high absolute SNR values is given in Fig. 3f showing a latitude (x-axis) versus pressure (y-axis) scatterplot. Two highlighted areas (indicated by orange ellipses) are centered horizontally around the tropical region in the remaining high pressure levels—this feature is discussed in more detail in Sec. 4.3. Another sensitive region is visible in the northern high latitudes in the lower stratosphere (green ellipse). Brushing this region, one can identify the corresponding feature belonging mainly to the negative (cooling) temperature trend (indicated by a blue ellipse) in Figs. 3b and 3c, respectively.

Generated hypothesis: The above described visual exploration process lead to the following hypothesis: A promising and robust indicator region with respect to climate change is seemingly located in the lower stratosphere (upper pressure levels in the ECHAM5 temperature field), geographically located in the northern latitudes as well as in the tropics. The corresponding cooling trend is considered to be a robust indicator over the whole investigated timespan. On the other hand, the observed positive trend in the troposphere can be considered less prominent according to visual exploration (some preliminary results from the statistical evaluation are given at the end of this section).

ERA-40 Reanalysis Data

In our study, we also examine the geopotential height field of the ERA-40 reanalysis dataset (Simmons and Gibson 2000) for the time period 1961 to 2002 where the derived parameters are based on a 15 year moving timeframe ($N = 15$). As done with ECHAM5, low absolute SNR values are excluded in the 2D scatterplot in Fig. 4a using a smooth NOT-brush (violet color). When examining the evolution of the derived geopotential height trend over time in a function graphs view, high variations in the early years can be observed (see Fig. 4b). According to the literature (Uppala et al. 2004), this is supposed to be a spurious feature. Thus, we restrict our selection to the post-1979 era, where also satellite data were assimilated.

As shown in the function graphs views in Figs. 4b and 4c, the main portion of the geopotential height trend is centered around the zeroline. We want to focus on the outliers, which diverge from the observable main data trend. Thus, we use a similarity-based NOT-brush (the violet brush located around the zeroline) in order to select curves with high variations—the resulting feature is highlighted in blue and red in Figs. 4b and 4c. Here, the red curves belong also to the high absolute SNR and post-1979 feature specified in the 2D scatterplot, while the blue curves (2^{nd} level focus) are only selected in the function graphs view by the similarity-based NOT-brush. The visual prominence of the features is moreover enhanced in Fig. 4b in order to allow the user to focus on all regions containing features (i.e., low γ value for the DOI enhancement). In order to show the actual significance of the feature it is depicted without enhancement in Fig. 4c.

The selection corresponding to the similarity NOT-brush is examined in a scatterplot

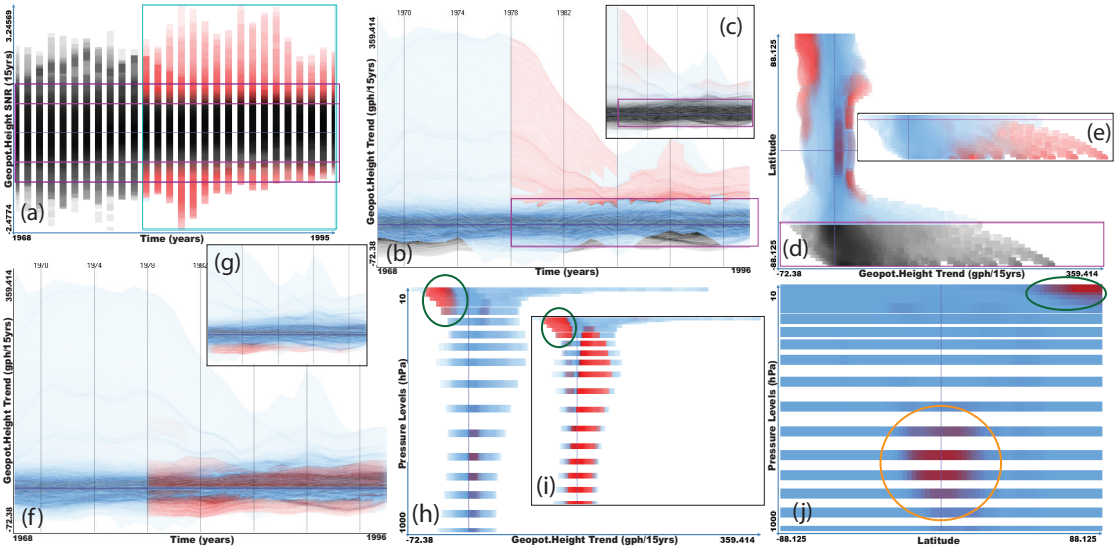

Figure 4: Hypothesis generation on derived trend in geopotential height fields (ERA-40 reanalysis dataset). (a) high SNR values over time (1968–1995) are brushed in a 2D scatterplot. The selection is restricted to the post-1979 era, where satellite measurements were incorporated. (b, c) similarity-based brushing of function graphs, which have a high variation, features are enhanced in (b). The resulting feature appears only in southern latitudes (e), which might be a spurious feature. These regions are therefore excluded from the selection in (d). (f, g) function graphs after 1979 having a high SNR are highlighted in red; features are additionally enhanced in (f). (h, i) geopotential height trends (x-axis) vs. pressure levels. A prominent feature is indicated by the green ellipse. features enhanced in (i). (j) sensitive regions with respect to climate change are highlighted in the scatterplot showing latitudes (x-axis) vs. pressure levels (y-axis). Here, two separable areas can be investigated (indicated by ellipses).

showing derived geopotential height trends (x-axis) vs. latitude (y-axis). The highlighted feature shows that the high trend variations brushed in the function graphs view is only prominent in southern latitudes, which seems to be a spurious feature (see Fig. 4e). According to Santer et al. (2004) the ERA-40 dataset contains deficiencies in these regions. Therefore, we exclude the latitudes 60°S–90°S from the selection. The result is shown in Fig. 4d highlighting high absolute SNR selections in the post-1979 era.

The variation of the geopotential height trend over time is visually examined in the function graphs view, highlighting the same features in red (post-1979 era, high absolute SNR selection, excluding southern latitudes). In Fig. 4f the features are visually enhanced in order to examine all areas containing brushed data items. One can see that the highlighted regions are vertically centered around the zeroline. On the other hand, the features are depicted without enhancement in Fig. 4g in order to focus on the prominence of the features. Since only the negative trend curves are enhanced, these are supposed to

be more significant with respect to climate change than the positive trends.

Generated hypothesis: The features (high SNR, post-1979 era, excluding southern latitudes) are highlighted in red in the scatterplot in Fig. 4j, showing latitudes (x-axis) vs. pressure levels (y-axis). Here two structures are very prominent (indicated by two ellipses) and are supposed to be the promising indicators for climate change (and thus part of the here generated hypothesis). The one sensitive region is located in the upper pressure levels and is prominent in northern latitudes (see green ellipse). This feature corresponds to the negative geopotential height trend indicated by a green ellipse in Figs. 4h and 4i. The other sensitive region can be examined in the tropical region in medium pressure levels centered around the 700 hPa level (see orange ellipse). Since the geopotential height has different properties as the temperature also the sensitive regions are differently located. While the promising indicators are mainly located in the uppermost pressure levels of the ECHAM5 temperature field, for the ERA-40 geopotential height field they appear also in the lower to middle troposphere.

Preliminary Results from Statistical Analysis

The hypotheses which were generated during interactive visual exploration are subject to statistical analysis. The employed *least-squares-fitting* method (Lackner et al. 2009) expects the timespan over which the curves are fitted, and the corresponding latitude range as prerequisites. Linear trends are calculated over the investigated timespan and region. The statistical significance of a trend is determined by the *Students t-test* and the *goodness-of-fit measure*, which is given by the coefficient of determination R^2 (compare to Wilks (2006)). We define the trend significance and the goodness-of-fit as the quantitative criteria for assessing the sensitivity and robustness of the explored parameter (for further details on the method see Lackner et al. (2009)). Since this paper focuses on hypothesis generation, we only give some preliminary results from this analysis. A detailed computational analysis is, however, subject of future work.

For the ECHAM5 dataset, for instance, the high significance for the highlighted features in the lower stratosphere could be confirmed applying the statistical analysis to the higher northern latitude region of 60°N–90°N at the 20hPa–30hPa pressure levels (see the prominent features in the scatterplots in Figs. 5a and 5b showing temperature trends (y-axis) vs. latitudes (x-axis), features in Fig.5b are enhanced). When evaluating the hypothesis generated for the geopotential height field the ERA-40 reanalysis dataset we also got similar results.

On the other hand, the southern latitudes 25°S–90°S over the timespan 2025–2050 were also evaluated. According to the explorative visualization, these areas had a relatively low significance—see the less prominent features in Fig. 5a. However, according to the statistics the same areas returned a strong significance for the chosen timespan stemming mainly from 25°S–45°S. Therefore, the features in this latitude region were again examined

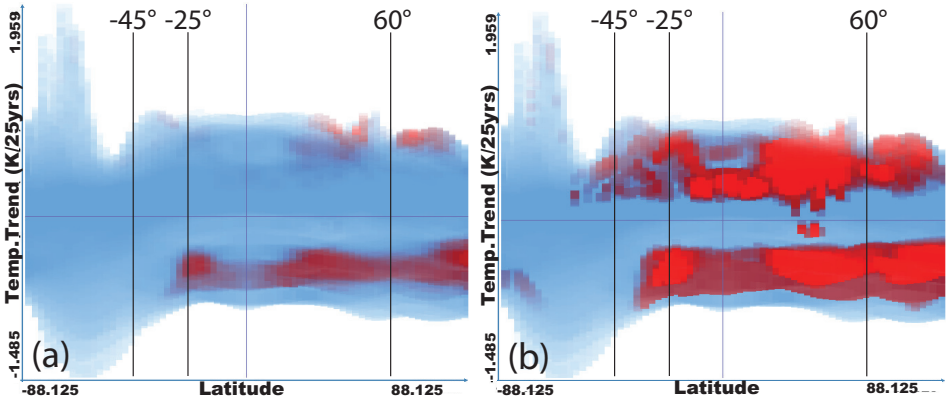

Figure 5: ECHAM5: Sensitive regions with respect to climate change highlighted in the scatterplot (latitude on x, temperature trend on y-axis) were handed over to statistics for further analysis. In (a) the averaged DOI attribution are depicted in order to visualize the importance of each feature. On the other hand, the visual representation of the features is enhanced in (b), showing the maximum DOI values.

using SIMVIS, but now displaying the maximum DOI values in order to focus on all areas containing features (see Fig. 5b). Still, only small areas with low prominence could be found, even though we already get a slightly improved agreement. Getting back to statistics, we varied the timespans for the least-squares-fit method, i.e., 2020–2045 and 2015–2040, respectively. With these modified parameters also the statistical analysis returned a noticeable lower significance for the respective latitude range, which shows that the least-squares-fit reacts very sensitively to the chosen timerange (the coupling of visualization and statistical analysis was crucial to identify this relation).

Using this iterative approach between visual exploration and computational analysis, we could benefit from the strengths of both domains: Finding the right parameters for statistics is usually cumbersome, however, using interactive visual explorations these parameter ranges could be efficiently narrowed down in an iterative process. Moreover, we could investigate that the applied statistical method reacts more sensitive with respect to the chosen timespan than expected. These examples show how the application of visual exploration techniques—used in an iterative process—contributed to an improved workflow in this application.

4.2 Parameter Optimization

As illustrated in Fig. 2 there are several parameters involved in the exploration scenario in this study. It is often challenging to come up with the optimal settings, affecting the respective exploration steps in the pipeline. For example, we derive climate parameters (linear trend, SNR) from the original data in order to form our hypotheses. Thereby, the

timeframe over which these calculations are performed significantly affects the derived data, and therefore also influences the following steps in the pipeline. Using interactive visual exploration we can assess the sensitivity of our results to the timeframe. To this end, we have derived the parameters over 10 and 25 years for ECHAM5 and over 10 and 15 years for ERA-40. On the example of ECHAM5, we briefly show how SIMVIS was used to come up with parameters that then were suitable for our analysis.

In order to be able to calculate meaningful linear trends, the original data is smoothed first using a moving average over a timespan of N years. Then, the *linear trend* of a year i is calculated as a moving difference between the smoothed data $\tilde{y}$, i.e., $trend_i = \frac{1}{N}(\tilde{y}_{i+N/2} - \tilde{y}_{i-N/2})$. The *linear trend fit curve* for each time frame over $N+1$ years is calculated using the derived trend values as a slope, i.e., $fit_{ij} = \tilde{y}_{i-N/2} + [j-(i-N/2)]trend_i$, where j runs from $i-N/2$ to $i+N/2$. As a next step, the fitted trend curve is removed from the original data y to obtain the detrended standard deviation s for the current timeframe, determining the natural variability of the climate data:

$$s_i = \Big[\frac{1}{N-1}\sum_{j=i-N/2}^{i+N/2}(y_j - fit_{ij})^2\Big]^{\frac{1}{2}} \tag{2}$$

Finally, the *signal-to-noise ratio* is computed as the ratio of the trend to the standard deviation, i.e., $SNR_i = \frac{trend_i}{s_i}$ (compare to Ladstädter et al. (2009)).

The resulting parameters are explored using SIMVIS, in a similar setting as described in Sec. 4.1. When the ECHAM5 data is smoothed over a shorter time frame (10 instead of 25 years) there are obviously more high-frequency features present in the data, which can also be observed in Fig. 6a showing SNR values (y-axis) over time (x-axis). Comparing Fig. 6b and Fig. 3b shows that averaging over less data points leads to less pronounced formation of features. For the long-term trend in which we are interested, a longer timeframe is clearly favorable, since the high-frequency characteristics are effectively flattened out and do not show up in the visual exploration.

When examining the linear temperature trends using a function graphs view one gets a high response in the upper and lower trend values (10-years), which also seem to contain a lot of noise (see Fig. 6c). Here, no clear highlighted trends can be identified in the visualization, in contrast to Figs. 3d and 3e, arrow 2. Using 25 years we obtain clearer signals and thus better-defined features. Accordingly, we used 25 years instead of 10 years in the ECHAM5 dataset, and 15 instead of 10 years in the ERA-40 dataset, respectively.

4.3 Analyzing Relations Between Selections

Up to now we were performing our investigation mainly in one direction, e.g., brushing high absolute SNR values and examining the resulting feature in other dimensions. In science, this principle is known as implication ($a \rightarrow b$). In the following, we want to check whether this interrelation also exists in the opposite direction, i.e., whether we we get a similar feature in one dimension when specifying a feature in another dimension ($a \leftarrow b$).

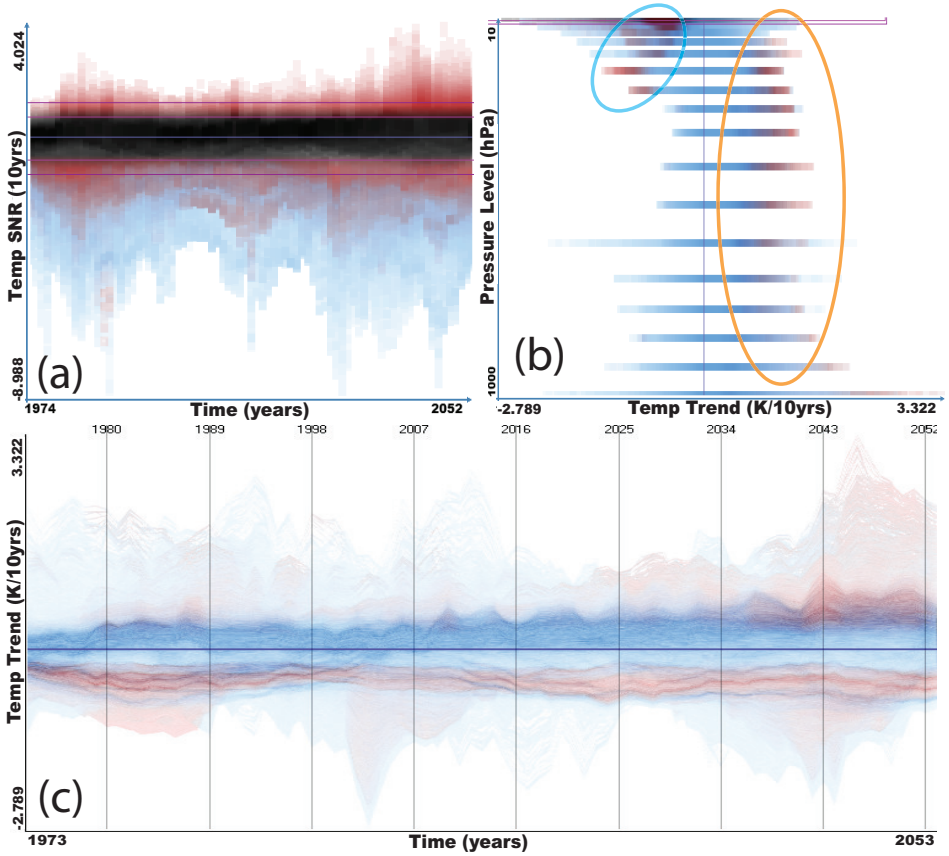

Figure 6: ECHAM5 temperature: derived parameters computed over 10 years instead of 25 years. The features which were barely visible with 25 years (Fig. 3b) are now highlighted in (b). The function plots of the derived temperature trend seem to contain a lot of noise.

If this interrelation can be confirmed the respective statement is stronger ($a \leftrightarrow b$).

When examining the derived temperature trends in the function graphs view (ECHAM5, 25 years, see Sec. 4.1), one can visually identify three streams of curves, which were very prominent in the visualization and also seemed to belong to the high absolute SNR feature (highlighted in red in Figs. 3d and 3e, indicated by small arrows). Using similarity-based brushing we can examine the interrelations between these visible trends and the other dimensions. In Fig. 7a such a brush is specified, aiming to approximate the visible structure of the respective curves. Here, similarity is evaluated based on the gradients of the function graphs and the target function. Three families of curves are emphasized in red and blue within the function graphs view (context data depicted in black). The bottom family of enhanced curves stems from the uppermost pressure level, which has been excluded, and is therefore colored in blue (second level feature).

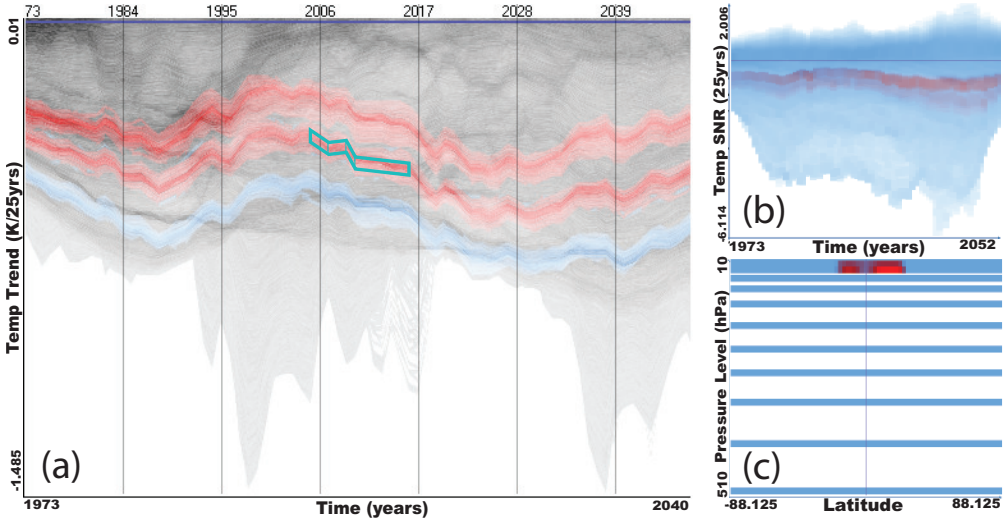

Figure 7: A prominent visual structure in the function plots view is brushed based on it's similarity to a user defined target function (a). Three families of curves are thereby highlighted. The respective feature contains a relatively high signal-to-noise ratio highlighted in (b), and can be located in the upper pressure levels, centered around the tropical region (c).

Examining the resulting feature in a scatterplot (SNR over time, see Fig. 7b), one can see that the highlighted curves have a relatively high (negative) signal-to-noise ratio—note, that the high SNR feature is disabled in the scatterplot. The similarity feature is highlighted in another 2D scatterplot (see Fig. 7c), where it is approximately horizontally centered around the zeroline (the tropical region), and located in the uppermost pressure levels. A similar feature can be examined in Fig. 3f—indicated by orange ellipses—when going into the opposite direction (i.e., selecting high absolute SNR values in a scatterplot). However, in the previous examination these two highlighed spots were not very dominant—they were occluded by other highlighted areas in the upper pressure levels, where the most prominent feature was in the high northern latitudes. Due to the use of similarity based brushing, the areas in the tropics containing these families of similar curves could be located. Since this relation seemingly exists in both directions ($a \leftrightarrow b$) the corresponding statement is supposed to be stronger and can be considered for further investigation (e.g., using statistics).

4.4 Further Results

When analyzing the ECHAM5 dataset (25 years) in the 2D scatterplot, a negative (cold) temperature trend feature (considering high absolute SNR values) visually emerged in the pressure level closest to the surface (indicated by a green ellipse in Fig. 3c). This feature varies from the more prominent warming trend features with high SNR also located in

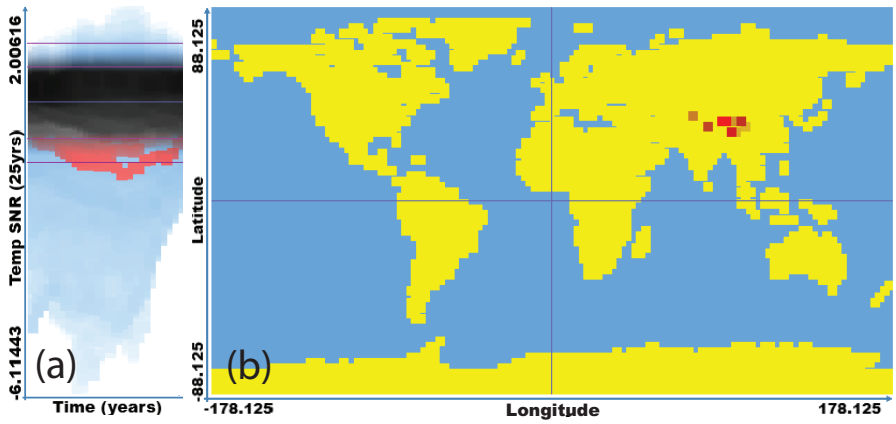

Figure 8: Cooling trend brushed in the lowest pressure level indicated by a green ellipse in Fig. 3c shows relatively low SNR values (a) and corresponds to a certain geographic area also including the Tibetan Plateau.

this pressure level. Brushing the area (green ellipse) with a rectangular brush reveals that this feature corresponds to relatively low SNR values in the timespan 2022 to 2052 (see Fig. 8a). When looking at the geographic location, one can identify that the brushed feature corresponds to a certain area which is mainly located at the Tibetan Plateau (see Fig. 8b, where also a land-sea coloring is incorporated). According to the process illustrated in Fig. 2, the next step would be to use statistical analysis in order to evaluate whether this geographical region has a special characteristic—this is subject of future work. However, using classical statistical analysis, it would have been very challenging to identify this region in the spatial context. Also when using a binary classification scheme instead of smooth brushing (e.g., with a hard selection of $|\text{SNR}| \geq 1$), this feature would have been challenging to detect.

4.5 Performance Issues

The presented study was carried out on a system consisting of the following components: The hardware used was a modern PC-based system (Intel Core2 Quad CPU, 4 GB RAM, 320 GB harddisk, 64bit Windows) with a NVIDIA GeForce 8800 graphics card. The SIMVIS software is written in C++, using OpenGL and Cg shader language.

The two datasets investigated during this case study consist of 180K cells, defined at 42 time steps (ERA-40) and 108 time steps (ECHAM5), respectively. The derived data of ECHAM5 resulted in approximately 2.3 GB of data, for example. Due to algorithmic optimizations and an effective data handling framework, we are able to handle analysis sessions with multiple linked views at interactive framerates. By the use of binning techniques, large amounts of function plots can be depicted and analyzed, while still providing full interactivity. To the best of our knowledge no other comparable system

can handle such large amounts of function graphs interactively on a PC.

5 Conclusion and Future Work

The generation of hypotheses in climate research is a crucial task. In this paper, we demonstrate the useful integration of state-of-the-art interactive visual exploration technology into the hypothesis generation process in climate research. The goal was to investigate atmospheric regions in space and time that are sensitive with respect to climate change. In order to rapidly come up with promising hypotheses, we explored derived parameter spaces using interactive visual exploration of complex features specified in multiple, linked attribute views. For analysis, the emerged hypotheses were handed over to statistical analysis. Up to now, the results from visual exploration could already be confirmed in some exemplary cases. We also applied visual exploration in individual cases where the correlation could not be established. Here, our visual exploration framework showed to be especially useful to further investigate these cases, and to improve the understanding of the influence of different parameters on computational analysis. The power of this approach is that no prior knowledge about the data is needed to rapidly formulate hypotheses. Therefore, parameter ranges affecting for instance the computational analysis can be narrowed down efficiently.

Lessons learned from this case study are that interactive visual exploration with the opportunity to interactively drill down into certain aspects of the data (through brushing) substantially supports the exploration and analysis process of climate researchers in many ways. Using interactive visual exploration allowed us to examine the whole field without knowing its characteristics in advance, which showed to be very useful. Interesting features or patterns can be found by browsing interactively through the field. The findings narrow down the scope for a later, more specialized treatment using statistical tools, which then are applied to gain quantitative results. For visualization research it is very rewarding to see how positively new technology is adopted in a challenging application domain. Generally, we see great potential for visualization when performing undirected exploration since it efficiently complements computational analysis (e.g., statistics). We think that the approach presented here of using visual exploration to come up with promising hypotheses and then quantitatively evaluating the results can be generalized to several other scenarios.

In future work we will focus on further fusing statistical methods yielding quantitative results in our visual exploration framework. We also want to perform a detailed quantitative evaluation of the results gained from this study using computational analysis. Here again, we want to show how visual exploration and statistics can interact in a feedback loop to gain in depth insight into the data.

Acknowledgments

The authors want to thank G. Kirchengast for important discussions, contributions and the supervision of F. Ladstädter, moreover, we thank B.C. Lackner for her help and results from the statistical analysis. The datasets are courtesy of the Max-Planck-Institute for Meteorology, Hamburg, Germany and the European Centre for Medium-Range Weather Forecasts, Reading, UK. This work was supported in part by the Austrian Science Fund (FWF) Project INDICATE P18733-N10.

PAPER C

Exploration of Climate Data Using Interactive Visualization

Florian Ladstädter[1], Andrea K. Steiner[1], Bettina C. Lackner[1], Barbara Pirscher[1], Gottfried Kirchengast[1], Johannes Kehrer[2], Helwig Hauser[2], Philipp Muigg[3], and Helmut Doleisch[3]

[1]Wegener Center for Climate and Global Change (WegCenter) and Institute for Geophysics, Astrophysics, and Meteorology (IGAM)/Institute of Physics, University of Graz, Graz, Austria

[2]Department of Informatics, University of Bergen, Bergen, Norway

[3]SimVis GmbH, Vienna, Austria

ABSTRACT

In atmospheric and climate research, the increasing amount of data available from climate models and observations provides new challenges for data analysis. We present interactive visual exploration as an innovative approach to handle large datasets. Visual exploration does not require any previous knowledge about the data as is usually the case with classical statistics. It facilitates iterative and interactive browsing of the parameter space in order to quickly understand the data characteristics, to identify deficiencies, to easily focus on interesting features, and to come up with new hypotheses about the data. These properties extend the common statistical treatment of data, and provide a fundamentally different approach. We demonstrate the potential of this technology by exploring atmospheric climate data from

This article was published in *Journal of Atmospheric and Oceanic Technology* 27.4 (2010), pp. 667–679. DOI: 10.1175/2009JTECHA1374.1

different sources including reanalysis datasets, climate models, and radio occultation satellite data. Results are compared to those from classical statistics revealing the complementary advantages of visual exploration. Combining both, the analytical precision of classical statistics and the holistic power of interactive visual exploration, the usual workflow of studying climate data can be enhanced.

1 Introduction

The ever increasing demand for insight into the Earth's climate system has led to an enormous amount of data produced in the last decades by the climate research community. The increasing complexity and number of General Circulation Models (GCMs), together with a great variety of observational data (Solomon et al. 2007a), result in large, multivariate and time-dependent datasets. Interactive visual exploration helps to quickly gain informative views on the data. It becomes a valuable complement to statistical data analysis methods.

Visualization can be seen in context of more general data mining concepts. Data mining, vaguely defined in literature, refers to identifying useful patterns in large observed datasets (Fayyad et al. 1996; Friedman 1997; Goebel and Gruenwald 1999). In *exploratory* data analysis (EDA) as one data mining task (Tukey 1977), interactive visualization plays an important role (Wong 1999; Keim et al. 2002; Oliveira and Levkowitz 2003). No assumptions of an underlying data model need to be presumed. This is in contrast to *confirmative* analysis methods, where visualization supports the verification of existing hypotheses about the data (Schumann and Müller 2000). Visual data exploration uses the unique ability of the human vision to detect patterns and thus can help the users in identifying relevant characteristics of the dataset, and to ultimately come up with hypotheses about the data.

In atmospheric and climate sciences, visualization is still most frequently applied in the form of simple unconnected plots (e.g., scatterplots, contour plots) to demonstrate characteristics of the data. Interactive visualization techniques for EDA tasks are hardly used so far. The reasons for this may be both a lack of suitable tools covering the specific needs of the geophysical community and that the available advanced visualization techniques are hardly known in this community (Hibbard et al. 2002; Nocke et al. 2008). Analyses were performed by Macêdo et al. (2000), who explored multivariate ocean-atmosphere datasets using the XGobi software tool (Swayne et al. 1998). In Doleisch et al. (2004b) the interactive visual field exploration tool SIMVIS (Doleisch et al. 2003) was used to visualize a simulated meteorological dataset of the hurricane Isabel, which struck the US east coast in 2003. SIMVIS was then later also applied to climate model data and to reanalysis datasets by Kehrer et al. (2008) and Ladstädter et al. (2009), showing the ability of the tool to explore large climate datasets. Hobbs et al. (2010) showed the

benefits of visual data exploration in a case study using geographic and atmospheric data. Cuntz et al. (2007) presented a framework for interactive visualization of flow data output from climate model simulations. Interactive visualization was also used by Sukharev et al. (2009) to analyze correlations in time-varying multivariate climate data. For concise surveys over available tools and related work see Hibbard et al. (2002); Nocke (2007); Aigner et al. (2008); Nocke et al. (2008); Fuchs and Hauser (2009).

It is important to point out that classical statistical methods usually need a hypothesis beforehand to work. Features which were not known or at least anticipated beforehand are hard to find. While providing meaningful quantitative analysis, these methods are less well suitable for the undirected search or for identifying hypotheses without prior knowledge. Classical statistics is therefore much better suited for hypothesis testing, while interactive visualization can aid in generating these hypothesis (Kehrer et al. 2008).

With interactive visualization techniques such as linked views and brushing (selecting) data items, interesting features of huge datasets can be effectively identified and interdependencies between parameters can be discovered. Local deviations in the datasets can be revealed easier by visual exploration than by classical statistical methods, where the domain of analysis is usually limited to certain areas of interest according to some hypotheses. Exploring the dataset interactively might easily unveil unexpected features, leading to a new view on the data characteristics.

Atmospheric and climate researchers can benefit from these properties of exploration techniques. The potential to explore the whole dataset at once is often convenient when dealing with large atmospheric datasets. Finding interrelations between parameters which were not anticipated can help to discover unexpected features. This is not easily achieved with simple plots as they are commonly used in atmospheric and climate sciences.

In this study we aim to introduce advanced interactive visualization to atmospheric, climate, and oceanic scientists. We apply the technology to two climate datasets, investigating trend characteristics of atmospheric parameters. In order to further illustrate the utility, some of the results are compared to the outcome of classical statistical analysis of trend data. Furthermore, we investigate processing differences in remote sensing satellite data.

This paper is structured as follows: In section 2 the concepts and the tool employed are presented. The climate datasets used for demonstration are introduced in section 3. This is followed in section 4 by a number of example results showing the application of the tool and concepts to climate data, combined with some comparative results from classical statistical methods. The final section presents conclusions.

2 Interactive Visual Exploration Methods

In this section we present key elements of advanced visualization techniques. As outlined in the introduction, a previously formulated hypothesis is not needed to start working with

the data. The aim is to enable the user to iteratively gain knowledge about interesting data characteristics. This knowledge ideally creates new questions or leads to hypotheses, which can then be explored and analyzed in more detail (Kehrer et al. 2008).

In this study the interactive field exploration tool SIMVIS is applied (Doleisch et al. 2003). SIMVIS integrates advanced visualization technology and was originally developed for the exploration and analysis of large, multivariate 4D data resulting from computational fluid dynamics simulations, as they are used, e.g., in the automotive sector. The framework has only recently been applied to other areas as well, such as meteorological and climatological datasets (Doleisch et al. 2004b; Kehrer et al. 2008). Even though being able to handle large datasets, SIMVIS can be run on desktop PCs typical for a standard scientists workplace (a large monitor as well as large RAM storage is useful for smooth interactive manipulation). Major concepts realized in SIMVIS are summarized in the following. For a better understanding of the concepts, a video[1] is provided showing an example of interactive exploration.

Interactive Feature-Based Visualization This concept is founded on reducing the overall data to subsets (*features*) which exhibit properties of interest (e.g., regions with a high Signal-to-Noise Ratio (SNR) ratio). To express interest in a certain feature, the user can *brush* parts of the data using the mouse. Brushing simply means to select data points directly within a visualization by, e.g., defining or modifying selection rectangles in a space spanned by two parameters such as temperature and humidity (Becker and Cleveland 1987). A numerical refinement of the brush selection constraints is also possible.

Brushing and Linking in Multiple Views Multiple concurrently shown views present different aspects of the data. These views not only act as passive representation of parts of the dataset, they are also used to interactively explore and select the data. The different views include spatial 3D views and various types of 2D plots such as histogram, scatterplot, parallel coordinates view, and a curve-view showing the variation of a parameter over time. Any of the parameters of the multivariate dataset can be assigned to the views. The user then expresses interest in a certain subdomain of the data via interactive brushing. Technically this process assigns a *degree of interest* (DOI $\in [0, 1]$) attribute to every data point. For a discrete feature classification this will be either 0 or 1 for *context* data and for *brushed* data, respectively. Through *smooth brushing* also fractional DOI values can be assigned (Doleisch and Hauser 2002). The information is immediately propagated and highlighted in all other views, providing the linking between the views and the displayed parameter spaces. With this brushing and linking concept the user can apply constraints to the data and instantly check the resulting distribution in all other representations (Baldonado et al. 2000).

[1] see online supplement

Focus & Context Visualization Data items with high DOI values are considered to be *in focus* and are drawn in an emphasized way, while low DOI values lead to a reduced style representation (*context*). This distinction is especially useful in the 3D view to deal with visual clutter. Here the focus & context concept helps to easily discriminate between the features and their context, the latter shown in transparent gray. The concept is employed in all available views, e.g., the scatterplot view emphasizes data items in focus by drawing them on top of the context items.

Derived-Data Attributes Depending on the type of data to be explored, the features of interest might not be directly accessible from the dataset. Climate researchers are often interested in temporal trends derived from some existing parameters. This can be achieved through a flexible derived-data concept, where every available data parameter set can be the source of new derived parameters. In order to transform these parameters, a variety of predefined mathematical operations is available (e.g., algebra, derivatives). Arbitrary operations can be combined to user-defined formulas.

3 Datasets

As examples to demonstrate interactive visual exploration in the field of climate research, representative types of datasets are investigated: (3.1) reanalysis and model data and (3.2) remote sensing data from radio occultation.

3.1 Reanalysis and Model Trend Data

The ERA-40 seasonal-mean reanalysis data[2] (Simmons and Gibson 2000) is used for the time period 1961 to 2002. Since it is based on observational data, incorporating many different meteorological observations, the time series is exposed to irregularities such as changing data sources, leading to varying data quality.

The second dataset consists of output of the fifth-generation atmosphere-ocean general circulation model (AOGCM) ECHAM5[3] (Roeckner et al. 2003), where a simulation of the B1 scenario of the Intergovernmental Panel on Climate Change (IPCC) 4$^{\text{th}}$ Assessment Report is taken for the time period 2001 to 2064. The run is chosen to be reasonably representative for a projected climate trend of the investigated time period, an evaluation that is based on trend calculations for several GCMs (Lackner et al. 2009). The simulation is complemented by the ECHAM5 20$^{\text{th}}$ century run before 2001 (back to 1961) in the example, where necessary. The model output data can be expected to be without non-stationarity deficiencies in the majority of the data regime.

[2]Obtained from the European Centre for Medium-Range Weather Forecasts (ECMWF) data server.
[3]Of the Max-Planck-Institute for Meteorology (MPI-M) Hamburg, Germany

For these two datasets, June-July-August (JJA) seasonal mean fields of temperature and geopotential height (corresponding to the geometric elevation above mean sea level normalized to standard Earth's surface gravity) on 18 pressure levels ranging from 1000 hPa to 10 hPa[4] and on a horizontal resolution of $2.5° \times 2.5°$ are explored. For ECHAM5, the top-most level (10 hPa) is left out in the exploration due to known limitations (Cordero and de Forster 2006).

To access trend characteristics of both datasets, they are complemented using the derived-data functionality of SIMVIS (see also Ladstädter et al. 2009). Being an interactive exploration framework, SIMVIS does not provide statistical functions as needed for regression analysis. To be able to access meaningful *features* of the dataset, we therefore use the available mathematical operations to derive the following new parameters. We define the signal-to-noise ratio as the ratio of the trend to the detrended standard deviation. The linear trend is calculated as a moving difference on smoothed data, where the time periods used for both trend calculation and smoothing are 25 years for ECHAM5 and 15 years for ERA-40, respectively. All these computations can be done in the SIMVIS framework during the investigation process. They are applied separately for each of the space-time grid points within the framework.

More specifically, the data y of any parameter are first smoothed using a moving arithmetic averaging, resulting in y^{av}. The linear trend b_i is then computed centered for each time-frame as a moving difference between the edge data points, i.e., $b_i = N^{-1}(y^{\mathrm{av}}_{i+N/2} - y^{\mathrm{av}}_{i-N/2})$, where i denotes the center point of the time-frame and N is the time period length. This gives the slope for the corresponding trend fit curve y^{FIT}_{ij} valid for all data points of the current time-frame $i - N/2 \leq j \leq i + N/2$, i.e., $y^{\mathrm{FIT}}_{ij} = y^{\mathrm{av}}_{i-N/2} + [j - (i - N/2)]b_i$. The trend fit curve is then used to remove the trend from the original data to obtain the detrended standard deviation s_i as a measure for the natural variability of the data for the current time-frame:

$$s_i = \Big[\frac{1}{N-1}\sum_{j=i-N/2}^{i+N/2}\Big(y_j - y^{\mathrm{FIT}}_{ij}\Big)^2\Big]^{\frac{1}{2}}. \tag{1}$$

The SNR is then simply defined as the ratio of the trend signal to the variability of the data,

$$\mathrm{SNR}_i = b_i/s_i. \tag{2}$$

This computation indicates well the utility of SIMVIS to provide derived data attributes (here SNR fields derived from basic fields of temperature and geopotential height) that are subsequently useful as complementary fields in the visual data exploration process.

[4]The pressure levels (hPa) are 1000, 925, 850, 775, 700, 600, 500, 400, 300, 250, 200, 150, 100, 70, 50, 30, 20, and 10.

3.2 GPS Radio Occultation Data

Global Positioning System (GPS) Radio Occultation (RO) satellite data originating from the CHAMP mission (Wickert et al. 2004) are investigated as further example. The GPS RO method is a remote sensing satellite technique delivering high quality atmospheric datasets with long-term stability and high vertical resolution (e.g., Kursinski et al. 1997; Foelsche et al. 2009). The raw RO measurements together with precise orbit data are first transformed into phase delay data, from which atmospheric profiles are retrieved, such as refractivity (closely equivalent to density), geopotential height, and temperature. While the RO technique possesses intrinsic self-calibrating properties, the processing of raw RO data leading to derived refractivity can introduce residual differences between the output of different processing centers (structural uncertainty, e.g., Ho et al. 2009b).

In this study, differences of monthly mean climatologies of refractivity retrieved by three different RO processing centers for the time period 2002 to 2006 are explored. The refractivity climatology data used stem from the Wegener Center[5] (WegC) and further two processing centers, denoted here Reference Center 1 (RefC1) and Reference Center 2 (RefC2). The data of two processing versions of the Wegener Center are used, WegC1 as used by Ho et al. (2009b) and WegC2 as used by Steiner et al. (2009a). WegC1 used phase delay and orbit data from RefC1 and WegC2 phase delay and orbit data from RefC2, respectively.

To compare the data of the four processing runs, monthly refractivity climatologies in 36 5° latitude bands (within 90°S to 90°N) and at 200 altitude levels (from 0.2 km to 40 km) are used. The difference between the individual datasets and their mean is explored, $\Delta x = x - \overline{x}$, with $\overline{x} = (x_1 + x_2 + x_3 + x_4)/4$. For the refractivity profiles, the relative difference $\Delta x/\overline{x}$ is used to account for the refractivity essentially decreasing exponentially with altitude.

Not aiming at a concise study of the topic (for a study on RO structural uncertainties see Ho et al. 2009b), the exploration of these datasets shall serve as another example of fast hypothesis generation using interactive visualization.

4 Application to Climate Data

In this section exemplary results for the exploration of atmospheric climate datasets are presented. A prominent topic in today's climate research is the detection of trends in atmospheric parameters caused by climate change. While most measured data is available from the Earth's surface, recent modeling efforts and a growing amount of data available for upper air parameters through satellite and radiosonde measurements (Solomon et al. 2007a; Steiner et al. 2009a) show that the Upper Troposphere–Lower Stratosphere (UTLS) region[6], reacts sensitively to climate change. We use interactive visual exploration to

[5] Wegener Center for Climate and Global Change, University of Graz, Austria
[6] The UTLS extends from about 5 km (≈500 hPa) to 35 km (≈10 hPa).

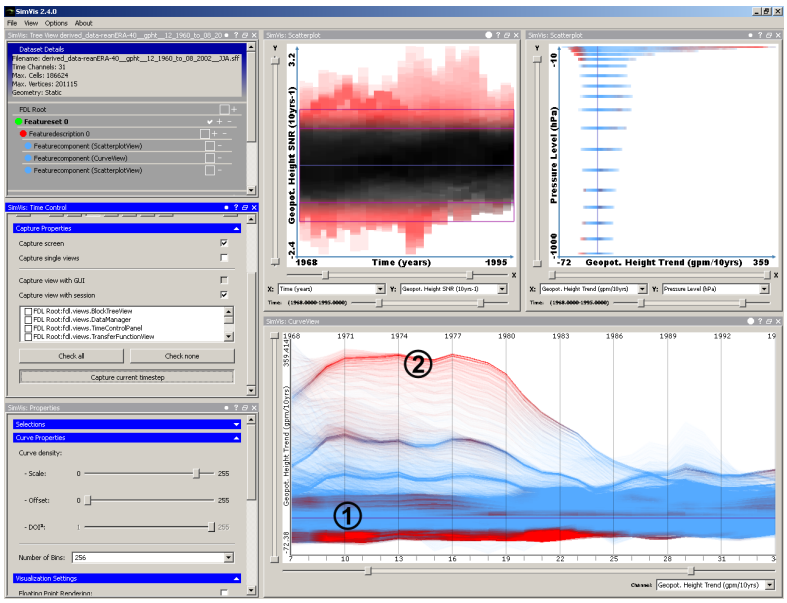

Figure 1: Exemplary visual exploration session with SIMVIS, exploring the geopotential height field of the ERA-40 reanalysis dataset. Top center: Scatterplot view showing time versus SNR. Smooth brushing is applied to select data points of high significance (violet rectangle). The other views (top right, bottom) are immediately updated, showing selected features in red, while the rest remains blue. Top right: Scatterplot view of the variation of the trend with pressure levels. Bottom: Curve-view of the variation of the trend with respect to time with labeling of the zero line (①) and of some deviating trends (②).

quickly get an overview over the various investigated datasets, to identify regions in time and space where robust indicators for climate change emerge, and to compare datasets from various radio occultation data processing centers. By comparing some of the results with classical statistics, we demonstrate the difference of the approaches and present an example, where the exploratory method revealed a feature of the dataset not found otherwise. All figures presented (except one from classical statistics) are screenshots directly captured from the work with the SIMVIS tool (with trivial annotations added). Being an *interactive* tool, the shown features are inherently better represented on-screen; the printed snapshot figures in particular show somewhat less color contrast.

4.1 Exploring Reanalysis Data

To demonstrate the basic steps of an interactive exploration session, we examine the geopotential height field of the ERA-40 reanalysis dataset. In Fig. 1, a scatterplot (top center, showing the time channel versus the SNR channel) is used in the SIMVIS framework to select data points in space and time where the trend signal emerges from the data noise

($|\text{SNR}| \geq 1$). As we do not want to define a sharp boundary between data with high and low significance, in order not to loose any potential feature close to the boundary, we do take advantage of *smooth brushing*[7]. The *smooth brush* effectively assigns fractional DOI values ($\in]0, 1[$) to data points in the range $1.0 \leq \text{SNR} \leq 1.5$ and $-1.5 \leq \text{SNR} \leq -1.0$ (since SNR represents a trend signal to noise, Eq. 2, it can also be negative).

The result of the brushing is immediately shown in all other open views, where the selected data points are highlighted in red according to their DOI value. It is notable in the curve-view (bottom) that although the bulk of data is located around the zero line (label ①), there are certain time series with high significance (in red, label ②, referred to as outliers in the following) that deviate from the main trends. The scatterplot vs. pressure levels (top right) shows that at the topmost levels the variation becomes much larger, and outliers with high significance and positive trends can be observed at stratospheric levels.

The outliers attract our interest, so we add another brush to the curve-view as shown in Fig. 2 (panel a). The brush selects all curves going through the selection box (turquoise rectangle) applied at the year-1974 layer. As a result, features selected in all views are shown in red, features selected only in the current view in blue, and the context information (not selected) is shown in black. The two scatterplots in Fig. 2 show that the feature distribution resulting from the combined selection of outlier trends and high values of SNR is related to the stratosphere region (panel b) and to southern high latitudes (panel c). Having found this, literature research reveals that the high variation in southern high latitudes in the ERA-40 dataset is a spurious feature (Santer et al. 2004). The improvement of the data quality with time (as can be observed, e.g., in the curve-view in Fig. 1) can be explained with the assimilation of satellite data after 1979 (Uppala et al. 2004). For ERA-40 such explanations are readily available. However, applying interactive visual exploration to new datasets can efficiently and effectively trigger new research on spotted characteristics of interest.

Based on what we learned on the outliers in Fig. 2, we proceed with applying a NOT-selection to all data south of 60°S and a selection of the post-1979 time period, i.e., deselecting domains including data of inferior quality. This results in a distribution of data points with high significance as shown in Fig. 3. The scatterplot in Fig. 3a shows a positive trend signal throughout the troposphere turning to a negative signal in the stratosphere. To locate the patterns of good trend signals geographically, the scatterplot in Fig. 3b[8] is underlaid with a land-sea mask showing the continents. High significance in the longitude-latitude distribution can be found above the continents in the tropics and at northern mid-latitudes. Note that in Fig. 3a red (tropospheric) domains emerge visually that have only weakly been seen in the pressure level view of Fig. 1; this occurs since in Fig. 1 the non-selected data (in blue) had quantitatively exceeded the selected

[7] The violet rectangle in Fig. 1, which is in fact a NOT-brush, deselects the part then shown in black.
[8] Note that all pressure level data are integrated into this view.

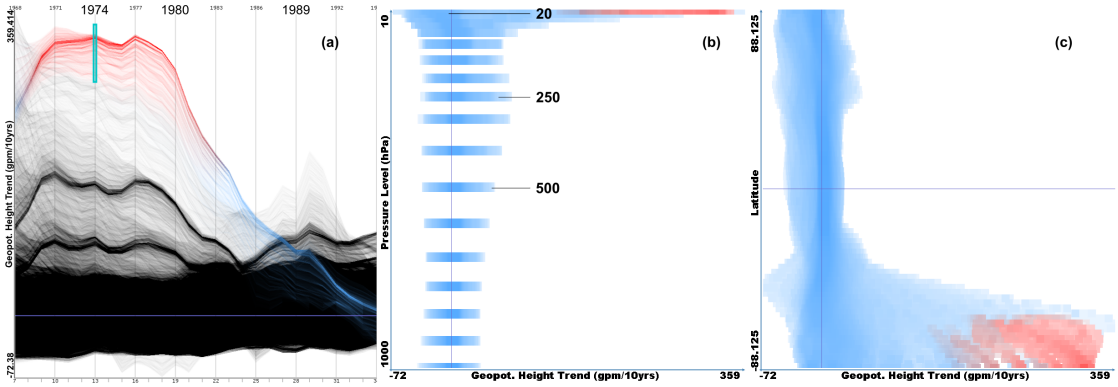

Figure 2: Inspecting outliers of the geopotential height trend field of ERA-40. Brushing outliers (turquoise rectangle) in the curve-view (a) and scatterplot views as a function of pressure levels (b) and latitude (c), with the selected outliers in red. Some pressure levels are labeled for better orientation.

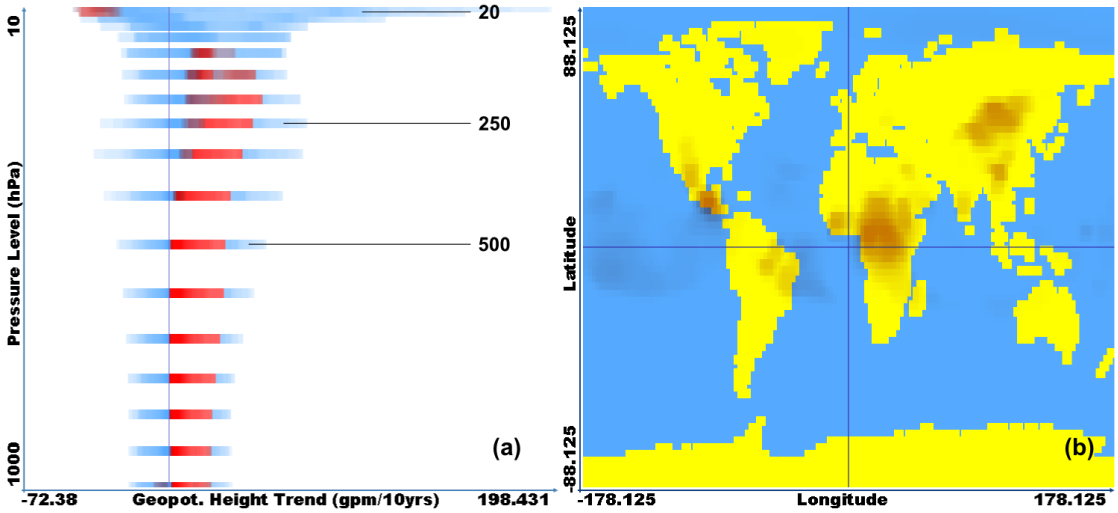

Figure 3: Removing the southern high latitudes and restricting the analysis to the post-1979 time. Scatterplot view as function of pressure levels (a) and of geographic location (b), with the selected data in red.

data (in red) due to including all pre-1979 information.

4.2 Exploring Climate Model Data

In this section the geopotential height and temperature fields for a B1 scenario run of ECHAM5 are explored. To underpin the effectiveness of the approach, the findings are compared to results from statistical analyses for the same B1 run.

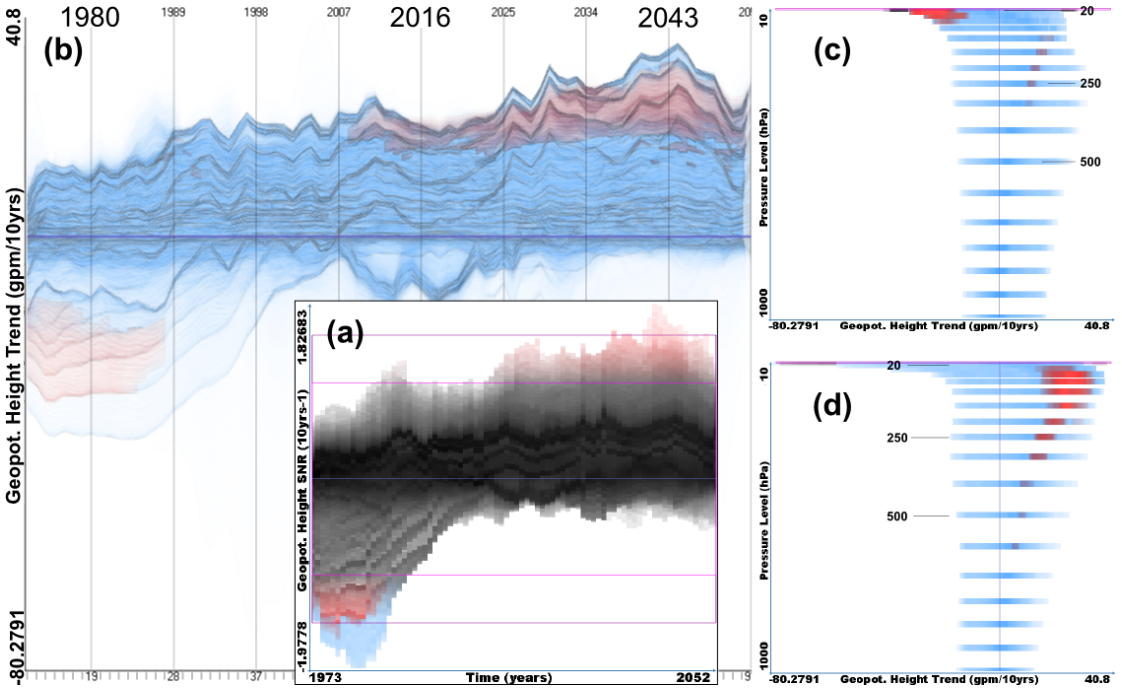

Figure 4: Exploration of the geopotential height field of an ECHAM5 run. As in Fig. 1 high SNR values are brushed (a). A curve-view (b) shows the time variation of the geopotential height trend (1961 to 2064), and scatterplot views of trends vs. pressure levels show the data for the time periods 1961 to 2001 (c) and 2001 to 2064 (d) separately, with the selected data in red.

A first example of the exploration of the ECHAM5 dataset is shown in Fig. 4. The geopotential height of pressure levels is a good indicator for global warming, since the pressure surfaces will rise when there is thermal expansion of the underlying air masses. In Fig. 4a the geopotential height field shows regions of high significance at the beginning and at the end of the 1961 to 2064 time period. The variation of the trend over time in Fig. 4b reveals a clearly visible reversion of the geopotential height trend from negative to positive. To further investigate this behavior, we select these features in subsequent scatterplots (not shown here) by brushing the first time period until 2001 and the second time period from 2001 to 2064 separately. The resulting pressure level distribution of the selected trend values is shown in Fig. 4c and 4d. Evidently the significantly negative trends in the time period before 1990 stem from the stratosphere (Fig. 4c), where cooling lowers the pressure levels. Later, past about 2010, this effect becomes outweighed by the raising of the layers in the troposphere due to warming there and significantly positive trends emerge in the upper troposphere (Fig. 4d). Interactive visual exploration was found to be an effective approach for revealing these features.

Figure 5 gives a first overview of the trends in the temperature field, with high SNR

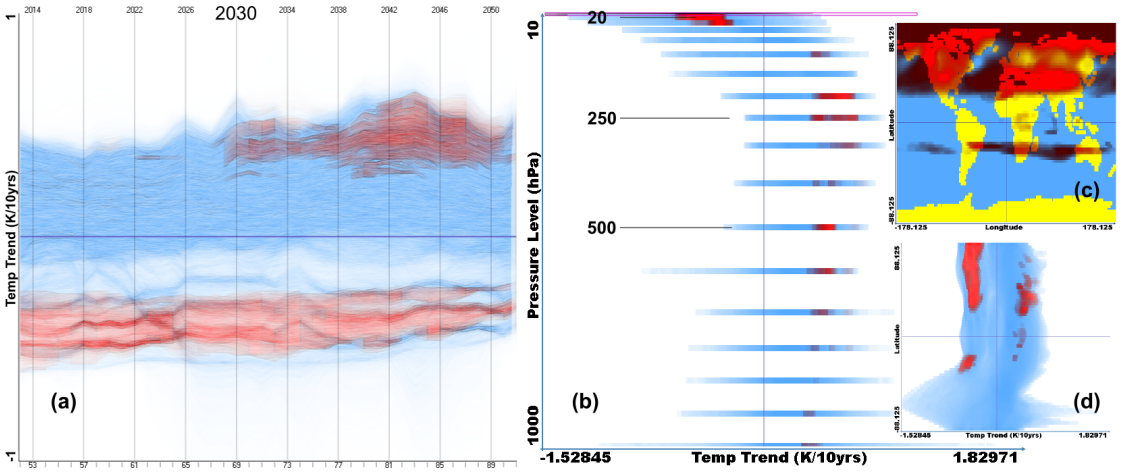

Figure 5: Exploration of the temperature field of the ECHAM5 run. High SNR values have been brushed as in Fig. 4 (not shown). Shown are a curve-view of temperature trends (2001 to 2064) (a), scatterplots of temperature trends vs. pressure levels (b), as function of geographic location (c), and vs. latitude (d), respectively, with the selected data in red.

values again depicted in red. Figure 5a shows the variation of the temperature trend over time from 2001 to 2064, where negative temperature trends show high significance throughout the whole time period. Positive trends become more significant around 2030 (recall that these are trends at individual grid points with no area or height layer averaging). It is important to emphasize again that the purpose of the interactive visual exploration is not to deliver quantitative results (as is usually the case in statistics), but rather to quickly come up with hypotheses about the data and to explore the data, without stating precise quantitative findings. Figure 5b indicates that the most sensitive region for detecting temperature trends can be found in the UTLS, with negative trends in the lower stratosphere and positive trends in the upper troposphere. The longitude-latitude distribution of significant trends is shown in Fig. 5c (northern hemisphere summer most visible in the JJA trends), and in Fig. 5d the respective latitude ranges for the positive (tropospheric) and negative (stratospheric) trends are highlighted. Interactive visualization proved effective for this fast first overview of the dataset.

Next we aim to compare our results with classical statistical trend testing (Wilks 2006). Using classical statistical analysis, linear trends were calculated over 2001 to 2050 at each pressure level and the significance of the trends was determined using Students t-test. Figure 6 (panel a) illustrates the regions for which this analysis was performed. For regions and pressure levels fulfilling the criteria of statistical significance above 90 %, and goodness-of-fit coefficient R^2 (the coefficient of determination) above 0.5, Fig. 6b shows the corresponding box colored. For details on the analysis see Lackner et al. (2009). We compare trends over 2001 to 2050 only, since a linear fit is not an adequate approximation

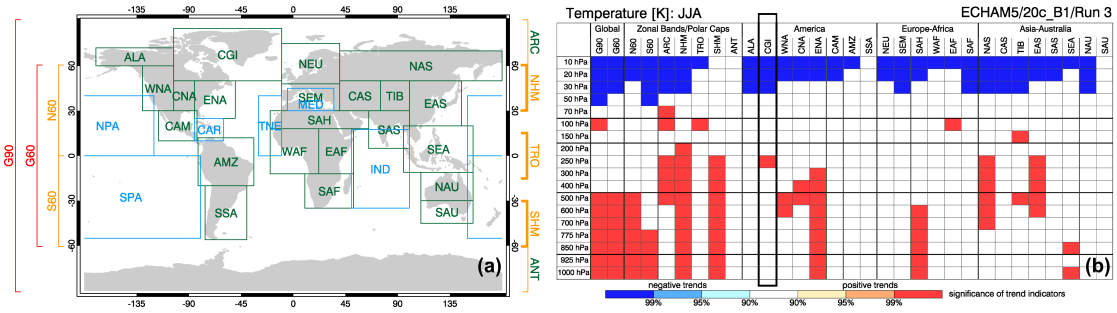

Figure 6: Regions used in a classical statistical analysis, corresponding mostly to the IPCC regions (Solomon et al. 2007b; Lackner et al. 2009) (a) and temperature trend results for the ECHAM5 run for the time period 2001 to 2050 (b). In (b) boxes of regions with statistically significant positive trends are marked in red, those with significant negative trends in blue.

for the changing trend over the whole time period starting 1961.

For comparison of the features shown in Fig. 5 with statistical results, we choose spatial subdomains according to the regions used in Fig. 6. This is one of the major strengths of interactive visual exploration—while in statistical analysis it can be hard to keep an eye on the whole domain at the same time, generally forcing to pre-select areas of interest, the visual exploration can be done on the whole dataset at once, selecting features interactively and iteratively.

Figure 7 illustrates this. We choose the Canada-Greenland-Iceland (CGI) region as an example, where we brush the region in a longitude-latitude scatterplot (Fig. 7a). The resulting distribution of values showing high SNR as function of pressure levels (Fig. 7b) can immediately be compared with the statistical result in Fig. 6b, where a significant negative temperature trend signal is shown for the top-most levels 30 hPa upwards, and a positive trend at the 250 hPa level. This indeed agrees very well with Fig. 7b, where the data points in red are clustered at the top-most levels and the 250 hPa level. Some less pronounced features can also be seen in other levels (better visible on-screen). Figure 7c shows that the trend significance over time is very stable at stratospheric levels, while the upper tropospheric signal appears most significant for the temporal center of the moving trend estimates around the year 2030.

Other investigated regions (not shown) compare similarly well with statistical results. This gives us confidence that the interactive visual approach, while not meant to give quantitatively precise results, is able to serve as a good exploratory complement to the classical statistical approach.

As a final example for the climate model data exploration illustrated in Fig. 8, we focus on the distinct band of data points with high SNR in the southern hemisphere subtropics in Fig. 5c. Brushing the range of about 20°S to 30°S (Fig. 8a), we see that it stems from the stratosphere with negative trend values (Fig. 8b; less pronounced features on, e.g.,

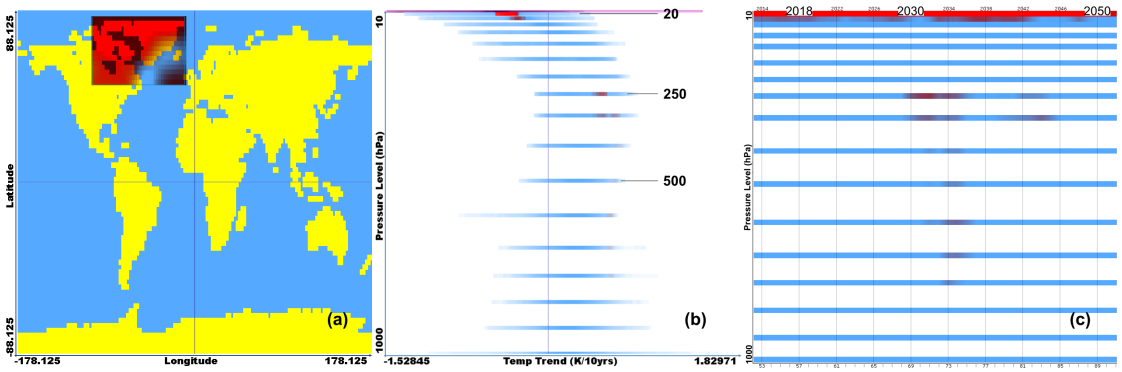

Figure 7: Inspecting the Canada-Greenland-Iceland (CGI) region of Fig. 6. Brushing the region (highlighted rectangle) (a), scatterplot of temperature trends vs. pressure levels (b), and curve-view showing the time variation of trend significances (c), with the selected data in red.

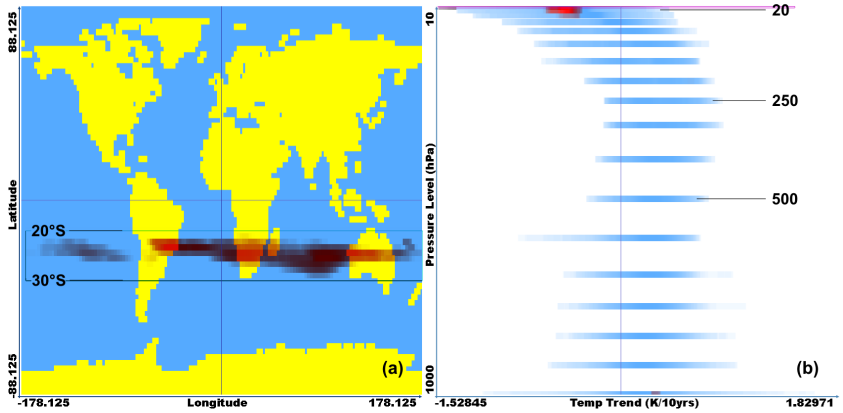

Figure 8: Inspecting the feature in the southern hemisphere subtropics found in Fig. 5. Shown are scatterplots as function of geographic location (with the 20°S to 30°S band marked) (a) and of pressure levels (b), respectively, with the selected data in red.

the near-surface 1000 hPa layer with positive trend values can be seen on-screen). We regard it as a good example for the power of visual, undirected exploration that this band was *not* part of the zonal bands defined in Fig. 6a (there is a gap between the tropical (TRO) and the Southern Hemisphere Mid-latitudes (SHM) band; see legend at the right of Fig. 6a) and that this pronounced feature has therefore been "overlooked" in the statistical analysis based on this definition.

4.3 Exploring GPS Radio Occultation Data

To introduce the RO datasets, the climatological temperature profiles of the WegC1 processing are shown in Fig. 9. The typical tropical temperature profile shape emerges

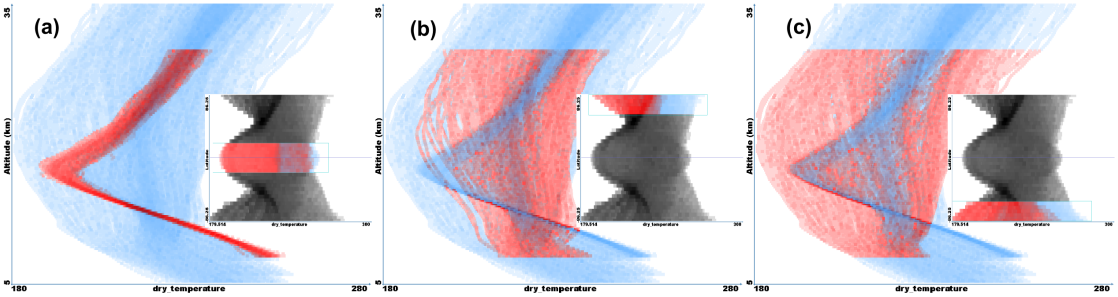

Figure 9: Zonal mean monthly-mean temperature profiles (5 km to 35 km) from the CHAMP GPS RO data for the time period 2002 to 2006, processed by WegC1 (cf. section 3). The brushes (shown in the inset) selected the tropics (a), the northern (b) and southern (c) high latitudes, respectively, and the selected data are shown in red. Data at altitude levels outside 8 km to 30 km are not in red because the corresponding refractivity data of all centers overlap fully in 8 km to 30 km only; removed by a NOT-brush in another view, not shown.

from the set of profiles very clearly (Fig. 9a). A higher variation of the profiles can be seen at high latitudes (Figs. 9b,c), with more isothermal shape as expected. Somewhat less variability occurs over the arctic region (Fig. 9b) than over the antarctic one (Fig. 9c), where also the absolutely coldest conditions prevail.

Having set this context, we explore relations between refractivity climatologies of the four processing versions (WegC1, WegC2, RefC1, RefC2), shown in Fig. 10. The number of contributing individual profiles to each monthly-mean climatological profile differs between the four datasets due to different quality criteria used in the processing systems. In Figs. 10a–d the relation between the relative difference of refractivities to the four-dataset mean and the corresponding difference of the number of profiles to the four-dataset mean number of profiles is shown. While RefC1 and RefC2 numbers (Figs. 10a,b) lie tentatively above average, the WegC processings (Figs. 10c,d) show a number of profiles tentatively below average. The reason is that the WegC processing uses somewhat more rigid quality criteria.

The relative differences show no obvious systematics in this view, so we inspect them further. The *Parallel Coordinates* view shows a set of chosen parameters as vertical coordinate axes that are placed next to each other (Inselberg and Dimsdale 1990). Each multi-variate data point is then represented as a polyline that connects the corresponding data values on the parallel axes. This makes it a suitable representation for detecting interdependencies between the parameters. For example, if most of the line segments between two adjacent coordinate axis are parallel to each other there is a strong correlation between the attributes represented by the respective axis. The view allows brushing for each coordinate separately. Figure 10e shows the result when choosing the altitude as one parameter of interest (left), followed by the relative refractivity differences to the four-dataset mean (from left to right) of RefC1, RefC2, WegC1, and WegC2, respectively,

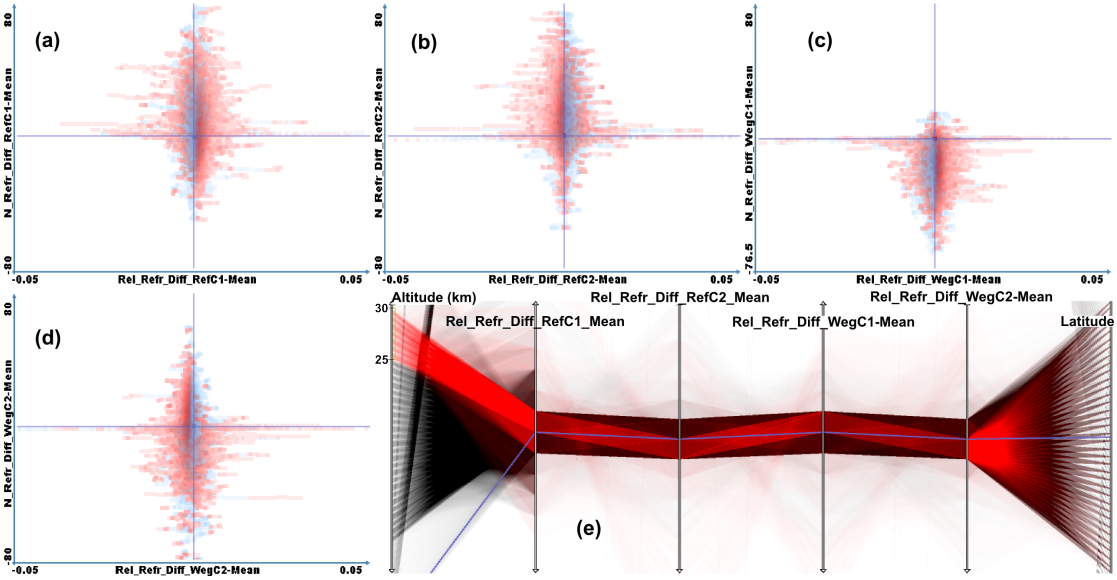

Figure 10: Relation between the number of profiles and relative refractivity differences against the four-dataset mean for RefC1 (a), RefC2 (b), WegC1 (c), and WegC2 (d). Data outside 8 km to 30 km deselected in a previous step (not shown) appear in blue, selected data in red. A parallel coordinates view (explained in the text) was brushed to select the altitude range from about 25 km to 30 km (leftmost coordinate), with the selected data in red (e). The other coordinates show relative refractivity differences of each dataset (four middle), and latitude (right). The blue line connects the (zero) origins of all coordinates.

and, as last coordinate (right), the latitude. For the selected 25 km to 30 km altitude range RefC1 and WegC1 show a tendency to larger relative refractivities than the mean, and vice versa for RefC2 and WegC2. This behavior is understood by recalling from section 3 that the main difference between the processing versions of WegC1 and WegC2 lies in the switch from using the raw data processed in a first step by RefC1 to the raw data processed by RefC2. The opposite tendency of the WegC1 and the WegC2 refractivity data compared to the mean suggests that the resulting climatologies from RO data are mainly influenced by this first processing step towards the phase delay and orbit data. A possible dependence on latitude could be easily spotted (rightmost coordinate), but appears not to exist.

Practically, such small residual processing differences, especially above 25 km, are well understood by the RO science community (e.g., Ho et al. 2009b; Steiner et al. 2009a) and further mitigated by improved processing; here it served as an instructive example how interactive visualization could spot these fast and effectively in a multi-center, multi-year remote sensing dataset for climate.

5 Conclusions

The amount of geophysical data available to scientists grows at a remarkable pace. The instrument to handle such large multivariate datasets is most commonly classical statistics. As an innovative approach, interactive visual exploration is shown to be a valuable technology to explore atmospheric and climate data and to be complementary to statistical analysis. It uses the power of human vision to detect features and relations within multiple parameters of a multi-dimensional dataset.

Here we presented some of these visualization concepts to the atmospheric, climate, and oceanic research community. Using the field exploration technology SIMVIS, the potential of undirected interactive exploration was shown for three representative example datasets, including reanalysis data, climate model data, and GPS Radio Occultation (RO) satellite data. We performed interactive exploration of atmospheric climate fields of temperature, geopotential height, and refractivity. Our approach efficiently detected deficiencies in the reanalysis dataset, and identified parameters and regions reacting most sensitive to climate change (for more details on this topic see Kehrer et al. (2008) and Ladstädter et al. (2009)). Small differences between satellite datasets were spotted fast and effectively in the context of quality assurance for climate applications of RO data.

We exploited that the visual exploration approach is clearly distinctive to classical statistical methods in that it does not require prior knowledge about the dataset. Features that attract the attention of the user can interactively be selected and iteratively explored in more detail. The resulting hypotheses about the data can then be quantitatively evaluated and confirmed by statistical analysis. We showed that the properties of the approach make it easy to get an overview over general characteristics of the dataset, to focus on certain subdomains of the parameter space, to generate hypotheses about the data, and to even spot relevant features which might have been overlooked in statistical analysis. Comparison with statistical results confirmed the utility of the technology, showing that interactive exploration forms a valuable complement to classical statistics, permitting a fast, efficient, and instructive analysis of the data.

Visualization enabling a direct and interactive access to atmospheric, climate, and oceanic datasets can support the process of gaining insight into the data characteristics. It is easy to visually analyze and explore features of interest such as trends, differences between datasets, or interdependencies between available parameters. Many more applications can be envisioned, dependent on the specific dataset; we see the potential to apply the presented approach to other climatological and geophysical datasets, beyond the example types of data used in this study. In conclusion, we encourage to combine the instruments of classical statistical analysis with advanced exploratory data analysis methods in an integrated workflow, helping to handle the vast amount of today's data output that geoscientific research is dealing with.

Acknowledgment The authors acknowledge GFZ (Potsdam, Germany) and UCAR (Boulder, CO, USA) for CHAMP RO data and ECMWF (Reading, UK) for the ERA-40 reanalysis data. We furthermore acknowledge the modeling groups, the PCMDI and WRCP's Working Group on Coupled Modelling (WGCM) for access to ECHAM5 data as part of CMIP3 multi-model data. SimVis GmbH is thanked for its efforts in SIMVIS development (www.simvis.at) and J. Fritzer, M. Borsche, and U. Foelsche (Wegener Center) for their efforts in RO processing development and climatology preparations, respectively. The work was financed by Austrian Science Fund (FWF) grants P18733-N10 and P18837-N10; RO processing development also by ESA and the Austrian Research Promotion Agency (FFG-ALR) via projects ProdexCN2 and EOPSCLIM.

PAPER D

An assessment of differences in lower stratospheric temperature records from (A)MSU, radiosondes, and GPS radio occultation

F. Ladstädter[1], A.K. Steiner[1], U. Foelsche[1], L. Haimberger[2], C. Tavolato[2], G. Kirchengast[1]

[1]Wegener Center for Climate and Global Change (WEGC) and Institute for Geophysics, Astrophysics, and Meteorology/Inst. of Physics (IGAM/IP), University of Graz, Austria
[2]Department of Meteorology and Geophysics, University of Vienna, Austria

ABSTRACT

Uncertainties for upper-air trend patterns are still substantial. Observations from the Radio Occultation (RO) technique offer new opportunities to assess the existing observational records there. Long-term time series are available from radiosondes and from the (Advanced) Microwave Sounding Unit ((A)MSU). None of them were originally intended to deliver data for climate applications. Demanding intercalibration and homogenization procedures are required to account for changes in instrumentation and observation techniques. In this comparative study three (A)MSU anomaly time series and two homogenized radiosonde records are compared to RO data from the CHAMP, SAC-C, GRACE-A and F3C missions for September 2001 to December 2010. Differences of monthly anomalies are examined to assess the differences in the datasets due to structural uncertainties. The difference of anomalies of the (A)MSU datasets relative to RO shows a statistically significant trend within about (-0.2 ± 0.1) K/10 yr (95 % confidence interval) at all latitudes. This signals a

This article was published in *Atmospheric Measurement Techniques* 4 (2011), pp. 1965–1977. DOI: 10.5194/amt-4-1965-2011

systematic deviation of the two datasets over time. The radiosonde network has known deficiencies in its global coverage, with sparse representation of most of the Southern Hemisphere, the tropics and the oceans. In this study the error that results from sparse sampling is estimated and accounted for by subtracting it from radiosonde and RO datasets. Surprisingly the sampling error correction is also important in the Northern Hemisphere (NH), where the radiosonde network is dense over the continents but does not capture large atmospheric variations in NH winter. Considering the sampling error, the consistency of radiosonde and RO anomalies is improving substantially; the trend in the anomaly differences is generally very small. Regarding (A)MSU, its poor vertical resolution poses another problem by missing important features of the vertical atmospheric structure. This points to the advantage of homogeneously distributed measurements with high vertical resolution.

1 Introduction

The Upper Troposphere–Lower Stratosphere (UTLS) region is known to react sensitively to climate change (Baldwin et al. 2007). High-quality observations are crucial to assess the anthropogenic influence on the climate system in the UTLS. It is well known that the temperature trend patterns in the troposphere and stratosphere can provide valuable information on the mechanisms of climate change (Karl et al. 2006; Solomon et al. 2007a; Thompson and Solomon 2005). Until now observational data exist primarily from radiosondes (since 1958) and from the (Advanced) Microwave Sounding Unit ((A)MSU) instrument flying on US National Oceanic and Atmospheric Administration (NOAA) polar orbiting satellites (since 1979). However, none of these existing long-term measurement systems for the upper-air were originally intended to be used for climate monitoring purposes. While surface temperature trends are in accordance amongst different groups (Solomon et al. 2007a), the uncertainties regarding trend values for the upper-air are still substantial (Randel et al. 2009; Randall and Herman 2008; Titchner et al. 2009). The main reasons for these uncertainties derive from demanding intercalibration and homogenization procedures. These *structural uncertainties* have been results of changing instrumentation and observation practice over the decades (Karl et al. 2006; Thorne et al. 2005). This is true for both main sources of upper-air temperature data. The radiosonde time series has specifically experienced numerous changes in their stations, types of sensors, and changes in data processing systems. Using advanced homogenization techniques, these artificial data discontinuities are reduced (Haimberger 2007; Haimberger et al. 2008). The sparse spatial sampling is causing further uncertainties in the global radiosonde stations' network (Free and Seidel 2005). Unlike radiosondes, (A)MSU data provide very good global coverage. The instrumentation biases introduced in the chain of NOAA satellites (most recent being NOAA-19) still need to be accounted for. Further

errors affecting (A)MSU data include shifts in the diurnal sampling, orbit variations and calibration changes (Karl et al. 2006). Many of these issues are addressed by calibrated datasets produced by different groups (Christy et al. 2007; Mears and Wentz 2009b; Zou et al. 2009).

There have been significant efforts in the past to create reliable climate records despite these obstacles (Mears and Wentz 2009b; Christy et al. 2003; Haimberger et al. 2008; Zou and Wang 2010). It has been argued that the uncertainties in upper-air temperature trends are inevitable due to structural uncertainties involved in the methodology (Thorne et al. 2005). Increasing the number of independent datasets decreases the structural uncertainty (Seidel et al. 2004). The need for new upper-air measurement systems has already been stated by the implementation plan for the Global Observing System for Climate (GCOS 2010). One already existing relatively new system is GPS Radio Occultation (RO) that can be considered as of potential benchmark quality (Steiner et al. 2009a). RO uses Global Positioning System (GPS) radio signals in limb sounding geometry to deliver observations in the UTLS region with high accuracy, global coverage, and high vertical resolution (Melbourne et al. 1994; Kursinski et al. 1997; Steiner et al. 2001; Hajj et al. 2002). Additionally it is self-calibrating, thus avoiding error-prone intercalibration procedures. These properties make the technique well qualified to be used for climate applications, as has been shown in a considerable number of publications (e.g., Scherllin-Pirscher et al. 2011a; Steiner et al. 2009a; Foelsche et al. 2009; Ho et al. 2009b; Leroy et al. 2006). Therefore RO can be considered a good choice to assess the adequacy of the observational data mentioned above for climate applications. This has been done in several previous studies for (A)MSU (Schrøder et al. 2003; Ho et al. 2007; Steiner et al. 2007, 2009b). Regarding radiosondes, Kuo et al. (2005), He et al. (2009), and Sun et al. (2010) concluded that RO soundings are of sufficient quality to differentiate between different types of radiosondes. Steiner et al. (2007, 2009b), and Ho et al. (2007) found significant differences between RO and (A)MSU records. Ho et al. (2009a) suggested to use RO data for calibration of (A)MSU temperatures.

This study advances previous work (Steiner et al. 2007), using the most recent datasets for RO, (A)MSU and radiosondes, and substantially longer records. It furthermore improves on previous work by analysing error characteristics of RO and radiosondes resulting from sparse spatial and temporal sampling. The data used in this study are briefly introduced in Sect. 2, the method of comparison and assessing sampling error characteristics is described in Sect. 3, the results are discussed in Sect. 4, followed by a summary of the results and conclusions of this comparative study.

2 Data

The comparison time range is limited by the availability of continuous RO data. The CHAMP satellite (Wickert et al. 2001) delivered data from September 2001 to September

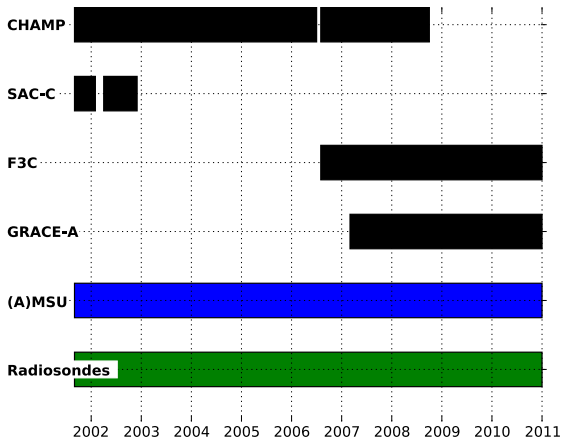

Figure 1: Time frames of datasets used (black, GPS RO datasets).

2008. Data from the FORMOSAT-3/COSMIC (F3C) mission (Anthes et al. 2008) are used starting from August 2006 until December 2010. Available data from SAC-C (2001, 2002) (Hajj et al. 2004) and GRACE-A (2007 to 2010) (Beyerle et al. 2005) are also used. The study time frame is therefore September 2001 to December 2010 (Fig. 1).

2.1 GPS Radio Occultation

We use CHAMP, SAC-C, GRACE-A, and F3C profiles from September 2001 to December 2010 as processed by the Wegener Center for Climate and Global Change (WEGC). We applied the current processing scheme OPSv5.4 (Occultation Processing System, version 5.4) to excess phase data and precise orbit information provided by the University Corporation for Atmospheric Research (UCAR) (Pirscher 2010). The data of the various instruments can be combined to a consistent single climate record as long as the processing chain is the same for all sources (Pirscher 2010; Foelsche et al. 2011). Only high-quality profiles are provided and can be downloaded from the global climate monitoring website[1]. We use dry-temperature profiles in an altitude range of 4 km to 35 km at a vertical resolution of 0.1 km. The RO specific dry-temperature is essentially the same as actual temperature at altitudes above 10 km where moisture is negligible (Scherllin-Pirscher et al. 2011b). Therefore it can be directly used to study the (A)MSU lower stratosphere channel of interest here (Steiner et al. 2007, 2009b). The number of profiles ranges from about 120 to 160 per day (single-satellite) up to about 2000 per day (multi-satellite); see the representative example months in Fig. 2. In both cases the observations are distributed approximately uniformly in space and time within each month.

[1] www.wegcenter.at/globclim

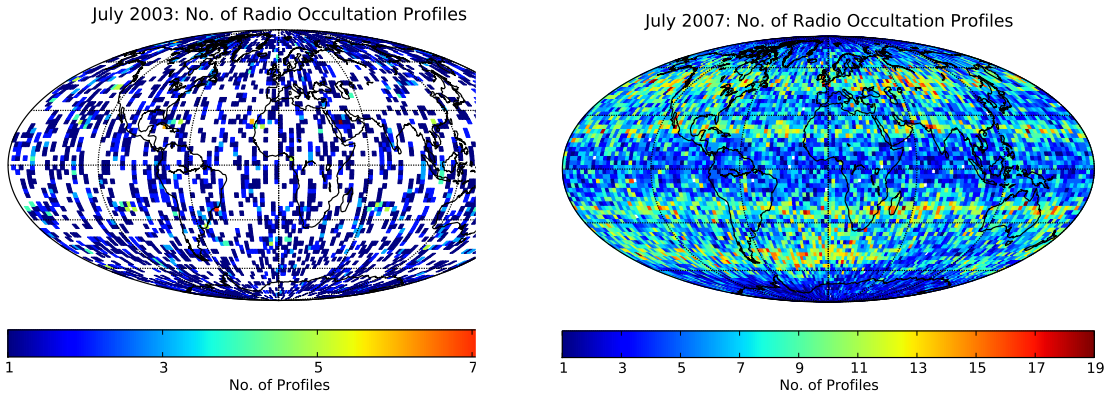

Figure 2: Global monthly coverage of RO profiles for July 2003 (left) single-satellite (CHAMP) and for July 2007 (right) multi-satellite data (CHAMP, COSMIC, GRACE-A). Number of profiles in $2.5° \times 2.5°$ bins are shown.

2.2 (Advanced) Microwave Sounding Unit

The (Advanced) Microwave Sounding Unit ((A)MSU) instruments provide satellite-based nadir measurements of layer-average brightness temperatures. The instruments fly on board of the NOAA series of polar orbiting satellites. We use calibrated post-processed data from three different groups, all of them provided at $2.5° \times 2.5°$ horizontal resolution. The AMSU instruments are in orbit since 1998, while the last NOAA satellite with an MSU instrument aboard was decommissioned in 2007 (NOAA-14), with decreasing data continuity after 2004. Therefore, during this overlap time contained in the study time frame, the (A)MSU datasets include data from both instrument types.

The bulk temperature of the lower stratosphere region (TLS) corresponds to MSU channel 4 and AMSU channel 9, respectively. These two channels match each other fairly well in order to ensure continuation of the temperature time series. Remaining differences between the MSU and the AMSU instrument are accounted for in the merging procedures of the processing groups so that the time series matches the MSU data (Mears and Wentz 2009a).

The layer between 150 hPa and 30 hPa ($\approx$ 13 km to 25 km) contributes most to the TLS layer mean temperature, peaking at around 90 hPa ($\approx$ 18 km) (Christy et al. 2003). The poor vertical resolution results in considerable influence of the troposphere to the TLS in the tropics.

TLS brightness temperatures were retrieved from the University of Alabama at Huntsville (UAH) (Christy et al. 2003) in version UAHv5.4;[2] from Remote Sensing Systems (RSS)

[2] http://vortex.nsstc.uah.edu/data/msu/

(Mears and Wentz 2009b) in version RSSv3.3;[3] and from the National Environmental Satellite, Data and Information Service (NESDIS) Center for Satellite Applications and Research (STAR) (Zou et al. 2009) in version STARv2.0.[4]

2.3 Radiosondes

For this comparison, we use the latest homogenized radiosonde datasets: The Radiosonde Observation Correction using Reanalyses (RAOBCORE) dataset (Haimberger 2007) and the Radiosonde Innovation Composite Homogenization (RICH) dataset (Haimberger et al. 2008), both in version 1.5. Compared to the already published version 1.4, the new version uses raw radiosonde data and background forecast data from ERA-Interim (Dee et al. 2011) instead of operational ECMWF analyses. More than 1000 stations are used. 00:00 UTC and 12:00 UTC launches are kept separately. Figure 3 shows the global coverage of these archives and indicates the launch times. The homogenization procedure works on daily data, which enables very effective breakpoint detection.

RAOBCORE uses time series of the ERA-Interim background forecasts as reference for homogenization. RAOBCORE is therefore, strictly speaking, not independent of satellite data, because ERA-Interim contains (A)MSU information. RICH uses the breakpoints detected by RAOBCORE, but relies only on up to 30 neighboring stations for the actual homogenization. It is therefore a completely independent dataset (Haimberger et al. 2008).

The radiosonde data are available on 12 pressure levels from 850 hPa to 30 hPa.[5] For both homogenized radiosonde time series, the University of Vienna used the Radiative Transfer for TOVS (RTTOV) model (Saunders 2008) to construct MSU-equivalent brightness temperature (TLS) anomalies. The TLS values were then binned into a 2.5° × 2.5° horizontal grid.[6]

2.4 ECMWF

As reference dataset in the estimation of sampling error characteristics of RO and radiosondes (see method description in Sect. 3), we use the ECMWF operational analysis fields. For each RO profile, OPSv5.4 extracts a collocated profile from the global ECMWF field at T42 resolution, comparable to the horizontal resolution of RO (Scherllin-Pirscher et al. 2011a). The analysis fields are available for four time layers, 00:00 UTC, 06:00 UTC, 12:00 UTC, and 18:00 UTC. The 00:00 UTC and 12:00 UTC time layers correspond to the radiosonde launch times and are used in 2.5° × 2.5° horizontal resolution on 25 pressure levels (from 1 hPa to 1000 hPa) as collocated fields to radiosonde data at station

[3] http://www.remss.com/msu/msu_browse.html
[4] ftp://ftp.orbit.nesdis.noaa.gov/pub/smcd/emb/mscat/data/v2.0/
[5] 850 hPa, 700 hPa, 500 hPa, 400 hPa, 300 hPa, 250 hPa, 200 hPa, 150 hPa, 100 hPa, 70 hPa, 50 hPa, 30 hPa
[6] http://www.univie.ac.at/theoret-met/research/raobcore/

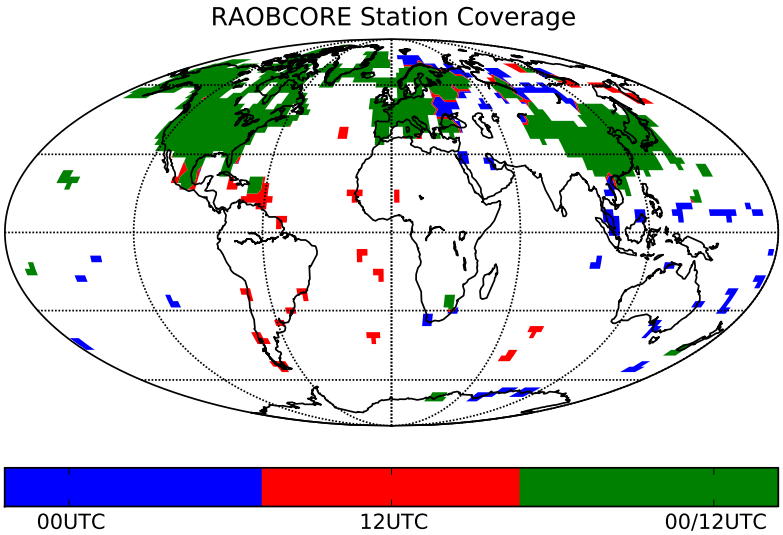

Figure 3: Global coverage of radiosonde launches used in the RAOBCORE and RICH datasets. The color code shows whether there are launches at 00:00 UTC (blue), 12:00 UTC (red), or at both times (green), in the corresponding 2.5° × 2.5° bin.

locations. The vertical resolution was increased in 2007, but additional levels after 2007 were introduced below 500 hPa only, which has no effect on the TLS. The averaged field over all time layers is used as reference for the radiosondes and RO, as described in the next section.

3 Method

The different comparisons in this study are based on TLS layer-average brightness temperatures ("MSU-equivalent"). We compare monthly and zonal means for regularly-spaced 20° bands and for four regions, tropics (20° S to 20° N), extra-tropics (70° S to 30° S and 30° N to 70° N), and quasi-global (70° S to 70° N).

3.1 Setup of comparable data

Consistent with the computational procedure applied for radiosonde profiles (see Sect. 2.3), we use RTTOV to compute layer-average TLS from RO and collocated ECMWF temperature profiles. RTTOV uses internally 43 vertical levels from 0.1 hPa to 1013 hPa. The input profiles are interpolated to these levels. To match the horizontal and temporal resolutions of the other datasets, we then bin the resulting TLS field into a 2.5° × 2.5° grid (monthly means). Averaging involves weighting by the cosine of the latitude, which accounts for

area changes between meridians of different latitudes (Foelsche et al. 2008b). This is only a minor effect at this resolution though. We do not distinguish between the various RO missions, all available RO profiles are incorporated into the respective monthly mean. As noted above, this procedure is justified given that the processing chain is the same for all sources (up to negligible differences in raw processing) and that the inter-satellite consistency is thus very high (Foelsche et al. 2011).

The ECMWF analysis field at $2.5° \times 2.5°$ resolution is also processed by RTTOV separately for all four available time layers. As a result, all datasets involved in this comparison are now available at the same monthly-means, $2.5° \times 2.5°$ resolution and in MSU-equivalent TLS. In Fig. 4 we show representative TLS fields for RO and differences of RO to STAR for two months (Northern Hemisphere (NH) winter and summer). TLS temperatures of RO and STAR show larger deviations at higher latitudes, but are generally in very good agreement, especially on a zonal mean scale as used below.

In the next step, we create latitudinal bands by simply averaging over all bins at each respective latitude. Then we aggregate those to larger bands. Here we apply weighting with the surface area of the bands involved. This approach accounts for the decreasing area of latitude bands of equal width (Foelsche et al. 2011).

3.2 Sampling error estimation

All observational datasets inherently differ from reality because of their finite sampling of the atmosphere. Depending on the sampling density and the variability of the atmosphere, it often is essential to account for this difference. A decent approach to estimate the magnitude of error made by discrete sampling is to compare atmospheric fields to a "true" reference field (Foelsche et al. 2008b). In this study, the sampling error estimation for RO and radiosondes is performed consistently. We do not consider sampling error for (A)MSU because we can assume that the error reaches virtually zero due to high horizontal resolution of the dataset. Potential temporal (A)MSU sampling errors caused by diurnal cycle drifts are already accounted for in the homogenized (A)MSU datasets (Christy et al. 1998; Mears and Wentz 2009a).

We use ECMWF analysis fields for all four time layers assuming that they are valid approximations of the "true" global field. The methodology for estimating the sampling error of RO is described in detail elsewhere (Pirscher 2010; Foelsche et al. 2008b). In short, the collocated ECMWF profiles are averaged to latitudinal bands and monthly means as described above. They represent the atmospheric state at the times and locations of RO measurements as seen by the reference field. We then subtract the full reference field, representing the "true" atmospheric state. We define this difference as *sampling error* of RO for the respective month and latitudinal band. We finally subtract the estimated de-seasonalized sampling error from RO anomalies. This substantially improves the quality of RO climatological fields as has been shown in several studies (Foelsche et al. 2011; Scherllin-Pirscher et al. 2011b). The actual data is thus not used for estimating the

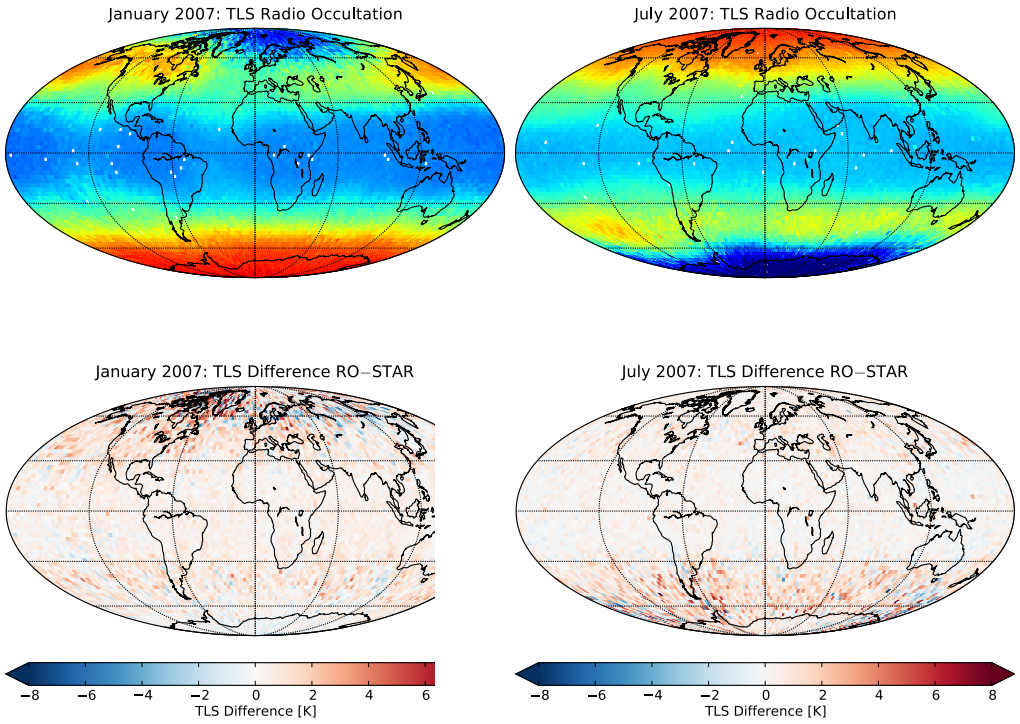

Figure 4: Brightness temperatures (TLS) for two monthly means at 2.5° × 2.5° resolution. (left) January 2007, (right) July 2007, (top) Radio occultation synthetic TLS, (bottom) Difference of RO synthetic TLS to AMSU TLS (STAR).

sampling error.

In contrast to satellite measurements, the global coverage of radiosondes is not uniform. Most notable, the Southern Hemisphere (SH), the tropics, and the oceans are sparsely represented. In other regions, especially over the NH continents, the coverage is very good. Free and Seidel (2005) stated that the concentration of stations in those regions does not necessarily improve the dataset because it oversamples those continental areas while under-representing the oceans. At most of the stations in the SH, radiosonde launches occur only once a day, see Fig. 3. Using an equivalent approach as for RO we estimate the sampling error for radiosondes. We take the ECMWF analysis fields for 00:00 UTC and 12:00 UTC separately, and sub-sample the 2.5° × 2.5° fields to bins where we have radiosonde data for the respective time. This results in a temporally and spatially collocated reference field, analogous to the method above described for RO. After averaging to latitudinal bands we subtract the full reference field containing all four time layers to get the sampling error for radiosondes. Finally we subtract the sampling error from the radiosonde data as we did for RO.

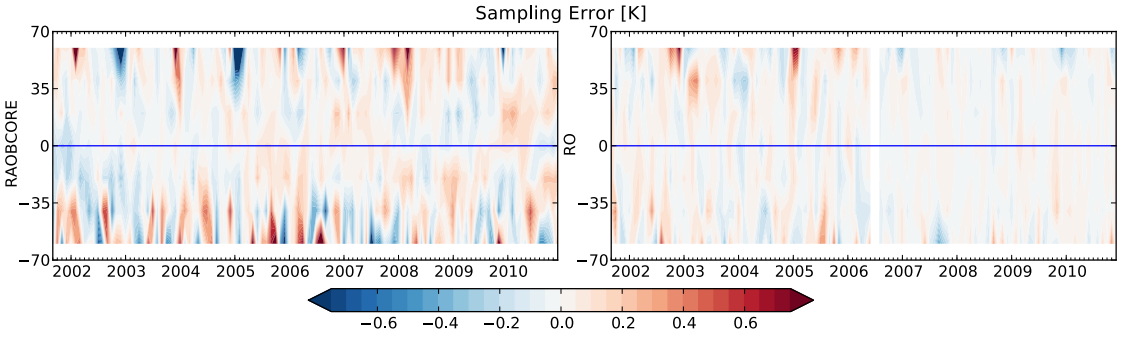

Figure 5: Sampling error of (left) radiosondes and (right) RO. Shown are latitudinal bands at 20° resolution.

3.3 Computation of TLS anomalies and anomaly differences

For RO and (A)MSU data, we calculate monthly TLS anomalies relative to the period 2002 to 2010 to de-seasonalize the data. The radiosonde time series are already provided in anomaly space for the same reference time period. After subtracting the respective de-seasonalized sampling error from RO and radiosonde anomalies (as described above), we compute differences of these anomaly time series. Thereby the climatological variability common to both datasets is removed. Then remaining are the differences due to structural uncertainties. We then compute the linear trends in the anomalies and anomaly differences and their statistical significance to assess deviations between the datasets. In particular, a statistically significant trend of the anomaly differences indicates that both datasets involved behave differently in their time evolution.

4 Results

4.1 Sampling error

Only by considering the sampling error for both RO and radiosonde records, a consistent comparison is possible. In Fig. 5 the resulting sampling error for radiosondes and RO is shown for 20° zonal bands from 70° S to 70° N.

For RO, the sampling error is generally very small (< 0.2 K), except at high latitudes, where it becomes increasingly difficult to capture atmospheric variability (Scherllin-Pirscher et al. 2011b). The additional F3C multi-satellite data as of 2006 provide only moderate reduction of the RO sampling error. For the monthly and zonal means considered in this study, the essential atmospheric variability is already captured by a single satellite (Pirscher et al. 2007; Foelsche et al. 2008a, 2009).

For radiosondes (cf. Fig. 5, left), the sampling error is rather small (< 0.3 K) between

Table 1: Trends of anomalies for the period of Sep. 2001 to Dec. 2010. The ± value defines the 95 % confidence intervals for the trends. Trend values which are significantly different from 0 at the 90 % and 95 % level are marked by a single and double asterisk, respectively.

Dataset	Trend (K/10 years)	$\text{StdDev}_{\text{Residuals}}$(K)
	70° S to 70° N	
RO	$+0.057 \pm 0.133$	0.19
RAOBCORE	$+0.137 \pm 0.128^{**}$	0.19
RICH	$+0.045 \pm 0.130$	0.19
UAH	$-0.140 \pm 0.130^{**}$	0.19
RSS	$-0.149 \pm 0.132^{**}$	0.19
STAR	$-0.162 \pm 0.126^{**}$	0.18
	20° S to 20° N	
RO	$+0.351 \pm 0.404^{*}$	0.59
RAOBCORE	$+0.342 \pm 0.443$	0.64
RICH	$+0.225 \pm 0.439$	0.64
UAH	$+0.137 \pm 0.374$	0.54
RSS	$+0.138 \pm 0.388$	0.56
STAR	$+0.111 \pm 0.364$	0.53
	30° N to 70° N	
RO	$+0.222 \pm 0.344$	0.50
RAOBCORE	$+0.237 \pm 0.333$	0.48
RICH	$+0.098 \pm 0.333$	0.48
UAH	-0.033 ± 0.330	0.48
RSS	-0.028 ± 0.336	0.49
STAR	-0.062 ± 0.321	0.47
	70° S to 30° S	
RO	$-0.743 \pm 0.451^{**}$	0.66
RAOBCORE	$-0.752 \pm 0.474^{**}$	0.69
RICH	$-0.712 \pm 0.470^{**}$	0.68
UAH	$-0.864 \pm 0.449^{**}$	0.65
RSS	$-0.905 \pm 0.456^{**}$	0.66
STAR	$-0.870 \pm 0.444^{**}$	0.65

Table 2: Trends of anomaly differences for the period of Sep. 2001 to Dec. 2010. The ± value defines the 95 % confidence intervals for the trends. Trend values which are significantly different from 0 at the 90 % and 95 % level are marked by a single and double asterisk, respectively.

Datasets	Trend (K/10 years)	$\mathrm{StdDev}_{\mathrm{Residuals}}$(K)
	70° S to 70° N	
RAOBCORE–RO	$+0.080 \pm 0.061^{**}$	0.09
RICH–RO	-0.013 ± 0.065	0.10
UAH–RO	$-0.198 \pm 0.042^{**}$	0.06
RSS–RO	$-0.206 \pm 0.043^{**}$	0.06
STAR–RO	$-0.220 \pm 0.045^{**}$	0.07
	20° S to 20° N	
RAOBCORE–RO	-0.012 ± 0.083	0.12
RICH–RO	$-0.129 \pm 0.089^{**}$	0.13
UAH–RO	$-0.216 \pm 0.061^{**}$	0.09
RSS–RO	$-0.215 \pm 0.058^{**}$	0.08
STAR–RO	$-0.242 \pm 0.071^{**}$	0.10
	30° N to 70° N	
RAOBCORE–RO	$+0.014 \pm 0.061$	0.09
RICH–RO	$-0.125 \pm 0.063^{**}$	0.09
UAH–RO	$-0.256 \pm 0.051^{**}$	0.07
RSS–RO	$-0.252 \pm 0.045^{**}$	0.06
STAR–RO	$-0.286 \pm 0.054^{**}$	0.08
	70° S to 30° S	
RAOBCORE–RO	-0.006 ± 0.139	0.20
RICH–RO	$+0.034 \pm 0.139$	0.20
UAH–RO	$-0.118 \pm 0.055^{**}$	0.08
RSS–RO	$-0.159 \pm 0.052^{**}$	0.08
STAR–RO	$-0.124 \pm 0.056^{**}$	0.08

about 50° S to 50° N. For higher latitudes the sampling error becomes large. We attribute this to greater variability of the atmosphere at higher latitudes and to the small number of stations in the SH. The sampling density in the tropics is also small but seems to be sufficient to capture the main features of atmospheric variability there. The patterns in southern and northern high latitudes differ substantially: While in the SH temporal evolution of the sampling error seems to be a rather random effect related to sparse sampling, the pattern in the NH shows a clear relation to the NH winter. Every NH winter the sampling error reaches a maximum. Comparing with Fig. 4 (top left), showing the TLS pattern in January, implies that the radiosonde network misses the large atmospheric variability in winter. This results in a larger sampling error.

Temporal sampling of radiosondes (00:00 UTC and 12:00 UTC) seems to basically capture the diurnal variation up to the semi-diurnal cycle. This was investigated by using only 00:00 UTC and 12:00 UTC time layers of the reference field for calculating the sampling error, instead of the "full" field of four time layers. Comparing the sampling error based on 00:00 UTC and 12:00 UTC time layers with that based on the "full" field showed very small differences only.

The effect of subtracting the respective sampling error from RO and radiosonde anomalies is shown in Fig. 6 for the large-scale zonal bands defined above. It is especially pronounced in NH and SH extratropics. The distinct influence of the sampling error correction in NH winter is clearly visible, as well as the all-year random effect in the SH extratropics. Generally, the radiosonde data get significantly closer to the RO time series after removing the sampling error. In the following, the RO and radiosonde datasets are always being used in the corrected form of having their respective sampling errors subtracted. We focus on 70° S to 70° N to avoid sampling problems at polar latitudes.

4.2 TLS anomalies and anomaly differences

The TLS anomalies of all datasets are shown in Fig. 7 at 20° latitudinal resolution for 70° S to 70° N. Overall, the anomaly patterns of the various datasets are consistent. Figure 8 shows TLS anomaly time series for the investigated large-scale zonal bands. The anomalies show good agreement over the whole time range. The anomaly trend values are summarized in Table 1. We observe statistically significant (at 95 % significance level) negative TLS trends in the global mean for all (A)MSU datasets. These negative trends mostly stem from the SH extratropics, where the trend values are in rough agreement with Randel et al. (2009). In the tropics the trend values are positive for the TLS brightness temperature anomalies for all datasets, though statistically not significant (except for RO, showing low significance). This probably is a result from the coarse vertical resolution of TLS MSU-equivalents, where TLS derives from integrating over upper troposphere/lower stratosphere parts of the tropics (Randel et al. 2009). As shown by Schmidt et al. (2010), RO detects a positive trend signal in the tropics around the tropical tropopause, most probably strongly influencing the integral TLS. We do not further enter here into a

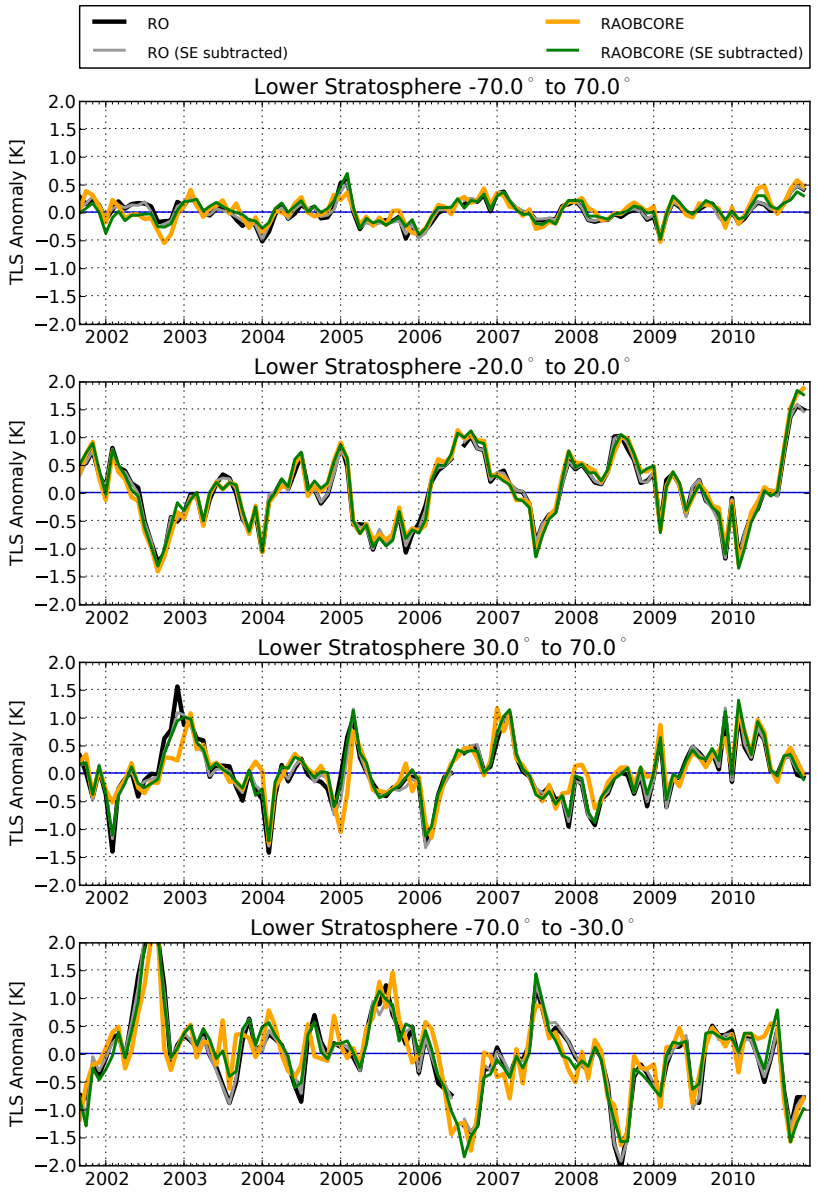

Figure 6: TLS anomalies before/after subtracting the sampling error for RO (black/grey) and for RAOBCORE (orange/green). Shown for quasi-global region, tropics, and for NH/SH extratropics (top to bottom).

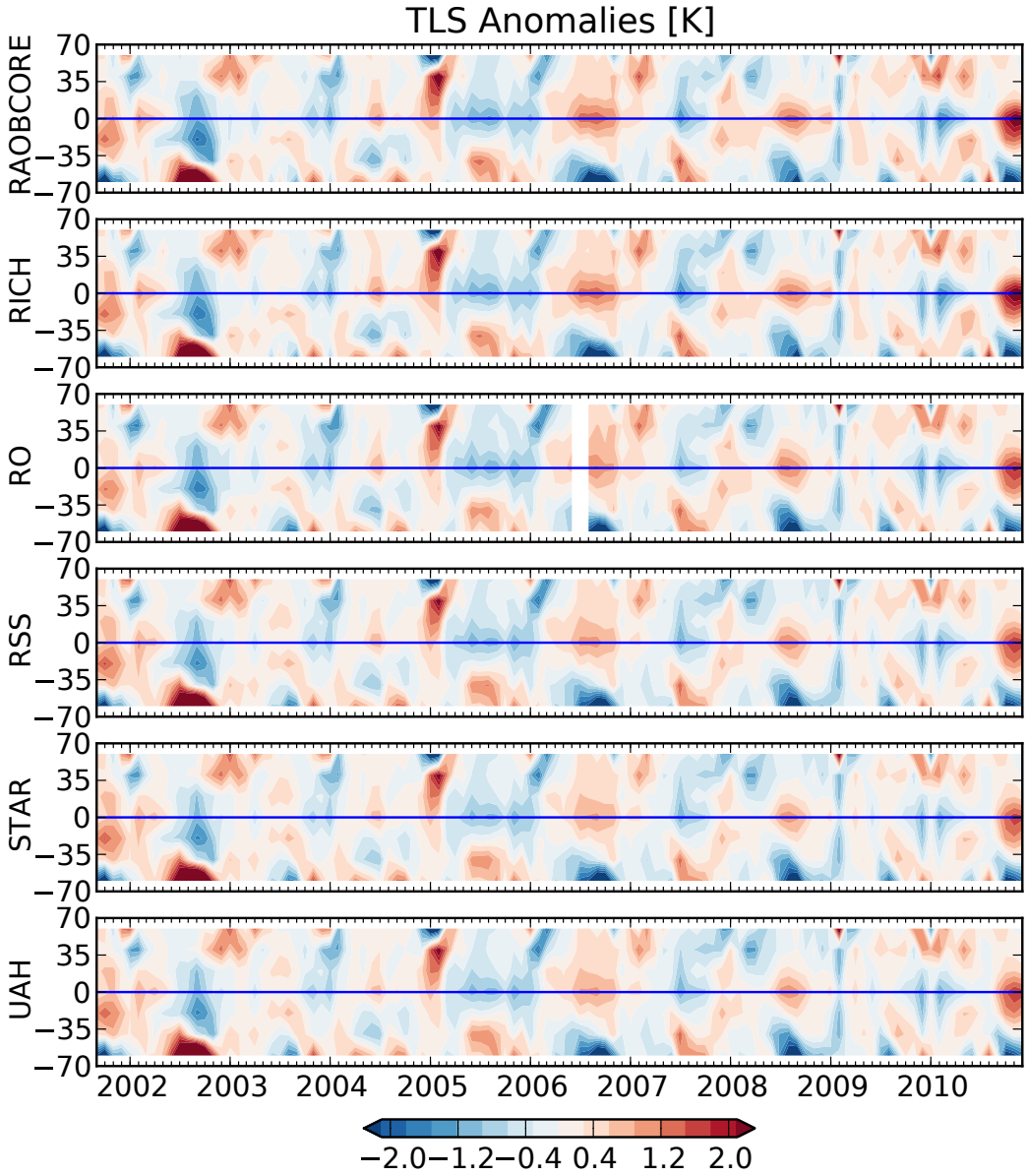

Figure 7: Evolution of TLS anomalies for radiosondes (RAOBCORE, RICH), RO, and (A)MSU (RSS, STAR, UAH) (top to bottom), shown at 20° resolution.

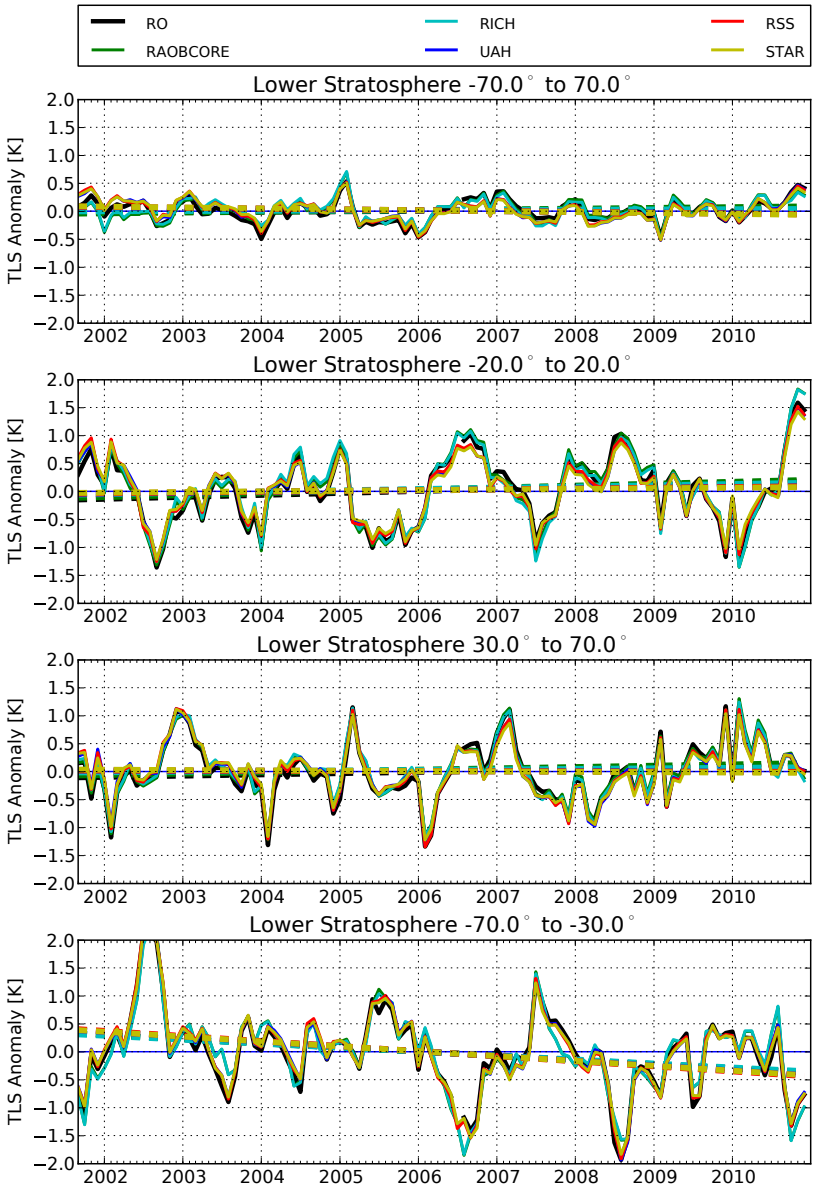

Figure 8: TLS anomaly time series for all datasets, shown for quasi-global, tropical, and NH/SH extratropical zonal bands (top to bottom). The linear regression lines are shown as dashed lines.

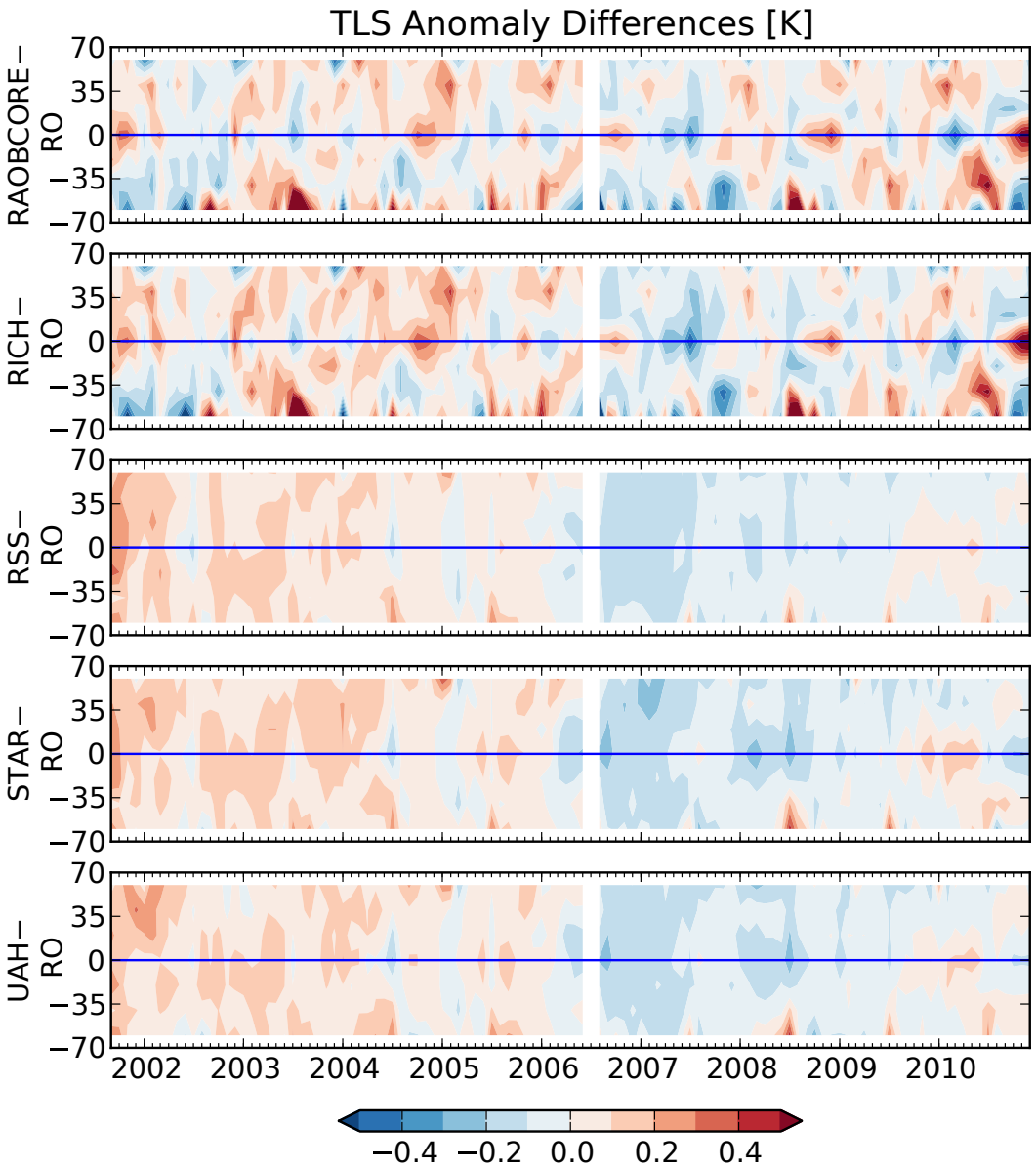

Figure 9: Evolution of TLS anomaly differences of radiosonde (RAOBCORE, RICH) and (A)MSU (RSS, STAR, UAH) datasets to RO at 20° resolution (top to bottom).

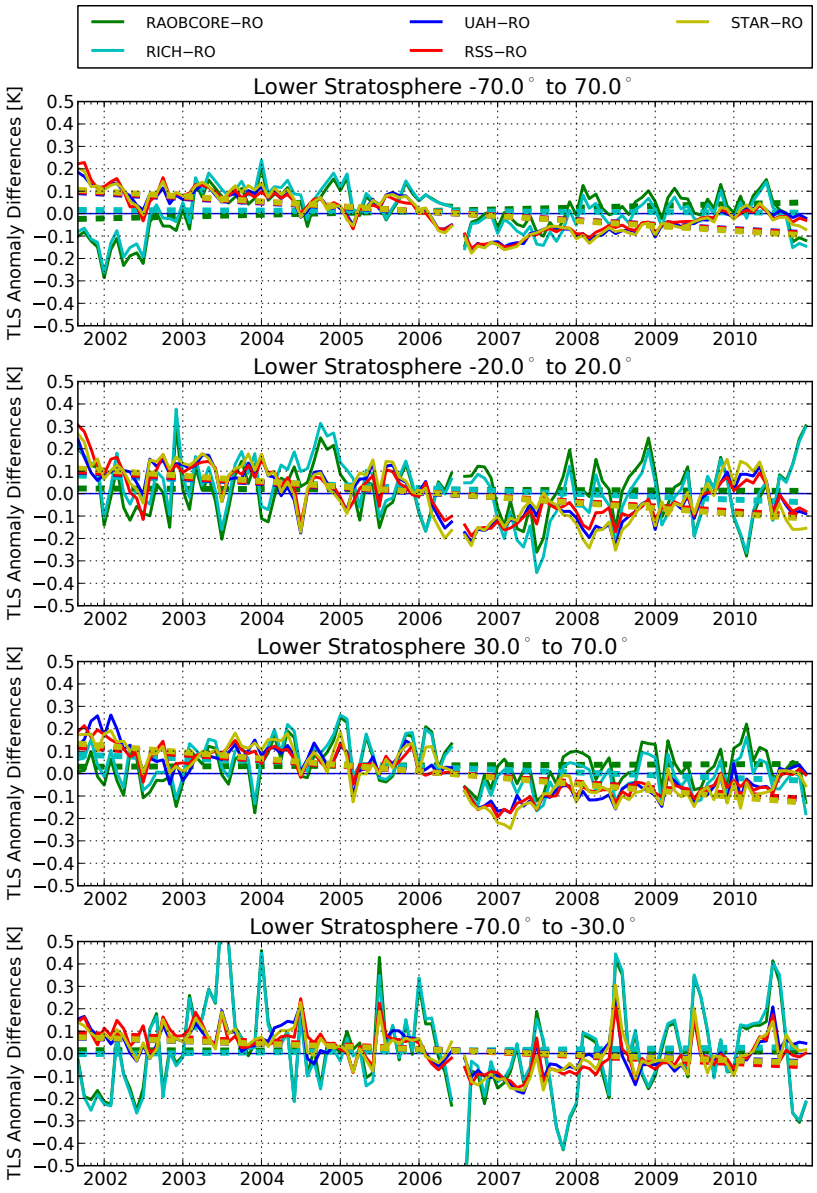

Figure 10: TLS anomaly difference time series for all datasets, shown for quasi-global, tropical, and NH/SH extratropical zonal bands (top to bottom). The linear regression lines are shown as dashed lines.

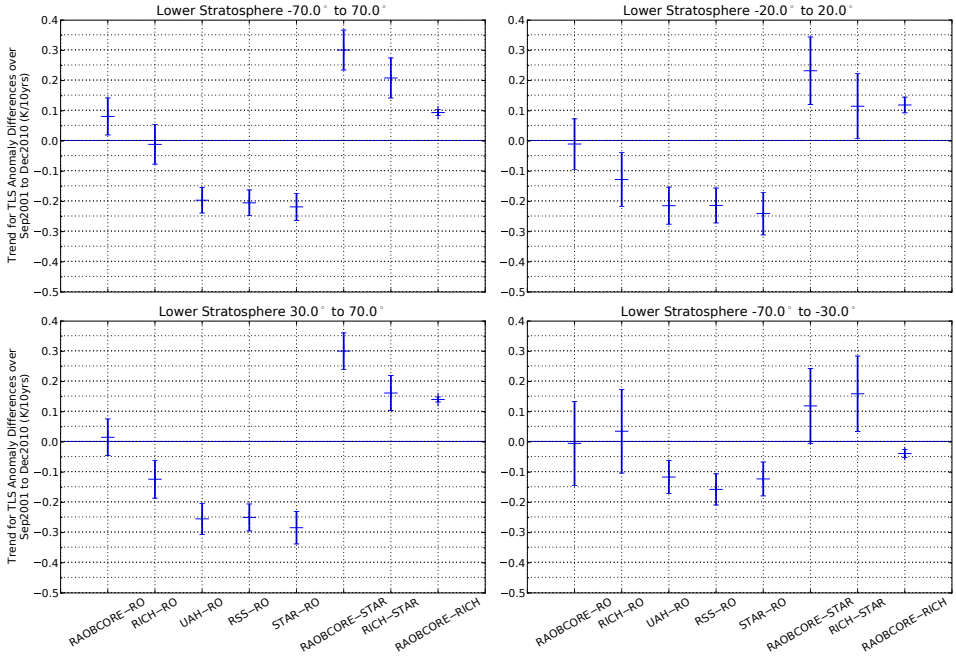

Figure 11: Trend values of anomaly differences with 95 % confidence interval for quasi-global, tropics, and NH/SH extratropics regions (top left to bottom right).

climatological interpretation of the trends (which is difficult because of the short time period involved) but focus below on the structural differences of the datasets.

The differences of radiosonde and (A)MSU anomalies to RO anomalies are shown in Fig. 9 at 20° latitudinal resolution and in Fig. 10 for the large-scale zonal regions. The anomaly difference trend values are summarized in Table 2. RAOBCORE and RICH show nearly negligible trends in their difference to RO, (0.08±0.06) K/10 yr and (−0.01±0.07) K/10 yr globally, which indicates that they do not diverge in time relative to RO. A moderate exception of this can be observed for the RICH dataset in the tropics and NH, with difference trend values of (-0.13 ± 0.09) K/10 yr and (-0.13 ± 0.06) K/10 yr. The above mentioned problem of the radiosonde network to correctly capture NH winter atmospheric variations is visible in the NH and quasi-global latitudinal bands. These differences are much more pronounced if the radiosonde datasets are not corrected for their sampling error (not shown; cf. Fig. 6).

The TLS anomaly difference trend of (A)MSU relative to RO is within about (-0.2 ± 0.1) K/10 yr throughout all latitude ranges, and statistically significant everywhere and for all three (A)MSU datasets (with relatively smallest values of about (-0.14 ± 0.05) K/10 yr in the SH and relatively largest ones of about (-0.26 ± 0.05) K/10 yr in the NH).

These results are visually summarized in Fig. 11, and also include the respective difference of the radiosonde datasets to a representative (A)MSU dataset (STAR) and the difference of RAOBCORE to RICH, all with their 95 % confidence interval.

5 Summary and conclusions

This study focused on comparing (A)MSU data and radiosonde data to radio occultation data, which are well qualified as reference dataset for climate applications. We included RO data from CHAMP, SAC-C, GRACE-A, and F3C satellites for the time period September 2001 to December 2010. All RO profiles were transformed to MSU-equivalent layer-average brightness temperatures (TLS) using a radiative transfer model (RTTOV). Using inter-satellite consistency, the RO data were combined to form a single TLS RO dataset. This dataset was compared to (A)MSU datasets (UAH, RSS, STAR) and recent homogenized radiosonde datasets (RAOBCORE, RICH).

We estimated the spatiotemporal sampling error of radiosonde and RO data. Comparing the RO reference anomalies with radiosonde anomalies, we showed the importance of taking into account these error characteristics also for radiosondes. The consistency of radiosondes and RO was improved substantially by subtracting their respective sampling errors. We thus compared radiosonde and RO datasets in corrected form, i.e., with their sampling errors subtracted. The resulting anomaly time series for TLS showed good agreement of radiosonde data with RO.

Rather surprisingly, we found that it is also important to take into account the sampling error for radiosondes in the Northern Hemisphere (NH) extratropics where radiosonde station coverage is generally very good. We conclude that this results from the radiosonde network missing the atmospheric variability, particularly in NH winter. The advantage of homogeneously distributed measurements is thus clearly visible. In the tropics the deviations of radiosonde TLS from RO TLS are relatively small. This implies that despite the small number of stations in this region the sampling of radiosondes seems to be sufficient to largely capture the relatively homogeneous atmosphere in the tropics. RAOBCORE showed small to insignificant differences compared to RO in all of the three subregions. RICH also showed insignificant differences in the global mean. While RICH shows more cooling than RO in the tropics and NH, its anomalies still agree clearly better with RO than (A)MSU data. Generally radiosonde data showed larger errors in SH than elsewhere because the station coverage is very sparse there. Trends in TLS anomaly differences of radiosondes compared to RO were found to be small to insignificant in the global mean, (0.08 ± 0.06) K/10 yr for RAOBCORE and (-0.01 ± 0.07) K/10 yr for RICH.

(A)MSU data do not need sampling error correction because they provide very dense horizontal sampling. We found statistically significant trend values within about (-0.2 ± 0.1) K/10 yr for the anomaly differences relative to RO in all large-scale zonal regions for all three (A)MSU datasets. This latitudinally consistent result somewhat deviates from

the results of Steiner et al. (2007), who showed significant difference trends mainly in the tropics for the time period 2001 to 2006. The difference trend values are smaller compared to Steiner et al. (2007), which we attribute to the longer time series, the most recent versions of RO and (A)MSU data, and to a change in the difference trend characteristics of the (A)MSU record in 2006 where the negative trend tendency ceased to continue. The overall conclusion of Steiner et al. (2007) that multiple independent datasets are needed for detecting weaknesses in climate records remains valid.

The good vertical resolution of the RO and radiosonde data (compared to the layer-average TLS of the (A)MSU instrument) will be of advantage to further analyze and understand the differences. We expect the remaining differences to be easiest to explain in the tropics (which we will analyze in a future study). The high quality of RO measurements and the good agreement of radiosonde and RO anomalies indicate that the detected differences mainly stem from the (A)MSU data.

Acknowledgement We are grateful to UCAR/CDAAC (USA) and WEGC (A) GPS RO operational team members for provision of RO data, at WEGC especially to J. Fritzer and B. Scherllin-Pirscher for their contributions to OPS system development and operations. We thank B. C. Lackner for fruitful discussions. UAH, RSS and NESDIS/STAR (all USA) are acknowledged for providing (A)MSU records. Furthermore we thank ECMWF (UK) for access to their atmospheric analysis data. This work was funded by the Austrian Science Fund (FWF; BENCHCLIM project P22293-N21, TRENDEVAL project P21642-N21, C. Tavolato and L. Haimberger supported by project P21772-N10). WEGC OPS development was co-funded by ESA/ESTEC Noordwijk, ESA/ESRIN Frascati, and FFG/ALR Austria.

Bibliography

Aigner, W., S. Miksch, W. Müller, H. Schumann, and C. Tominski (2008).
"Visual Methods for Analyzing Time-Oriented Data."
In: *IEEE Trans. Visualization and Computer Graphics* 14.1, pp. 47–60 (cit. on p. 89).

Allison, I., N. L. Bindoff, R. A. Bindschadler, et al. (2009).
The Copenhagen Diagnosis, 2009: Updating the world on the Latest Climate Science.
Tech. rep. Sydney, Australia: The University of New South Wales Climate Change Research Centre (CCRC). URL: http://www.copenhagendiagnosis.org/
(cit. on pp. 7–9, 13).

Anthes, R. A., D. Ector, D. C. Hunt, et al. (2008).
"The COSMIC/FORMOSAT-3 mission: Early results."
In: *B. Am. Meteorol. Soc.* 89.3, pp. 313–333. DOI: 10.1175/BAMS-89-3-313
(cit. on p. 108).

Arrhenius, S. (1896).
"On the Influence of Carbonic Acid in the Air upon the Temperature of the Ground."
In: *Philosophical Magazine and Journal of Science* 41, pp. 237–276 (cit. on p. 6).

Baldonado, M. Q. W., A. Woodruff, and A. Kuchinsky (2000).
"Guidelines for Using Multiple Views in Information Visualization."
In: *Proceedings of the Workshop on Advanced Visual Interfaces.* (Palermo, Italy).
New York, NY, USA: ACM, pp. 110–119. DOI: 10.1145/345513.345271
(cit. on pp. 35, 90).

Baldwin, M. P., M. Dameris, and T. G. Shepherd (2007).
"How will the stratosphere affect climate change?"
In: *Science* 316.5831, pp. 1576–1577. DOI: 10.1126/science.1144303
(cit. on pp. 21, 106).

Becker, R. A. and W. S. Cleveland (1987). "Brushing Scatterplots."
In: *Technometrics* 29.2, pp. 127–142. ISSN: 0040-1706. DOI: 10.2307/1269768
(cit. on p. 90).

Beyerle, G., T. Schmidt, G. Michalak, S. Heise, J. Wickert, and C. Reigber (2005).
"GPS radio occultation with GRACE: Atmospheric profiling utilizing the zero difference technique." In: *Geophys. Res. Lett.* 32, L13806.
DOI: 10.1029/2005GL023109 (cit. on p. 108).

Biastoch, A., T. Treude, L. H. Rüpke, U. Riebesell, C. Roth, E. B. Burwicz, W. Park, M. Latif, C. W. Böning, G. Madec, and K. Wallmann (2011). "Rising Arctic Ocean temperatures cause gas hydrate destabilization and ocean acidification." In: *Geophys. Res. Lett.* 38, L08602. DOI: 10.1029/2011GL047222 (cit. on p. 8).

Borsche, M., G. Kirchengast, and U. Foelsche (2007). "Tropical tropopause climatology as observed with radio occultation measurements from CHAMP compared to ECMWF and NCEP." In: *Geophys. Res. Lett.* 34, L03702. DOI: 10.1029/2006GL027918 (cit. on p. 32).

Broecker, W. S. (1975). "Climatic Change: Are We on the Brink of a Pronounced Global Warming?" In: *Science* 189.4201, pp. 460–463. DOI: 10.1126/science.189.4201.460 (cit. on pp. 7, 8).

Christy, J. R., R. W. Spencer, and E. S. Lobl (1998). "Analysis of the merging procedure for the MSU daily temperature time series." In: *J. Climate* 11, pp. 2016–2041. DOI: 10.1175/1520-0442-11.8.2016 (cit. on p. 112).

Christy, J. R., R. W. Spencer, W. B. Norris, W. D. Braswell, and D. E. Parker (2003). "Error estimates of version 5.0 of MSU-AMSU bulk atmospheric temperatures." In: *J. Atmos. Ocean. Tech.* 20.5, pp. 613–629. DOI: 10.1175/1520-0426(2003)20<613:EEOVOM>2.0.CO;2 (cit. on pp. 19, 107, 109).

Christy, J. R., W. B. Norris, R. W. Spencer, and J. J. Hnilo (2007). "Tropospheric temperature change since 1979 from tropical radiosonde and satellite measurements." In: *J. Geophys. Res.* 112, D06102. DOI: 10.1029/2005JD006881 (cit. on p. 107).

Christy, J., D. Seidel, and S. Sherwood (2006). "What kinds of atmospheric temperature variations can the current observing systems measure and what are their strengths and limitations, both spatially and temporally?" In: ed. by T. Karl, S. Hassol, C. Miller, and W. Murray. Washington, DC: U.S. Climate Change Science Program/Subcommittee on Global Change Research. Chap. 2, pp. 29–46 (cit. on p. 19).

Cordero, E. C. and P. M. de Forster (2006). "Stratospheric Variability and Trends in Models Used for the IPCC AR4." In: *Atmos. Chem. Phys.* 6.12, pp. 5369–5380 (cit. on pp. 55, 75, 92).

Cuntz, N., A. Kolb, M. Leidl, C. R. Salama, and M. Böttinger (2007). "GPU-based Dynamic Flow Visualization for Climate Research Applications." In: *In Simulation und Visualisierung 2007 (SimVis 2007)*, pp. 371–384 (cit. on p. 89).

Dee, D. P., S. M. Uppala, A. J. Simmons, et al. (2011). "The ERA-Interim reanalysis: configuration and performance of the data assimilation system."
In: *Q. J. Roy. Meteor. Soc.* 137.656, pp. 553–597. ISSN: 1477-870X.
DOI: 10.1002/qj.828 (cit. on p. 110).

Dee, D., P. Berrisford, P. Poli, and M. Fuentes (2009).
ERA-Interim for climate monitoring. ECMWF Newsletter No. 119–Spring 2009
(cit. on pp. 18, 20).

Doleisch, H. (2004).
"Visual Analysis of Complex Simulation Data using Multiple Heterogenous Views."
see also http://www.VRVis.at/via/resources/diss-HD/.
PhD thesis. Technical University of Vienna (cit. on p. 56).

Doleisch, H. and H. Hauser (2002).
"Smooth Brushing for Focus+Context Visualization of Simulation Data in 3D."
In: *WSCG 2002 Conference Proceedings*. (Plzeň, Czech Republic), pp. 147–154
(cit. on pp. 56, 71, 74, 90).

Doleisch, H., M. Mayer, M. Gasser, R. Wanker, and H. Hauser (2004a).
"Case Study: Visual Analysis of Complex, Time-Dependent Simulation Results of a Diesel Exhaust System."
In: *Proc. Eurographics/IEEE-TCVG Symp. on Visualization (VisSym 2003)*,
pp. 91–96 (cit. on pp. 66, 70).

Doleisch, H., P. Muigg, and H. Hauser (2004b).
Interactive Visual Analysis of Hurricane Isabel—a Description in More Detail.
Technical Report TR-VRVis-2004-058. VRVis Research Center, p. 6
(cit. on pp. 35, 88, 90).

Doleisch, H., M. Gasser, and H. Hauser (2003). "Interactive Feature Specification for Focus+Context Visualization of Complex Simulation Data."
In: *VISSYM '03: Proceedings of the Symposium on Data Visualisation 2003*.
(Grenoble, France). Aire-la-Ville, Switzerland, Switzerland: Eurographics Association,
pp. 239–248 (cit. on pp. 54, 70, 71, 88, 90).

Doleisch, H., M. Mayer, M. Gasser, P. Priesching, and H. Hauser (2005).
"Interactive Feature Specification for Simulation Data on Time-Varying Grids."
In: *In Conference on Simulation and Visualization 2005 (SimVis 2005)*, pp. 291–304
(cit. on pp. 35, 55).

Douglass, D. H., J. R. Christy, B. D. Pearson, and S. F. Singer (2008).
"A comparison of tropical temperature trends with model predictions."
In: *Int. J. Climatol.* 28.13, pp. 1693–1701. DOI: 10.1002/joc.1651 (cit. on p. 15).

EPICA community members (2004). "Eight glacial cycles from an Antarctic ice core."
In: *Nature* 429, pp. 623–628. DOI: 10.1038/nature02599 (cit. on p. 6).

Fayyad, U., G. Piatetsky-Shapiro, and P. Smyth (1996).
"From Data Mining to Knowledge Discovery in Databases."
In: *AI Magazine* 17, pp. 37–54 (cit. on pp. 34, 88).

Foelsche, U., G. Kirchengast, A. Steiner, L. Kornblueh, E. Manzini, and L. Bengtsson (2008a). "An observing system simulation experiment for climate monitoring with GNSS radio occultation data: setup and testbed study."
In: *J. Geophys. Res.* 113, D11108. DOI: 10.1029/2007JD009231
(cit. on pp. 54, 68, 114).

Foelsche, U., M. Borsche, A. Steiner, A. Gobiet, B. Pirscher, G. Kirchengast, J. Wickert, and T. Schmidt (2008b). "Observing upper troposphere–lower stratosphere climate with radio occultation data from the CHAMP satellite."
In: *Clim. Dynam.* 31 (1), pp. 49–65. DOI: 10.1007/s00382-007-0337-7
(cit. on pp. 32, 40, 54, 112).

Foelsche, U., B. Pirscher, M. Borsche, G. Kirchengast, and J. Wickert (2009).
"Assessing the climate monitoring utility of radio occultation data: From CHAMP to FORMOSAT-3/COSMIC." In: *Terr. Atmos. Ocean. Sci.* 20.1, pp. 155–170.
DOI: 10.3319/TAO.2008.01.14.01(F3C) (cit. on pp. 54, 93, 107, 114).

Foelsche, U., B. Scherllin-Pirscher, F. Ladstädter, A. Steiner, and G. Kirchengast (2011).
"Refractivity and temperature climate records from multiple radio occultation satellites consistent within 0.05 %." In: *Atmos. Meas. Tech.* 4, pp. 2007–2018.
DOI: 10.5194/amt-4-2007-2011 (cit. on pp. 32, 108, 112).

Fourier, J. B. J. (1824). "Remarques générales sur les températures du globe terrestre et des espaces planétaires." In: *Annales de Chimie et de Physique* 27 (cit. on p. 6).

Free, M. and D. J. Seidel (2005).
"Causes of differing temperature trends in radiosonde upper air data sets."
In: *J. Geophys. Res.* 110, D07101. DOI: 10.1029/2004JD005481
(cit. on pp. 106, 113).

Free, M. and D. J. Seidel (2006).
"Observed El Niño–Southern Oscillation temperature signal in the stratosphere."
In: *J. Geophys. Res.* 114, D23108. DOI: 10.1029/2009JD012420 (cit. on p. 23).

Free, M., D. J. Seidel, J. K. Angell, J. Lanzante, I. Durre, and T. C. Peterson (2005).
"Radiosonde Atmospheric Temperature Products for Assessing Climate (RATPAC): A new data set of large-area anomaly time series." In: *J. Geophys. Res.* 110, D22101.
DOI: 10.1029/2005JD006169 (cit. on p. 17).

Friedman, J. H. (1997). "Data Mining and Statistics: What's the Connection?"
In: *Proceedings of the 29th Symposium on the Interface Between Computer Science and Statistics*. (Houston, Texas, USA) (cit. on pp. 34, 88).

Fuchs, R. and H. Hauser (2009). "Visualization of Multi-variate Scientific Data." In: *Computer Graphics Forum* 28.6, pp. 1670–1690 (cit. on p. 89).

Furnas, G. W. (1986). "Generalized fisheye views." In: *Proc. Human Factors in Computing Systems (CHI '86)*, pp. 16–23 (cit. on p. 71).

GCOS (2010). *Implementation plan for the Global Observing System for Climate in support of the UNFCCC, (2010 Update).* WMO-TD/No. 1523 GCOS-138 (GOOS-184, GTOS-76). WMO (cit. on pp. 15, 27, 29, 107).

Gobiet, A., U. Foelsche, A. Steiner, M. Borsche, G. Kirchengast, and J. Wickert (2005). "Climatological validation of stratospheric temperatures in ECMWF operational analyses with CHAMP radio occultation data." In: *Geophys. Res. Lett.* 32, L12806. DOI: 10.1029/2005GL022617 (cit. on p. 32).

Gobiet, A., G. Kirchengast, G. L. Manney, M. Borsche, C. Retscher, and G. Stiller (2007). "Retrieval of temperature profiles from CHAMP for climate monitoring: intercomparison with Envisat MIPAS and GOMOS and different atmospheric analyses." In: *Atmos. Chem. Phys.* 7.13, pp. 3519–3536. DOI: 10.5194/acp-7-3519-2007 (cit. on p. 32).

Goebel, M. and L. Gruenwald (1999). "A Survey of Data Mining and Knowledge Discovery Software Tools." In: *ACM SIGKDD Explorations* 1.1, pp. 20–33 (cit. on pp. 34, 88).

Grieneisen, M. L. and M. Zhang (2011). "The current status of climate change research." In: *Nature Clim. Change* 1, pp. 72–73. DOI: 10.1038/nclimate1093 (cit. on p. 33).

Haimberger, L. (2007). "Homogenization of radiosonde temperature time series using innovation statistics." In: *J. Climate* 20, pp. 1377–1403. DOI: 10.1175/JCLI4050.1 (cit. on pp. 18, 106, 110).

Haimberger, L., C. Tavolato, and S. Sperka (2008). "Toward elimination of the warm bias in historic radiosonde temperature records—Some new results from a comprehensive intercomparison of upper-air data." In: *J. Climate* 21, pp. 4587–4606. DOI: 10.1175/2008JCLI1929.1 (cit. on pp. 18, 23, 106, 107, 110).

Hajj, G. A., E. R. Kursinski, L. J. Romans, W. I. Bertiger, and S. S. Leroy (2002). "A technical description of atmospheric sounding by GPS occultation." In: *J. Atmos. Sol-Terr. Phy.* 64.4, pp. 451–469. DOI: 10.1016/S1364-6826(01)00114-6 (cit. on p. 107).

Hajj, G. A., C. O. Ao, B. A. Iijima, D. Kuang, E. R. Kursinski, A. J. Mannucci, T. K. Meehan, L. J. Romans, M. de la Torre Juarez, and T. P. Yunck (2004). "CHAMP and SAC-C atmospheric occultation results and intercomparisons." In: *J. Geophys. Res.* 109, D06109. DOI: 10.1029/2003JD003909 (cit. on pp. 32, 108).

Hauser, H. (2005). "Generalizing Focus+Context Visualization." In: *Scientific Visualization: The Visual Extraction of Knowledge from Data (Proceedings of the Dagstuhl 2003 Seminar on Scientific Visualization)*, pp. 305–327. ISBN: 3-540-26066-8 (cit. on pp. 56, 71).

He, W., S.-p. Ho, H. Chen, X. Zhou, D. Hunt, and Y.-H. Kuo (2009). "Assessment of radiosonde temperature measurements in the upper troposphere and lower stratosphere using COSMIC radio occultation data." In: *Geophys. Res. Lett.* 36, L17807. DOI: 10.1029/2009GL038712 (cit. on pp. 40, 107).

Healy, S. B., A. M. Jupp, and C. Marquardt (2005). "Forecast impact experiment with GPS radio occultation measurements." In: *Geophys. Res. Lett.* 32, L03804. DOI: 10.1029/2004GL020806 (cit. on p. 32).

Hester, K. C. and P. G. Brewer (2009). "Clathrate Hydrates in Nature." In: *Annu. Rev. Mar. Sci.* 1.1, pp. 303–327. DOI: 10.1146/annurev.marine.010908.163824 (cit. on p. 8).

Hibbard, B., M. Böttinger, M. Schultz, and J. Biercamp (2002). "Visualization in Earth System Science." In: *SIGGRAPH Computer Graphics* 36.4, pp. 5–9. ISSN: 0097-8930. DOI: 10.1145/637357.637361 (cit. on pp. 88, 89).

Ho, S.-P., Y.-H. Kuo, Z. Zeng, and T. Peterson (2007). "A comparison of lower stratosphere temperature from microwave measurements with CHAMP GPS RO data." In: *Geophys. Res. Lett.* 34, L15701. DOI: 10.1029/2007GL030202 (cit. on pp. 32, 40, 107).

Ho, S.-P., M. Goldberg, Y. H. Kuo, C. Z. Zou, and W. Schreiner (2009a). "Calibration of temperature in the lower stratosphere from microwave measurements using COSMIC Radio Occultation data: preliminary results." In: *Terr. Atmos. Ocean. Sci.* 20.1, pp. 87–100. DOI: 10.3319/TAO.2007.12.06.01(F3C) (cit. on p. 107).

Ho, S.-P., G. Kirchengast, S. Leroy, et al. (2009b). "Estimating the uncertainty of using GPS radio occultation data for climate monitoring: Intercomparison of CHAMP refractivity climate records from 2002 to 2006 from different data centers." In: *J. Geophys. Res.* 114, D23107. DOI: 10.1029/2009JD011969 (cit. on pp. 32, 93, 102, 107).

Hobbs, J., H. Wickham, H. Hofmann, and D. Cook (2010).
"Glaciers Melt as Mountains Warm: A Graphical Case Study."
In: *Computational Statistics*. to appear (cit. on p. 88).

Immler, F. J., J. Dykema, T. Gardiner, D. N. Whiteman, P. W. Thorne, and H. Vömel (2010). "Reference Quality Upper-Air Measurements: guidance for developing GRUAN data products." In: *Atmos. Meas. Tech.* 3.5, pp. 1217–1231.
DOI: 10.5194/amt-3-1217-2010 (cit. on p. 27).

Inselberg, A. and B. Dimsdale (1990).
"Parallel coordinates: a tool for visualizing multi-dimensional geometry."
In: *Proceedings of IEEE Visualization '90*. (San Francisco, California).
Los Alamitos, CA, USA: IEEE Computer Society Press, pp. 361–378 (cit. on p. 101).

Johansson, J., P. Ljung, M. Jern, and M. Cooper (2005).
"Revealing Structure within Clustered Parallel Coordinates Displays."
In: *Proc. IEEE Symp. Information Visualization (InfoVis 2005)*, pp. 125–132.
ISBN: 0-7803-9464-x. DOI: 10.1109/INFOVIS.2005.30 (cit. on p. 72).

Kalnay, E., M. Kanamitsu, R. Kistler, et al. (1996).
"The NCEP/NCAR 40-Year Reanalysis Project."
In: *B. Am. Meteorol. Soc.* 77.3, pp. 437–471.
DOI: 10.1175/1520-0477(1996)077<0437:TNYRP>2.0.CO;2 (cit. on p. 20).

Karl, T. R., S. J. Hassol, C. D. Miller, and W. L. Murray, eds. (2006). *Temperature trends in the lower atmosphere: Steps for understanding and reconciling differences*.
Washington, DC: U.S. Climate Change Science Program/Subcommittee on Global Change Research (cit. on pp. 9, 12, 15, 21, 22, 27, 68, 106, 107).

Kehrer, J. (2007). "Integrating interactive visual analysis of large time series data into the SimVis system."
MA thesis. VRVis Research Center, Technical University of Vienna
(cit. on pp. 54, 57).

Kehrer, J., F. Ladstädter, P. Muigg, H. Doleisch, A. Steiner, and H. Hauser (2008).
"Hypothesis Generation in Climate Research with Interactive Visual Data Exploration."
In: *IEEE Transactions on Visualization and Computer Graphics* 14.6, pp. 1579–1586.
DOI: 10.1109/TVCG.2008.139 (cit. on pp. 22, 36, 51, 88–90, 103).

Kehrer, J. (2011). "Interactive Visual Analysis of Multi-faceted Scientific Data."
PhD thesis. Institute for Informatics, University of Bergen (cit. on p. 34).

Keim, D., W. Mueller, and H. Schumann (2002). "Visual Data Mining."
In: *Eurographics 2002 State of the Art Reports*, pp. 49–68 (cit. on p. 88).

Kistler, R., W. Collins, S. Saha, G. White, J. Woollen, E. Kalnay, M. Chelliah, W. Ebisuzaki, M. Kanamitsu, V. Kousky, H. van den Dool, R. Jenne, and M. Fiorino (2001). "The NCEP-NCAR 50-Year Reanalysis: Monthly Means CD-ROM and Documentation." In: *B. Am. Meteorol. Soc.* 82.2, pp. 247–267. DOI: 10.1175/1520-0477(2001)082<0247:TNNYRM>2.3.CO;2 (cit. on p. 20).

Kuo, Y.-H., W. S. Schreiner, J. Wang, D. L. Rossiter, and Y. Zhang (2005). "Comparison of GPS radio occultation soundings with radiosondes." In: *Geophys. Res. Lett.* 32, L05817. DOI: 10.1029/2004GL021443 (cit. on pp. 32, 40, 107).

Kursinski, E. R., G. A. Hajj, J. T. Schofield, R. P Linfield, and K. R. Hardy (1997). "Observing Earth's atmosphere with radio occultation measurements using the Global Positioning System." In: *J. Geophys. Res.* 102, pp. 23429–23465 (cit. on pp. 27, 31, 32, 93, 107).

Lackner, B. (2010). "Exploring Trend Indicators of Climate Change From Radio Occultation and Optimal Trend Detection." PhD thesis. Wegener Center for Climate et al. (cit. on p. 32).

Lackner, B., A. Steiner, F. Ladstädter, and G. Kirchengast (2009). "Trend Indicators of Atmospheric Climate Change Based on Global Climate Model Scenarios." In: *New Horizons in Occultation Research: Studies in Atmosphere and Climate*. Ed. by A. K. Steiner, B. Pirscher, U. Foelsche, and G. Kirchengast. Berlin Heidelberg: Springer, pp. 247–259. DOI: 10.1007/978-3-642-00321-9_20 (cit. on pp. 54, 67, 72, 73, 78, 91, 98, 99).

Ladstädter, F., A. Steiner, B. Lackner, G. Kirchengast, P. Muigg, J. Kehrer, and H. Doleisch (2009). "SimVis: An Interactive Visual Field Exploration Tool Applied to Climate Research." In: *New Horizons in Occultation Research: Studies in Atmosphere and Climate*. Ed. by A. K. Steiner, B. Pirscher, U. Foelsche, and G. Kirchengast. Berlin Heidelberg: Springer, pp. 235–245. DOI: 10.1007/978-3-642-00321-9_19 (cit. on pp. 34, 51, 80, 88, 92, 103).

Ladstädter, F., A. Steiner, B. Lackner, B. Pirscher, G. Kirchengast, J. Kehrer, H. Hauser, P. Muigg, and H. Doleisch (2010). "Exploration of Climate Data Using Interactive Visualization." In: *J. Atmos. Ocean. Tech.* 27.4, pp. 667–679. DOI: 10.1175/2009JTECHA1374.1 (cit. on pp. 37, 52).

Ladstädter, F., A. Steiner, U. Foelsche, L. Haimberger, C. Tavolato, and G. Kirchengast (2011). "An assessment of differences in lower stratospheric temperature records from (A)MSU, radiosondes, and GPS radio occultation." In: *Atmos. Meas. Tech.* 4, pp. 1965–1977. DOI: 10.5194/amt-4-1965-2011 (cit. on pp. 40, 52).

Laramee, R. S., C. Garth, H. Doleisch, J. Schneider, H. Hauser, and H. Hagen (2005). "Visual Analysis and Exploration of Fluid Flow in a Cooling Jacket." In: *Proc. IEEE Visualization Conf. (Vis 2005)*, pp. 623–630 (cit. on p. 66).

Laštovička, J., R. A. Akmaev, G. Beig, J. Bremer, and J. T. Emmert (2006). "Global Change in the Upper Atmosphere." In: *Science* 314.5803, pp. 1253–1254. DOI: 10.1126/science.1135134 (cit. on p. 22).

Leroy, S., J. Dykema, and J. Anderson (2006). "Climate Benchmarking Using GNSS Occultation." In: *Atmosphere and Climate: Studies by Occultation Methods*. Ed. by U. Foelsche, G. Kirchengast, and A. Steiner. Springer Berlin Heidelberg, pp. 287–301. ISBN: 978-3-540-34121-5. DOI: 10.1007/3-540-34121-8_24 (cit. on pp. 29, 31, 54, 107).

Leroy, S., J. G. Anderson, and G. Ohring (2008). "Climate signal detection times and constraints on climate benchmark accuracy requirements." In: *J. Climate* 21.4, pp. 841–846. DOI: 10.1175/2007JCLI1946.1 (cit. on pp. 29, 32).

Macêdo, M, D Cook, and T. Brown (2000). "Visual Data Mining in Atmospheric Science Data." English. In: *Data Mining and Knowledge Discovery* 4.1, 69–80. ISSN: 1384-5810 (cit. on p. 88).

Manabe, S. and R. T. Wetherald (1975). "The Effects of Doubling the CO2 Concentration on the climate of a General Circulation Model." In: *J. Atmos. Sci.* 32.1, pp. 3–15. DOI: 10.1175/1520-0469(1975)032<0003:TEODTC>2.0.CO;2 (cit. on p. 9).

Mears, C. A. and F. J. Wentz (2009a). "Construction of the remote sensing systems V3.2 atmospheric temperature records from the MSU and AMSU microwave sounders." In: *J. Atmos. Ocean. Tech.* 26, pp. 1040–1056. DOI: 10.1175/2008JTECHA1176.1 (cit. on pp. 109, 112).

– (2009b). "Construction of the RSS V3.2 lower-tropospheric temperature dataset from the MSU and AMSU microwave sounders." In: *J. Atmos. Ocean. Tech.* 26, pp. 1493–1509. DOI: 10.1175/2009JTECHA1237.1 (cit. on pp. 19, 107, 110).

Melbourne, W. G., E. S. Davis, C. B. Duncan, G. A. Hajj, K. R. Hardy, E. R. Kursinski, T. K. Meehan, L. E. Young, and T. P. Yunck (1994). "The application of spaceborne GPS to atmospheric limb sounding and global change monitoring." In: *JPL Publication* 94-18, p. 147 (cit. on pp. 22, 68, 107).

Muigg, P., J. Kehrer, S. Oeltze, H. Piringer, H. Doleisch, B. Preim, and H. Hauser (2008). "A Four-level Focus+Context Approach to Interactive Visual Analysis of Temporal Features in Large Scientific Data."
In: *IEEE Computer Graphics Forum* 27.3, pp. 775–782.
DOI: 10.1111/j.1467-8659.2008.01207.x (cit. on pp. 57, 71, 72).

Nakícenović, N., J. Alcamo, G. Davis, et al. (2000).
IPCC Special Report on Emissions Scenarios. Ed. by N. Nakícenović and R. Swart.
Cambridge, UK: Cambridge University Press.
URL: http://www.ipcc.ch/ipccreports/sres/emission/index.htm
(cit. on p. 20).

Nocke, T., T. Sterzel, M. Böttinger, and M. Wrobel (2008).
"Visualization of Climate and Climate Change Data: An Overview." In: *Digital Earth Summit on Geoinformatics 2008: Tools for Global Change Research (ISDE'08)*.
Ed. by Ehlers et al. Heidelberg: Wichmann, pp. 226–232 (cit. on pp. 34, 88, 89).

Nocke, T. (2007). "Visuelles Data Mining und Visualisierungsdesign für die Klimaforschung (Visual data mining and visualization design for climate research)."
(in German). PhD thesis. Inst. f. Computer Science, Dept. of Computer Science and Electrical Engineering, Univ. of Rostock, p. 246 (cit. on pp. 34, 70, 89).

Norris, R. D. and U. Rohl (1999). "Carbon cycling and chronology of climate warming during the Palaeocene/Eocene transition." In: *Nature* 401, pp. 775–778.
DOI: 10.1038/44545 (cit. on p. 8).

Novotný, M. and H. Hauser (2006).
"Outlier-Preserving Focus+Context Visualization in Parallel Coordinates."
In: *IEEE Trans. Visualization and Computer Graphics* 12.5, pp. 893–900.
ISSN: 1077-2626. DOI: 10.1109/TVCG.2006.170 (cit. on p. 72).

Ohring, G., ed. (2007).
Achieving Satellite Instrument Calibration for Climate Change (ASIC3). National Oceanic and Atmospheric Administration. Center for Satellite Applications et al.
URL: http://www.star.nesdis.noaa.gov/star/documents/ASIC3-071218-webversfinal.pdf (cit. on p. 27).

Oliveira, M. C. F. de and H. Levkowitz (2003).
"From Visual Data Exploration to Visual Data Mining: A Survey."
In: *IEEE Transactions on Visualization and Computer Graphics* 9.3, pp. 378–394.
DOI: 10.1109/TVCG.2003.1207445 (cit. on p. 88).

Onogi, K., J. Tsutsui, H. Koide, M. Sakamoto, S. Kobayashi, H. Hatsushika, T. Matsumoto, N. Yamazaki, H. Kamahori, K. Takahashi, S. Kadokura, K. Wada, K. Kato, R. Oyama, T. Ose, N. Mannoji, and R. Taira (2007). "The JRA-25 Reanalysis." In: *J. Meteorol. Soc. Jpn.* 85.3, pp. 369–432. DOI: 10.2151/jmsj.85.369 (cit. on p. 20).

Pirscher, B. (2010). *Multi-satellite climatologies of fundamental atmospheric variables from radio occultation and their validation (Ph.D. thesis), Sci. Rep. No. 33.* Wegener Center Verlag Graz, Austria. ISBN: 978-3-9502940-3-3 (cit. on pp. 30, 31, 108, 112).

Pirscher, B., U. Foelsche, B. Lackner, and G. Kirchengast (2007). "Local time influence in single-satellite radio occultation climatologies from Sun-synchronous and non-Sun-synchronous satellites." In: *J. Geophys. Res.* 112, D11119. DOI: 10.1029/2006JD007934 (cit. on p. 114).

Pirscher, B., U. Foelsche, M. Borsche, G. Kirchengast, and Y. Kuo (2010). "Analysis of migrating diurnal tides detected in FORMOSAT-3/COSMIC temperature data." In: *J. Geophys. Res.* 115, D14108. DOI: 10.1029/2009JD013008 (cit. on p. 32).

President's Science Advisory Committee (1965). *Restoring the quality of our environment. Report.* Washington: White House (cit. on p. 7).

Rahmstorf, S., A. Cazenave, J. A. Church, J. E. Hansen, R. F. Keeling, D. E. Parker, and R. C. J. Somerville (2007). "Recent Climate Observations Compared to Projections." In: *Science* 316.5825, p. 709. DOI: 10.1126/science.1136843 (cit. on p. 11).

Randall, R. M. and B. M. Herman (2008). "Using limited time period trends as a means to determine attribution of discrepancies in microwave sounding unit-derived tropospheric temperature time series." In: *J. Geophys. Res.* 113, D05105+. DOI: 10.1029/2007JD008864 (cit. on p. 106).

Randel, W. J. and F. Wu (2006). "Biases in Stratospheric and Tropospheric Temperature Trends Derived from Historical Radiosonde Data." In: *J. Climate* 19.10, pp. 2094–2104. DOI: 10.1175/JCLI3717.1 (cit. on p. 23).

Randel, W. J., K. P. Shine, J. Austin, J. Barnett, C. Claud, N. P. Gillett, P. Keckhut, U. Langematz, R. Lin, C. Long, C. Mears, A. Miller, J. Nash, D. J. Seidel, D. W. J. Thompson, F. Wu, and S. Yoden (2009). "An update of observed stratospheric temperature trends." In: *J. Geophys. Res.* 114.D2, D02107. DOI: 10.1029/2008JD010421 (cit. on pp. 19, 22, 23, 106, 117).

Roberts, J. C. (2004). "Exploratory Visualization with Multiple Linked Views." In: *Exploring Geovisualization*. Ed. by A. MacEachren, M.-J. Kraak, and J. Dykes. Elseviers, pp. 159–180 (cit. on p. 70).

Rocken, C., R. Anthes, M. Exner, D. Hunt, S. Sokolovskiy, R. Ware, M. Gorbunov, W. Schreiner, D. Feng, B. Herman, Y. Kuo, and X. Zou (1997). "Analysis and validation of GPS/MET data in the neutral atmosphere." In: *J. Geophys. Res.* 102.D25, pp. 29849–29866. DOI: 10.1029/97JD02400 (cit. on p. 32).

Roeckner, E., G. Bäuml, L. Bonaventura, R. Brokopf, M. Esch, M. Giorgetta, S. Hagemann, I. Kirchner, L. Kornblueh, E. Manzini, A. Rhodin, U. Schlese, U. Schulzweida, and A. Tompkins (2003). *The Atmospheric General Circulation Model ECHAM5*. Report No. 349. 127 pp. Max-Planck-Insitute for Meteorology, Hamburg, Germany (cit. on pp. 55, 69, 91).

Rübel, O., G. H. Weber, S. V. E. Keränen, C. C. Fowlkes, C. L. L. Hendriks, L. Simirenko, N. Y. Shah, M. B. Eisen, M. D. Biggin, H. Hagen, D. Sudar, J. Malik, D. W. Knowles, and B. Hamann (2006). "PointCloudXplore: Visual analysis of 3D Gene Expression Data Using Physical Views and Parallel Coordinates." In: *Proc. Eurographics/IEEE-VGTC Symp. on Visualization (EuroVis 2006)*, pp. 203–210. DOI: 10.2312/VisSym/EuroVis06/203-210 (cit. on p. 66).

Santer, B. D., T. M. L. Wigley, J. S. Boyle, D. J. Gaffen, J. J. Hnilo, D. Nychka, D. E. Parker, and K. E. Taylor (2000). "Statistical significance of trends and trend differences in layer-average atmospheric temperature time series." In: *J. Geophys. Res.* 105.D6, pp. 7337–7356. DOI: 10.1029/1999JD901105 (cit. on p. 23).

Santer, B. D., T. M. L. Wigley, C. Doutriaux, J. S. Boyle, J. E. Hansen, P. D. Jones, G. A. Meehl, E. Roeckner, S. Sengupta, and K. E. Taylor (2001). "Accounting for the effects of volcanoes and ENSO in comparisons of modeled and observed temperature trends." In: *J. Geophys. Res.* 106.D22, pp. 28033–28059. DOI: 10.1029/2000JD000189 (cit. on p. 23).

Santer, B. D., T. M. L. Wigley, A. J. Simmons, P. W. Kallberg, G. A. Kelly, S. M. Uppala, C. Ammann, J. S. Boyle, W. Bruggemann, C. Doutriaux, M. Fiorino, C. Mears, G. A. Meehl, R. Sausen, K. E. Taylor, W. M. Washington, M. F. Wehner, and F. J. Wentz (2004). "Identification of Anthropogenic Climate Change using a Second-Generation Reanalysis." In: *J. Geophys. Res.* 109, D21104. DOI: 10.1029/2004JD005075 (cit. on pp. 62, 77, 95).

Santer, B. D., P. W. Thorne, L. Haimberger, K. E. Taylor, T. M. L. Wigley, J. R. Lanzante, S. Solomon, M. Free, P. J. Gleckler, P. D. Jones, T. R. Karl, S. A. Klein, C. Mears, D. Nychka, G. A. Schmidt, S. C. Sherwood, and F. J. Wentz (2008). "Consistency of modelled and observed temperature trends in the tropical troposphere." In: *Int. J. Climatol.* 28.13, pp. 1703–1722. DOI: 10.1002/joc.1756 (cit. on pp. 15, 16).

Saunders, R. (2008). *RTTOV-9 Science and Validation Report.* NWP SAF NWPSAF-MO-TV-020. EUMETSAT (cit. on p. 110).

Scherllin-Pirscher, B., A. Steiner, G. Kirchengast, Y.-H. Kuo, and U. Foelsche (2011a). "Empirical analysis and modeling of errors of atmospheric profiles from GPS radio occultation." In: *Atmos. Meas. Tech.* 4, pp. 1875–1890. DOI: 10.5194/amt-4-1875-2011 (cit. on pp. 32, 107, 110).

Scherllin-Pirscher, B., G. Kirchengast, A. Steiner, Y.-H. Kuo, and U. Foelsche (2011b). "Quantifying uncertainty in climatological fields from GPS radio occultation: An empirical-analytical error model." In: *Atmos. Meas. Tech.* 4, pp. 2019–2034. DOI: 10.5194/amt-4-2019-2011 (cit. on pp. 31, 32, 40, 108, 112, 114).

Schmidt, S., O. Schögl, R. Kirchberger, H. Doleisch, P. Muigg, H. Hauser, M. Grabner, A. Bornik, and D. Schmalstieg (2005a). "Novel Visualization and Interaction Techniques for Gaining Insight into Fluid Dynamics in Internal Combustion Engines." In: *Proc. of the NAFEMS World Congress Conference 2005* (cit. on p. 55).

Schmidt, T., J. Wickert, G. Beyerle, and C. Reigber (2004). "Tropical tropopause parameters derived from GPS radio occultation measurements with CHAMP." In: *J. Geophys. Res.* 109, D13105. DOI: 10.1029/2004JD004566 (cit. on p. 32).

Schmidt, T., S. Heise, J. Wickert, G. Beyerle, and C. Reigber (2005b). "GPS radio occultation with CHAMP and SAC-C: global monitoring of thermal tropopause parameters." In: *Atmos. Chem. Phys.* 5.6, pp. 1473–1488. DOI: 10.5194/acp-5-1473-2005 (cit. on p. 32).

Schmidt, T, J Wickert, and A Haser (2010). "Variability of the upper troposphere and lower stratosphere observed with GPS radio occultation bending angles and temperatures." In: *J. Adv. Space Res.* 46.2, pp. 150–161. DOI: 10.1016/j.asr.2010.01.021 (cit. on pp. 32, 117).

Schrøder, T., S. Leroy, M. Stendel, and E. Kaas (2003). "Validating the microwave sounding unit stratospheric record using GPS occultation." In: *Geophys. Res. Lett.* 30.14, p. 1734. DOI: 10.1029/2003GL017588 (cit. on pp. 32, 40, 107).

Schumann, H. and W. Müller (2000).
Visualisierung – Grundlagen und allgemeine Methoden. (in German). Springer, p. 370. ISBN: 978-3-540-64944-1 (cit. on pp. 66, 88).

Seidel, D. J., J. K. Angell, J. Christy, M. Free, S. A. Klein, J. R. Lanzante, C. Mears, D. Parker, M. Schabel, R. Spencer, A. Sterin, P. Thorne, and F. Wentz (2004).
"Uncertainty in signals of large-scale climate variations in radiosonde and satellite upper-air temperature datasets." In: *J. Climate* 17.11, pp. 2225–2240.
DOI: 10.1175/1520-0442(2004)017<2225:UISOLC>2.0.CO;2 (cit. on p. 107).

Sherwood, S. C., C. L. Meyer, R. J. Allen, and H. A. Titchner (2008). "Robust Tropospheric Warming Revealed by Iteratively Homogenized Radiosonde Data."
In: *J. Climate* 21.20, pp. 5336–5352. DOI: 10.1175/2008JCLI2320.1 (cit. on p. 17).

Shine, K. P., M. S. Bourqui, P. M. d. F. Forster, et al. (2003).
"A comparison of model-simulated trends in stratospheric temperatures."
In: *Q. J. Roy. Meteor. Soc.* 129.590, pp. 1565–1588. DOI: 10.1256/qj.02.186 (cit. on p. 22).

Simmons, A. J. and J. K. Gibson (2000). *The ERA-40 project plan.*
ERA-40 Project Report Series No. 1 (cit. on pp. 55, 69, 76, 91).

Simmons, A., S. Uppala, D. Dee, and S. Kobayashi (2006).
ERA-Interim: New ECMWF reanalysis products from 1989 onwards.
ECMWF Newsletter No. 110–Winter 2006/07 (cit. on p. 20).

Smith, E. K. and S. Weintraub (1953).
"The constants in the equation for atmospheric refractive index at radio frequencies."
In: *Proceedings of the I.R.E.* Pp. 1035–1037 (cit. on p. 31).

Solomon, S., D. Qin, M. Manning, Z. Chen, M. Marquis, K. Averyt, M. Tignor, and H. Miller, eds. (2007a). *IPCC, 2007: Climate Change 2007: The Physical Science Basis. Contribution of Working Group I to the Fourth Assessment Report of the Intergovernmental Panel on Climate Change.*
Cambridge, United Kingdom and New York, NY, USA: Cambridge University Press (cit. on pp. 5–7, 9, 11, 13, 15, 88, 93, 106).

Solomon, S., D. Qin, M. Manning, et al. (2007b). "Technical Summary."
In: *Climate Change 2007: The Physical Science Basis. Contribution of Working Group I to the Fourth Assessment Report of the Intergovernmental Panel on Climate Change.*
Ed. by S. Solomon, D. Qin, M. Manning, Z. Chen, M. Marquis, K. B. Averyt, M. Tignor, and H. L. Miller.
Cambridge, United Kingdom and New York, NY, USA: Cambridge University Press, pp. 19–91 (cit. on pp. 68, 99).

Spencer, R. W. and J. R. Christy (1990).
"Precise Monitoring of Global Temperature Trends from Satellites."
In: *Science* 247.4950, pp. 1558–1562. DOI: 10.1126/science.247.4950.1558
(cit. on pp. 15, 18).

Steiner, A. and G. Kirchengast (2000).
"Gravity Wave Spectra from GPS/MET Occultation Observations."
In: *J. Atmos. Ocean. Tech.* 17.4, pp. 495–503.
DOI: 10.1175/1520-0426(2000)017<0495:GWSFGM>2.0.CO;2 (cit. on p. 32).

– (2005). "Error analysis for GNSS radio occultation data based on ensembles of profiles from end-to-end simulations." In: *J. Geophys. Res.* 110, D15307.
DOI: 10.1029/2004JD005251 (cit. on p. 32).

Steiner, A., K. Kirchengast, U. Foelsche, L. Kornblueh, E. Manzini, and L. Bengtsson (2001). "GNSS occultation sounding for climate monitoring."
In: *Phys. Chem. Earth* 26.3, pp. 113–124. DOI: 10.1016/S1464-1895(01)00034-5
(cit. on p. 107).

Steiner, A., G. Kirchengast, M. Borsche, U. Foelsche, and T. Schoengassner (2007).
"A multi-year comparison of lower stratospheric temperatures from CHAMP radio occultation data with MSU/AMSU records." In: *J. Geophys. Res.* 112, D22110.
DOI: 10.1029/2006JD008283 (cit. on pp. 32, 40, 54, 107, 108, 125).

Steiner, A., G. Kirchengast, B. Lackner, B. Pirscher, M. Borsche, and U. Foelsche (2009a).
"Atmospheric temperature change detection with GPS radio occultation 1995 to 2008."
In: *Geophys. Res. Lett.* 36, L18702. DOI: 10.1029/2009GL039777
(cit. on pp. 29, 32, 93, 102, 107).

Steiner, A., G. Kirchengast, M. Borsche, and U. Foelsche (2009b).
"Lower stratospheric temperatures from CHAMP RO compared to MSU/AMSU records: An analysis of error sources."
In: *New Horizons in Occultation Research: Studies in Atmosphere and Climate.*
Ed. by A. Steiner, B. Pirscher, U. Foelsche, and G. Kirchengast.
Berlin Heidelberg: Springer. DOI: 10.1007/978-3-642-00321-9_18
(cit. on pp. 40, 107, 108).

Steiner, A., B. Lackner, F. Ladstädter, B. Scherllin-Pirscher, U. Foelsche, and G. Kirchengast (2011).
"GPS radio occultation for climate monitoring and change detection."
In: *Radio Sci.* revision submitted (cit. on p. 32).

Sukharev, J., C. Wang, K.-L. Ma, and A. T. Wittenberg (2009). "Correlation Study of Time-Varying Multivariate Climate Data Sets." In: *Proceedings of IEEE VGTC Pacific Visualization Symposium 2009*. Beijing, China, pp. 161–168. DOI: 10.1109/PACIFICVIS.2009.4906852 (cit. on p. 89).

Sun, B., A. Reale, D. J. Seidel, and D. C. Hunt (2010). "Comparing radiosonde and COSMIC atmospheric profile data to quantify differences among radiosonde types and the effects of imperfect collocation on comparison statistics." In: *J. Geophys. Res.* 115, D23104. DOI: 10.1029/2010JD014457 (cit. on pp. 40, 107).

Swayne, D. F., D. Cook, and A. Buja (1998). "XGobi: Interactive Dynamic Data Visualization in the X Window System." In: *Journal of Computational and Graphical Statistics* 7, pp. 113–130 (cit. on p. 88).

Thomas, J. and K. Cook (2006). "A visual analytics agenda." In: *IEEE Computer Graphics and Applications* 26.1, pp. 10–13. DOI: 10.1109/MCG.2006.5 (cit. on p. 66).

Thompson, D. W. J. and S. Solomon (2005). "Recent stratospheric climate trends as evidenced in radiosonde data: Global structure and tropospheric linkages." In: *J. Climate* 18.22, pp. 4785–4795. DOI: 10.1175/JCLI3585.1 (cit. on p. 106).

Thorne, P. W., D. E. Parker, S. F. B. Tett, P. D. Jones, M. McCarthy, H. Coleman, and P. Brohan (2005). "Revisiting radiosonde upper air temperatures from 1958 to 2002." In: *J. Geophys. Res.* 110, D18105. DOI: 10.1029/2004JD005753 (cit. on p. 17).

Thorne, P. W., D. E. Parker, J. R. Christy, and C. A. Mears (2005). "Uncertainties in climate trends: Lessons from upper-air temperature records." In: *B. Am. Meteorol. Soc.* 86, pp. 1437–1442. DOI: 10.1175/BAMS-86-10-1437 (cit. on pp. 15, 17, 42, 106, 107).

Thorne, P. W., J. R. Lanzante, T. C. Peterson, D. J. Seidel, and K. P. Shine (2011). "Tropospheric temperature trends: history of an ongoing controversy." In: *Wiley Interdisciplinary Reviews: Climate Change* 2.1, pp. 66–88. DOI: 10.1002/wcc.80 (cit. on pp. 15, 16, 22, 23).

Titchner, H. A., P. W. Thorne, M. P. McCarthy, S. F. B. Tett, L. Haimberger, and D. E. Parker (2009). "Critically reassessing tropospheric temperature trends from radiosondes using realistic validation experiments." In: *J. Climate* 22, pp. 465–485. DOI: 10.1175/2008JCLI2419.1 (cit. on pp. 23, 106).

Trenberth, K. E., P. Jones, P. Ambenje, D. Bojariu, D. Easterling, A. Klein Tank, D. Parker, F. Rahimzadeh, J. Renwick, M. Rusticucci, B. Soden, and P. Zhai (2007). "Observations: Surface and Atmospheric Climate Change." In: *Climate Change 2007: The Physical Science Basis. Contribution of Working Group I to the Fourth Assessment Report of the Intergovernmental Panel on Climate Change*. Cambridge, UK and New York, NY, USA: Cambridge University Press. Chap. 3, pp. 237–336. URL: http://www.ipcc.ch/pdf/assessment-report/ar4/wg1/ar4-wg1-chapter3.pdf (cit. on p. 22).

Tsuda, T., M. Nishida, C. Rocken, and R. H. Ware (2000). "A Global Morphology of Gravity Wave Activity in the Stratosphere Revealed by the GPS Occultation Data (GPS/MET)." In: *J. Geophys. Res.* 105.D6, pp. 7257–7273. DOI: 10.1029/1999JD901005 (cit. on p. 32).

Tukey, J. W. (1977). *Exploratory Data Analysis*. Reading, MA: Addison-Wesley (cit. on pp. 34, 66, 88).

Uppala, S., P. Kållberg, A. Hernandez, S. Saarinen, M. Fiorino, X. Li, K. Onogi, N. Sokka, U. Andrae, and V. Da Costa Bechtold (2004). *ERA-40: ECMWF 45-year reanalysis of the global atmosphere and surface conditions 1957–2002*. ECMWF Newsletter No. 101–Summer/Autumn 2004 (cit. on pp. 20, 62, 76, 95).

Uppala, S., D. Dee, S. Kobayashi, P. Berrisford, and A. Simmons (2008). *Towards a climate data assimilation system: status update of ERA-Interim*. ECMWF Newsletter No. 115–Spring 2008 (cit. on p. 20).

Vermeer, M. and S. Rahmstorf (2009). "Global sea level linked to global temperature." In: *P. Natl. Acad. Sci.* 106.51, pp. 21527–21532. DOI: 10.1073/pnas.0907765106 (cit. on p. 13).

Wallace, J. M. and P. V. Hobbs (2006). *Atmospheric Science—An Introductory Survey*. Elsevier Academic Press, USA (cit. on pp. 67–69).

Ward, M. (1994). "XmdvTool: Integrating Multiple Methods for Visualizing Multivariate Data." In: *Proc. IEEE Visualization Conf. (Vis '94)*, pp. 326–336 (cit. on p. 71).

Ware, R., C. Rocken, F. Solheim, M. Exner, W. Schreiner, R. Anthes, D. Feng, B. Herman, M. Gorbunov, S. Sokolovskiy, K. Hardy, Y. Kuo, X. Zou, K. Trenberth, T. Meehan, W. Melbourne, and S. Businger (1996). "GPS Sounding of the Atmosphere from Low Earth Orbit: Preliminary Results." In: *B. Am. Meteorol. Soc.* 77.1, pp. 19–40. DOI: 10.1175/1520-0477(1996)077<0019:GSOTAF>2.0.CO;2 (cit. on p. 32).

Wickert, J., T. Schmidt, G. Beyerle, R. König, C. Reigber, and N. Jakowski (2004). "The radio occultation experiment aboard CHAMP: Operational data analysis and validation of vertical atmospheric profiles." In: *J. Meteorol. Soc. Jpn.* 82, pp. 381–395 (cit. on p. 93).

Wickert, J., G. Beyerle, R. König, S. Heise, L. Grunwaldt, G. Michalak, C. Reigber, and T. Schmidt (2005). "GPS radio occultation with CHAMP and GRACE: A first look at a new and promising satellite configuration for global atmospheric sounding." In: *Ann. Geophys.* 23.3, pp. 653–658. DOI: 10.5194/angeo-23-653-2005 (cit. on p. 32).

Wickert, J., C. Reigber, G. Beyerle, R. König, C. Marquardt, T. Schmidt, L. Grunwaldt, R. Galas, T. K. Meehan, W. G. Melbourne, and K. Hocke (2001). "Atmosphere sounding by GPS radio occultation: First results from CHAMP." In: *Geophys. Res. Lett.* 28.17, pp. 3263–3266. DOI: 10.1029/2001GL013117 (cit. on pp. 32, 107).

Wigley, T. M. L. (2006). "Statistical Issues Regarding Trends." In: *Temperature Trends in the Lower Atmosphere: Steps for Understanding and Reconciling Differences.* Ed. by T. R. Karl, S. J. Hassol, C. D. Miller, and W. L. Murray. Washington, DC: U.S. Climate Change Science Program/Subcommittee on Global Change Research. Chap. Appendix A (cit. on p. 43).

Wilks, D. S. (2006). *Statistical methods in the atmospheric sciences.* 2nd. Burlington; San Diego; London: Academic Press Inc., p. 648 (cit. on pp. 33, 69, 78, 98).

Wong, P. (1999). "Visual Data Mining." In: *IEEE Computer Graphics and Applications* 19.5 (cit. on p. 88).

Zalasiewicz, J., M. Williams, W. Steffen, and P. Crutzen (2010). "The New World of the Anthropocene." In: *Environ. Sci. Technol.* 44.7, pp. 2228–2231. DOI: 10.1021/es903118j (cit. on p. 12).

Zou, C.-Z. and W. Wang (2010). "Stability of the MSU-derived atmospheric temperature trend." In: *J. Atmos. Ocean. Tech.* 27.11, pp. 1960–1971. DOI: 10.1175/2009JTECHA1333.1 (cit. on p. 107).

Zou, C.-Z., M. Gao, and M. D. Goldberg (2009). "Error structure and atmospheric temperature trends in observations from the Microwave Sounding Unit." In: *J. Climate* 22.7, pp. 1661–1681. DOI: 10.1175/2008JCLI2233.1 (cit. on pp. 19, 107, 110).

Abstract

While the efforts of the scientific community have lead to a remarkable knowledge of the climate system, there are still many open topics left to be resolved. One of these topics is concerned with upper-air climate change. There has been a debate about upper-air trends in the last decades, and the controversy is still ongoing. Climate model data, reanalysis datasets, and observational records show large uncertainty ranges in their trend values, many of them even disagree in important aspects of trend characteristics. This thesis investigates methods to analyze upper-air climate data. Firstly, an innovative approach to deal with large atmospheric datasets is presented: Interactive visual exploration is shown to be a valuable tool to complement classical statistical methods. It opens new opportunities for data analysis because it does not require prior knowledge of data characteristics, thus enabling the user to come up with new hypothesis about the data. Several datasets from climate models, reanalyses and observations are explored with sophisticated interactive visualization techniques, showing how these methods make it easy to determine potentially unknown patterns and characteristics in the data. Secondly, Radio Occultation (RO) as a recent upper-air dataset with high accuracy is employed as reference for stratospheric radiosonde and (Advanced) Microwave Sounding Unit ((A)MSU) climatologies. Special care is taken to account for sparse sampling in the radiosonde and RO climatologies. The results show good agreement of radiosondes and RO, while (A)MSU and RO trends are found to differ significantly. The advantages of RO with homogeneously distributed observations, high vertical resolution and accuracy are confirmed, helping to overcome problems of conventional upper-air data. The suitability to serve as reference for other observational records is demonstrated, thus narrowing the large structural uncertainties involved in today's upper-air climate records.

Wegener Center for Climate and Global Change
University of Graz
Leechgasse 25
A-8010 Graz, Austria
www.wegcenter.at
ISBN 978-3-9503112-3-5